

m.m.B.

Journal of
**Geophysical
Research**

VOLUME 64

JUNE 1959

NUMBER 6

THE SCIENTIFIC PUBLICATION
OF THE AMERICAN GEOPHYSICAL UNION

Journal of Geophysical Research

An International Scientific Publication

OFFICERS OF THE UNION

MAURICE EWING, *President*
LLOYD V. BERKNER, *Vice President*
A. NELSON SAYRE, *General Secretary*
WALDO E. SMITH, *Executive Secretary*

OFFICERS OF THE SECTIONS

Geodesy
MILTON O. SCHMIDT, *President*
CHARLES PIERCE, *Vice President*
FRANK L. CULLEY, *Secretary*

Seismology
HUGO BENIOFF, *President*
LEONARD M. MURPHY, *Vice President*
JAMES A. PEOPLES, JR., *Secretary*

Meteorology
HELMUT E. LANDSBERG, *President*
THOMAS F. MALONE, *Vice President*
WOODROW C. JACOBS, *Secretary*

Geomagnetism and Aeronomy
H. R. JOESTING, *President*
L. R. ALLREDGE, *Vice President*
ROBERT E. GEBHARDT, *Secretary*

Oceanography
ROGER R. REVELLE, *President*
HENRY STOMMEL, *Vice President*
DONALD W. PRITCHARD, *Secretary*

Volcanology, Geochemistry, and Petrology
J. FRANK SCHAIRER, *President*
FRANCIS G. WELLS, *Vice President*
L. T. ALDRICH, *Secretary*

Hydrology
RAY K. LINSLEY, *President*
HARRY F. BLANEY, *Vice President*
RALPH N. WILSON, *Secretary*

Tectonophysics
HARRY H. HESS, *President*
PATRICK M. HURLEY, *Vice President*
BENJAMIN F. HOWELL, JR., *Secretary*

Beginning with the January 1959 issue (Vol. 64, No. 1) the *Journal of Geophysical Research* is published monthly by the American Geophysical Union, 1515 Massachusetts Ave., Northwest, Washington 5, D. C. with the support of the Carnegie Institution of Washington and the National Science Foundation. This new monthly combines the type of scientific material formerly published in the bi-monthly *Transactions, American Geophysical Union*, and the quarterly *Journal of Geophysical Research*. The *Transactions, American Geophysical Union* will continue as a quarterly publication for Union business and items of interest to members of the Union.

BOARD OF EDITORS

Editors: PHILIP H. ABELSON and J. A. PEOPLES, JR.

ASSOCIATE EDITORS

1959

JULIUS BARTELS
JOHN W. EVANS
H. W. FAIRBAIRN
JOSEPH KAPLAN
THOMAS MADDOCK, JR.

D. F. MARTYN
TOR J. NORDENSON
HUGH ODISHAW
E. H. VESTINE
J. LAMAR WORZEL

1959-1960

HENRY G. BOOKER
E. C. BULLARD
JULE CHARNEY
GEORGE T. FAUST
DAVID G. KNAPP

WALTER B. LANGBEIN
ERWIN SCHMID
HENRY STOMMEL
J. TH. THIJSSSE
A. H. WAYNICK

J. TUZO WILSON

1959-1961

HENRY BADER
K. E. BULLEN
CONRAD P. MOOK
WALTER H. MUNK

T. NAGATA
FRANK PRESS
A. NELSON SAYRE
MERLE A. TUVE

JAMES A. VAN ALLEN

This Journal welcomes original scientific contributions on the physics of the earth and its environment. Manuscripts should be transmitted to J. A. Peoples Jr., Geology Department, University of Kansas, Lawrence, Kansas. Authors' institutions, if in the United States or Canada, are requested to pay a publication charge of \$15 per page, which, if honored, entitles them to 100 free reprints.

Subscriptions to the *Journal of Geophysical Research and Transactions, AGU* are included in membership dues.

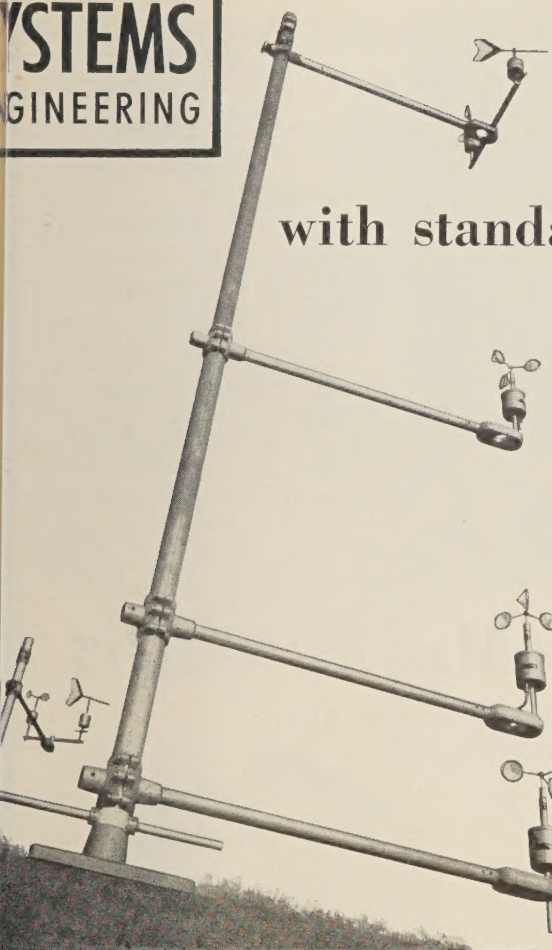
Non-member subscriptions, *Journal of Geophysical Research*.....\$16 per calendar year, \$2 per copy

Non-member subscriptions, *Transactions, AGU*.....\$4 per calendar year, \$1.25 per copy

Subscriptions, renewals, and orders for back numbers should be addressed to American Geophysical Union, 1515 Massachusetts Ave., Northwest, Washington 5, D. C. Suggestions to authors are available on request.

Advertising Representative: Howland and Howland, Inc., 114 East 32nd St., New York 16, N. Y.

SYSTEMS
ENGINEERING



with standard components

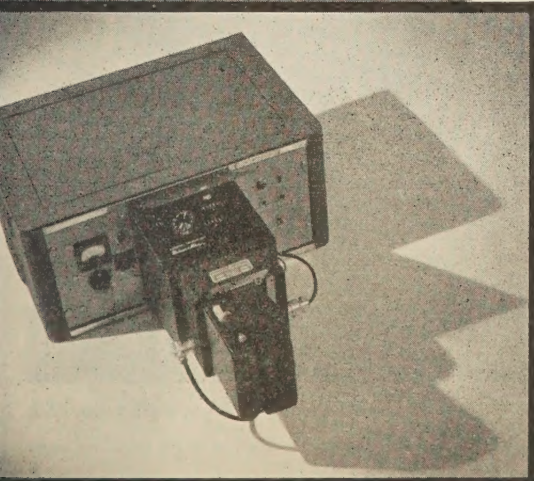
Where a complete meteorological system is required, Beckman & Whitley offers everything you need: 1. Time-tried and proved anemometers, wind-direction units, thermal radiometers, soil heat-flow transducers, etc., of the highest quality and performance, and 2. A knowledgeable and experienced engineering and meteorological group prepared to develop these elements into a complete met system to meet your particular needs.

EXAMPLE: Illustrated here is a complete automatic wind-profile system created for IGY glacier studies. The logarithmic pickup array is composed of standard transmitters mounted on a standard meteorological mast and telemetered to standard translator units driving a special photographic recording unit.

Shown below, this device automatically records the readings from digital counters representing the four wind-speed pickups, together with the indication from a clock face, operating on an interval basis which can be anything from seconds to hours. Wind direction is written on a standard strip-chart recorder.

There are many other examples ranging from small portable weather stations to rocket-motor test-tower instrumentation running into dozens of pickup points on numerous towers, and data presentation on punch cards, typewriters, calculator tapes, and the like.

Check with us on your particular problems.



Beckman & Whitley INC.
SAN CARLOS 15, CALIFORNIA



Type Gf6
after Schmidt

Field proven for decades
In actual use throughout the world

Reading accuracy: up to 1 gamma

Direct measuring range: 1200 gamma

Magnet Systems for vertical and horizontal components

Also suitable for recording of the magnetic variations

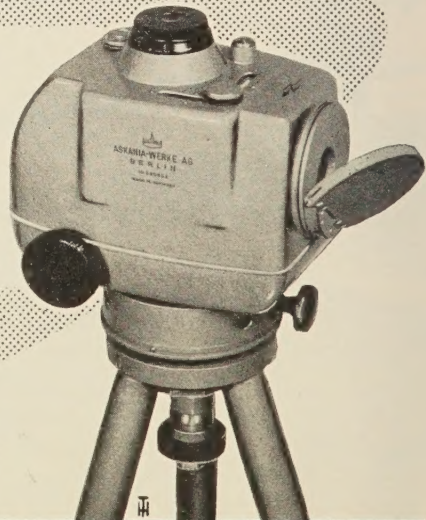
Precision Magnetometers

Type Gfz

for measuring of the vertical component

Easy to operate and time saving
only 40 sec. per measuring station
Reading accuracy: better than 2 gamma

Direct measuring range: 65000 gamma



Ask for detailed information for these and other geophysical instruments of our extensive manufacturing program

ASKANIA-WERKE AG. · BERLIN-FRIEDENAU

U. S. Branch Office & Service Dept.

4913 Cordell Ave., Bethesda, Md.

Please mention JOURNAL OF GEOPHYSICAL RESEARCH, when writing to advertisers



EXPLORER
FIRST ALL-TRANSISTORIZED
24-TRACE
SEISMOGRAPH SYSTEM

**CUT EXPLORATION COSTS . . .
SAVE 50% to 80% IN POWER, WEIGHT, SIZE**

Texas Instruments Incorporated has developed a completely new, high-performance seismograph around the functional magic of transistors.

YOU SAVE ON PORTAGE AND TRANSPORTATION . . . For the first time, a 24-channel seismograph, complete with control and test circuitry, is contained in a compact, *one-man* portable case 18" x 26" x 8" weighing only 57 pounds. Other systems require from three to six cases for components performing the same functions. Also, the entire seismograph system, with camera and magnetic recorder (*TECHNO's* new all-transistorized magnetic recorder is a highly compatible system with the EXPLORER) may be mounted in one Jeep or transported in one helicopter trip.

YOU SAVE ON POWER . . . the EXPLORER requires only one 12-volt battery and consumes nine amperes (normally only six amperes after

first breaks) . . . no warmup time is required. This is better than a five-to-one power savings over other present seismographs.

YOU SAVE ON MAINTENANCE . . . after initial system checks, 80 per cent of all amplifier difficulties are attributable to vacuum tubes. Transistors used in the EXPLORER, for practical purposes, have infinite life.

Furthermore, the EXPLORER offers a wide practical frequency range, 5 to 200 cps; broad dynamic range; and wide operational latitude in AGC speeds, initial suppression, filtering, inputs, outputs, and test circuitry.

The EXPLORER is literally *jumps* ahead of the exploration industry . . . it pays for itself in REDUCED OPERATING COSTS, INCREASED PRODUCTION, and UN-EQUALLED RELIABILITY.

Write for complete EXPLORER information . . . specify Bulletin S-324.

**TEXAS INSTRUMENTS**
INCORPORATED
INDUSTRIAL INSTRUMENTATION DIVISION
3609 BUFFALO SPEEDWAY • HOUSTON, TEXAS • CABLE: HOULAB

Other TI/IID Products

- Complete Seismic Instrumentation
- TI-Warden Gravity Meters
- DATA-GAGE Measurement and Control Systems
- "recti/rate" Recorders and Accessories
- Automatic Test Equipment

(TI handles export sales and service
for *TECHNO* transistorized recorder)

SPRENGNETHER'S DIRECT WRITING VISUAL RECORDER PROVIDES 24 HOUR REGISTRATION.

For a moderate initial investment, seismological laboratories can obtain this superior drum-type recorder. Its advantages include continuous registration and easy visual access to all information on the recorder. It also requires less storage space for records than a tape recorder.

Drum is completely enclosed to protect against dust or accidental damage. For greatest possible convenience in changing records, the large, curved plastic cover can be fully opened.

The pen drive galvanometer is a high torque, frictionless, torsion-type moving coil system. It operates in the field of large Alnico V magnet with special pole pieces and core.

Pen-drive is rigidly mounted on inside of back panel of recorder. Ink-well is mounted on the axis of moving coil to eliminate inking problems.

Recorder box is of heavy steel and has a beautiful, baked enamel finish.

SPECIFICATIONS:

Dimensions: 31" long, 16" wide, 15" high (not including motor housing) — Weight: 90 lbs. net — Drum Speed: 30 or 60 mm/min. — Translation Rate: 2.5 or 5 mm/rev. Power Requirements: 110 V. or 240 V. AC, 50 or 60 cy. Paper Size: 36" x 12" — Pen Galvanometer Sensitivity: .1 milliamperes/mm.



Series VR-40-0

Shown with controls as used with our VR-30-A Amplifier.

Write for complete technical information today.

Internationally Known Mfrs. of Seismological, Geophysical Instruments
W. F. SPRENGNETHER INSTRUMENT COMPANY INC.
4567 SWAN AVE. • ST. LOUIS 10, MO.

BULLETIN (IZVESTIYA), ACADEMY OF SCIENCES, U.S.S.R.

Subscriptions for 1958 volume now available

This monthly Russian publication, perhaps the leading journal of Geophysics of the U.S.S.R., is being translated and published in an English edition for the year 1958 by the American Geophysical Union. The twelve numbers in Russian cover 1536 pages. Published with the aid of a grant from the National Science Foundation.

Send subscriptions now to

AMERICAN GEOPHYSICAL UNION

1515 Massachusetts Avenue, N.W.
Washington 5, D.C., U.S.A.

Subscription rates: \$25.00 for the volume of 12 numbers (\$12.50 for individuals subscribing for personal use; introductory offer)
Numbers will be mailed as issued.

The English edition of this publication for 1957 has been translated and published for the American Geophysical Union by Pergamon Press. This volume may also be ordered through the American Geophysical Union at a price of \$25.00 plus a service charge of \$3.00. The March 1959 issue of the *Transactions*, AGU, will carry the titles of the papers of the first nine numbers of this volume.



... applying the earth sciences
since 1930



Since 1930 GSI has conducted geophysical exploration throughout the world.

We offer complete seismic, gravity and magnetic investigation services, data processing and data re-interpretation. Write for our descriptive literature.

... continuing leadership through research

GEOPHYSICAL SERVICE INC.

900 EXCHANGE BANK BUILDING • DALLAS 35, TEXAS

... offices throughout the world

GSI is the geophysical exploration subsidiary of Texas Instruments Incorporated.

Please mention JOURNAL OF GEOPHYSICAL RESEARCH, when writing to advertisers

GEOPHYSICAL MONOGRAPH SERIES

AMERICAN GEOPHYSICAL UNION

1515 MASSACHUSETTS AVENUE, N.W.

WASHINGTON 5, D.C., U.S.A.

Antarctica in the International Geophysical Year—Geophysical Monograph No. 1 (Publication No. 462, National Academy of Sciences—National Research Council); Library of Congress Catalogue Card No. 56-60071; 133 pp. and large folded map of the Antarctic, 1956, 7" x 10"

\$6.00

Contains 16 separate papers by various American authorities on the Antarctic under the headings: General, Geographic and Meteorological, Geological and Structural, Upper Atmospheric Physics, and Flora and Fauna. Map (41" x 41") compiled by the American Geographical Society. Introduction by L. M. Gould, President of Carleton College and internationally recognized authority on the Antarctic.

Geophysics and the IGY—Geophysical Monograph No. 2 (Publication No. 590, National Academy of Sciences—National Research Council); Library of Congress Catalogue Card No. 58-60035; 210 pp., 1958, 7" x 10"

\$8.00

Contains 30 separate papers by leading American authorities under the headings: Upper Atmospheric Physics, The Lower Atmosphere and the Earth, and The Polar Regions. Preface by Joseph Kaplan, Chairman of the U. S. National Committee for the IGY.

Atmospheric Chemistry of Chlorine and Sulfur Compounds—Geophysical Monograph No. 3 (Publication No. 652, National Academy of Sciences—National Research Council); Library of Congress Catalogue Card No. 59-60039; about 110 pp., 1959, 7" x 10"

\$5.50

Based on a symposium held jointly with the Robert A. Taft Sanitary Engineering Center of the U. S. Public Health Service in Cincinnati in November, 1957. Contains 23 papers (some as summaries) with discussion. Preface by James P. Lodge, Jr., of the Taft Sanitary Engineering Center and Chairman of AGU's Committee on Chemistry of the Atmosphere.

Prices plus postage, unless payment accompanies order. Quantity discounts: 5–19 copies, 10%; 20–49 copies, 15%; 50 or more copies, 20%.

It is anticipated that Geophysical Monographs 4 and 5 will be issued during 1959. Watch "Special Announcements" in the *Transactions* for word of these.

Purchase Order

To AMERICAN GEOPHYSICAL UNION

1515 Massachusetts Avenue, N.W., Washington 5, D.C., U.S.A.

Please enter our order for the following:

_____ copies of Geophysical Monograph No. 1, *Antarctica in the International Geophysical Year*, at \$6.00* \$ _____
_____ copies of Geophysical Monograph No. 2, *Geophysics and the IGY*, at \$8.00* \$ _____
_____ copies of Geophysical Monograph No. 3, *Atmospheric Chemistry of Chlorine and Sulfur Compounds*, at \$5.50* \$ _____

Payment of \$_____ is enclosed.

Please send invoice, adding postage charges.

Enter our standing order for _____ copies of subsequent Geophysical Monographs at the special prepublication rates (e.g., prepublication rate for Monograph No. 3 for non-members was \$4.00, payment in advance, or \$4.75 on invoice).

* List price for quantities up to four; see advertisement above for discounts on quantity purchases. Special discounts to members.

Typed name _____ Signature _____

Address _____

The Evolution of North America

by PHILIP B. KING

The story of the continent of North America through geologic time, from its earliest beginnings, is set forth here by one of America's leading structural geologists. Writing in an informal style, Dr. King treats each region separately, illustrating principles and significant stages of continental evolution. The regions selected are those with which the author, through his 35 years of geological experience and research in North America, is particularly familiar. Each chapter includes extensive bibliographical references and is clearly and beautifully illustrated with numerous maps and cross sections to bring out special geologic features.

208 pages. Illustrated. $8\frac{1}{2} \times 11"$. \$7.50

Order from your bookstore, or

PRINCETON UNIVERSITY PRESS
Princeton, New Jersey

Advances in Geophysics

Edited by H. E. LANDSBERG and J. VAN MIEGHEM

Volume 6

Ready July 1959

Atmospheric Diffusion and Air Pollution

Proceedings of a Symposium held at Oxford, August 1958
under the joint auspices of the International Union
of Theoretical and Applied Mechanics and the
International Union of Geodesy and Geophysics

Edited by

F. N. FRENKIEL
Applied Physics Laboratory
The Johns Hopkins
University

P. A. SHEPPARD
Imperial College
University of London

July 1959, about 480 pp., illus., \$12.00

Also available: Volumes 1-5

Descriptive literature available upon request

ACADEMIC PRESS, NEW YORK and LONDON

111 Fifth Avenue, New York 3, New York 40 Pall Mall, London, S. W. 1



COMMAND DESTRUCT

The flight testing of second generation missiles—more versatile and powerful than their predecessors—requires a device for sure termination of any missile flight that might endanger the test range or surrounding area.

Ramo-Wooldridge engineers, under a United States Army Signal Corps contract, have successfully developed and delivered the first sub-miniature, completely transistorized radio "command destruct" receivers.

Specifically designed for missile flight safety operations, the receiver (AN/DRW-11) can actuate safety mechanisms or destruct devices. It has three command channels, each of which actuates a control relay.

The "command destruct" receiver accepts frequency modulated signals in the UHF radio command band. It is designed to operate with closer radio frequency and command frequency channel spacing than has been used to date, thus making possible more efficient use of the available radio spectrum.

Compact and rugged, the radio receiver's modular construction permits rapid and complete accessibility to all components. One module houses the basic receiver. The second module contains the three command channels and relays. This integrated package occupies 115 cubic inches, and weighs 4 pounds. The receiver requires no pressurization and operates reliably under the adverse environmental conditions encountered in missile flight testing.

Engineers and scientists interested in being associated with some of the nation's most advanced research and development programs are invited to acquaint themselves with current opportunities at Ramo-Wooldridge. The areas of activity listed below are those in which R-W is now engaged and in which openings exist.

Missile electronics systems

Advanced radio and wireline communications

Information processing systems

Electronic language translation

Anti-submarine warfare

Air navigation and traffic control

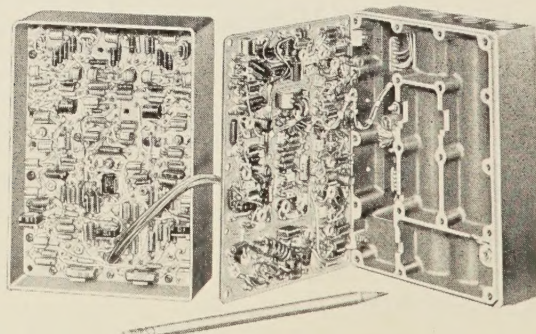
Analog and digital computers

Infrared systems

Electronic reconnaissance and countermeasures

Basic and applied physical research

For a copy of our brochure, *An Introduction to Ramo-Wooldridge*, or other additional information write to Mr. Donald L. Pyke.



RAMO-WOOLDRIDGE

P. O. BOX 90534, AIRPORT STATION • LOS ANGELES 45, CALIFORNIA

a division of **Thompson Ramo Wooldridge Inc.**

Journal of GEOPHYSICAL RESEARCH

VOLUME 64

JUNE, 1959

No. 6

Some Wind Determinations in the Upper Atmosphere Using Artificially Generated Sodium Clouds

EDWARD MANRING,* J. F. BEDINGER,* AND H. B. PETTIT*

*Geophysics Research Directorate
Air Force Cambridge Research Center
Bedford, Massachusetts*

AND
C. B. MOORE
*A. D. Little, Inc.
Cambridge, Massachusetts*

Abstract—Observation of the motion of trails produced by ejecting sodium vapor from rockets has allowed determination of some upper atmospheric winds. Simultaneous three-site photography was used to determine the position of the trail over a period of several minutes. As the result of three rocket flights, twilight wind measurements have been made over the altitude region 77 to 200 km.

Observations—Sodium vapor ejected into the earth's upper atmosphere during twilight produces a clearly visible trail which persists for several minutes [Bedinger and others, 1958]. During this period the shape of the trail undergoes continuous changes due to the wind at various altitudes. If the trail expansion is radial in a coordinate system moving with the wind, the magnitude and direction of motion of the trail center is a direct measure of the prevailing winds in that region. Such information has been obtained from the trails produced during three firings of Aerobee rockets from Holloman Air Force Base, New Mexico. Measurement of winds was not the primary objective for the first two flights, and the results and methods employed have been published. The first firing took place during evening twilight on October

12, 1955 and yielded accurate wind measurements at only two altitudes, 85 km and 110 km [Edwards and others, 1956]. The second firing occurred during evening twilight on April 11, 1956, at which time winds in the region from 77 to 109 km were measured [Bedinger and others, 1957]. Measurement of winds was a primary objective in the third flight which occurred during morning twilight on November 26, 1957 and winds in the region of 100 to 200 km were determined.

The positions of the trail at various altitudes and times were obtained from analyses of photographs taken simultaneously at three widely separated stations located at Socorro, Deming, and Mayhill, New Mexico. The positions of these stations relative to the launching site are shown in Figure 1. Pictures were taken at 15-second intervals for a period of 16 minutes. Simultaneity was assured by the use of a specially built synchronizing system at each sta-

* Present affiliation: Geophysics Corporation of America, 700 Commonwealth Avenue, Boston, Massachusetts.

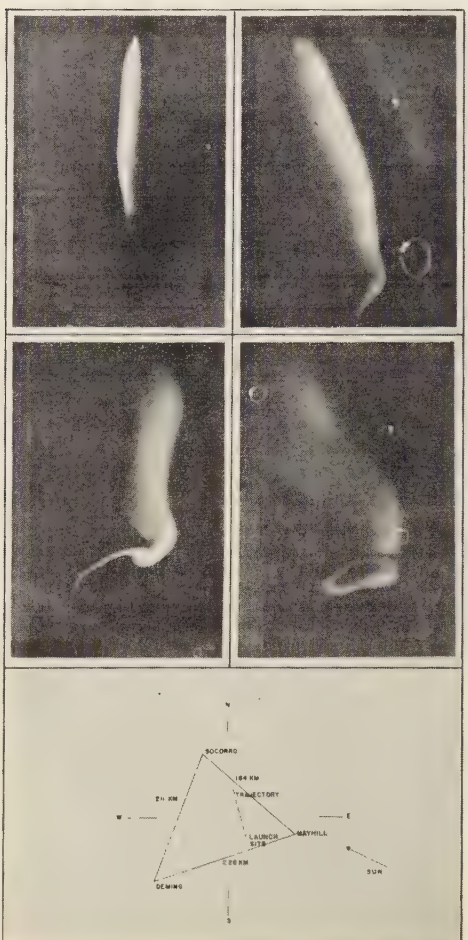


FIG. 1—Simultaneous photographs of the sodium trail during the morning twilight on November 26, 1957. The photographic stations were located at Socorro (left-hand set) and Deming (right-hand set), New Mexico. The two upper photographs were taken as the rocket approached the zenith of the trajectory, and the burning vapor may be seen at the top of the trail. The lower set was taken five minutes later.

tion. Seven-inch focal length Aero Ektar lenses were used at speeds up to f/2.5 and exposure times of from one to several seconds to insure positive registration of major stars against a varying sky brightness. Both Tri X and Royal X Pan films were used.

Data reduction—In order to eliminate the extensive and laborious computations required for reduction by direct measurements from the negatives, a complete analogue system was devised. A scaled-down model of the observational region was constructed ($\frac{1}{2}$ cm = 1 km). Slide projectors with gimbal-mounted project lenses were constructed, and the lens centers were placed exactly over the photographic stations. Large screens were placed opposite each projector and fastened securely. The positions of at least two major stars recorded on the photographs from each station were computed and points were carefully placed on the screens at the corresponding positions. Since the distances to the screens were known accurate glass slides could be made with the proper magnification to maintain angular position of the scale projection. Coincidence of the projected stars on these slides with the computed star points assured proper orientation and magnification of the slides. During the reduction of data, properly aligned slides were simultaneously projected from each station.

It may be noted in the photographs of Figure 1 that the lower altitude portion of the trail, 100 to 120 km, remained small in diameter with clearly defined edges and possessed several easily recognizable sharp discontinuities. The exact positions of these positively identified points were determined easily by stretching a string from each station to the same visually identified point on the proper screen and noting the string intersection. The positions were then read as x , y , and z coordinates of the intersections.

This method of direct reading could not be applied to the upper portion of the trail in the region of 120 to 200 km since corresponding points could not be located from visual inspection. A sketch of the method used for the higher portion of the trail is shown in Figure 1. In this method, after three 'simultaneous' slides had been properly positioned, an outline of the cloud was drawn on a thin paper fastened to the screen. The slide and projector lenses were then removed from each projector, and the lens was replaced with an opaque plate containing a small aperture carefully placed to coincide with the lens center. The cloud outline on each screen was then illuminated only by



FIG. 2—Illustration of the data reduction method

ight which passed through the center of the corresponding projection system. A vertically-adjustable thin glass plate was placed parallel to the ground plane at the intersection of the light from the three projectors. The point of a fountain pen placed on the glass plate cast a shadow on the screen. The pen was moved so that the shadow followed the cloud outline on one of the screens and left an ink mark on the glass. This procedure was followed for all three of the slides. The result is a six-sided figure on the glass plate, from which the actual position of the cloud center may be read directly. Also the radius of the photographed cloud may be directly determined. This procedure was followed for positions of the glass plate corresponding to 10-km height intervals over the region from 120 to 202 km for each set of simultaneous slides.

Wind velocity—The tabulated x , y , z , and t values were used to obtain difference values, Δx , Δy , Δz , and Δt , from which the magnitude and direction of the wind were obtained. Below 20 km changes in Δz were too small to be measured by the procedures used. From the experimental limitations, however, it can be stated that vertical winds in this region would have been detected if a steady velocity of 2 meters/sec were maintained during the period of observation. Above 120 km values of Δz could not be determined by the method used.

The results from both flights are given in Table 1. Figure 3 is a composite wind rose containing data from both flights. It may be noted that the results obtained from the evening twilight flight of April 11, 1956 show a continuous change in wind direction up to 105 km where there is a reversal, and the results from the morning twilight flight of November 26, 1957 show similar changes in wind directions over this range of altitude. Additional changes in direction are present at 140 and 170 km. The effects of these varying velocities are evident in Figure 4.

TABLE 1—*Tabulated wind velocities*

Altitude above sea level (km)	Wind speed (meters/sec)	Wind direction (degrees)
77*	43	118
84*	175	82
85**	80	320
92.5*	107	47
93*	125	48
102*	100	287
102.3*	91	290
104	125	250
105*	179	276
106	115	280
108	43	360
109	153	350
110**	45	120
110	75	30
114	63	50
119	36	60
122	20	120
126	28	155
132	33	240
142	40	270
152	30	245
162	20	230
172	40	200
182	41	210
192	42	220
202	38	240

* April 11, 1956, 1905 MST

** October 12, 1955, 1800 MST

November 26, 1957, 0556 MST

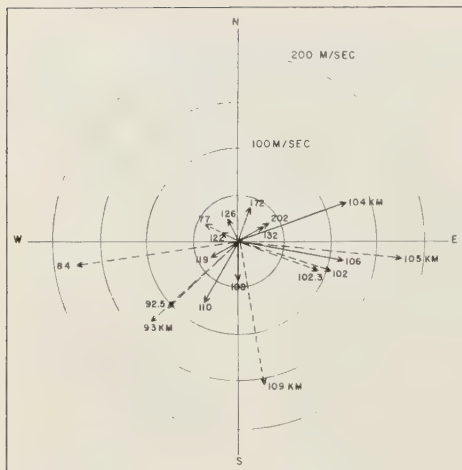


FIG. 3—Composite wind rose of morning of November 26, 1957 (solid arrow) and evening of April 11, 1956 (dotted arrow) twilight wind measurements

Diffusion—After an initial expansion in which the released sodium cloud expands until ambient density is attained, additional expansion will be governed by diffusion processes. The effect of varying atmospheric density along the trail, and the resulting expansion, is shown in Figure 4. Accurate determination of the cloud diameter as a function of time at a specific height should give a measure of the diffusion rate and hence density and temperature information at that height.

For a long trail the diffusion is described by

$$\frac{\partial n}{\partial t} = D \left(\frac{1}{r} \frac{\partial n}{\partial r} + \frac{\partial^2 n}{\partial r^2} \right)$$

where n is the density of sodium atoms, r the filament, and D the coefficient of diffusivity. For the specific case in which the cloud is photographed with the illuminating sunlight coming from behind, the cloud will possess uniform surface brightness over those portions which are optically dense. At the absorption maximum, the cross section for absorption by a sodium atom is about 10^{-11} cm 2 ; hence regions can be considered optically dense when the average density of sodium atoms along a line of sight through the cloud is greater than 10^{19}

atoms/cm 2 . Near the photographed cloud edges, densitometry of the images can, with proper precautions, yield the information necessary to evaluate densities (at least on a relative scale) and radii so that from a time sequence of photographs the coefficient of diffusivity can be evaluated from the above treatment.

In order to obtain data for wind evaluation, photographic sites were selected for ease in triangulation, and exposures were selected to record the star background. The resulting cloud images were therefore overexposed, and cloud edges cannot be determined with the precision required to evaluate the coefficient of diffusivity as a function of height with enough accuracy to be useful. At only one altitude were sodium densities such that an approximate evaluation of diffusion could be made. At 180 km $D = 6 \times 10^{-8}$ cm 2 /sec for the diffusion coefficient was obtained. Calculations using the Standard Atmosphere of Minzner and Ripley [1956] and the equation for diffusivity developed by Chapman and Cowling [1939], give the value as 2.97×10^{-8} cm 2 /sec. Photography from selected positions with exposures tailored specifically to de-

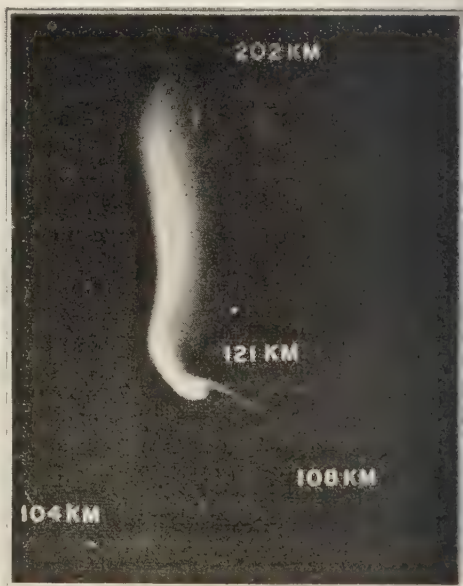


FIG. 4—Photograph of trail of ejected sodium. Heights of some portions are indicated

determine the cloud edges should provide data from which the diffusivity as a function of height from about 100 to above 200 km can be determined. An independent means of determining pressures and temperatures of the upper atmosphere would thus be provided.

Conclusions—Although measurements can only be made during twilight periods, the method has several desirable features which indicate its potential value for accurate and intensive study of upper atmospheric winds. Since the sodium vapor trail rapidly expands until ambient density is attained, the motion of the trail accurately displays the true motion of the atmospheric gases. The continuous trail technique allows determination of a complete altitude profile over a wide altitude range. The lower limit is determined by aerodynamic effects, since the thrust of the sodium vapor may cause instability or an erratic trajectory during the early part of the flight. The upper limit is determined by vehicle capability or the accuracy of the time lapse photography; the trail brightness decreases rapidly because of a high diffusion rate, and the response of the vapor to the mass motion of the medium is sluggish because of the long mean free path.

The trail technique may cause difficulty in data reduction since corresponding points from different triangulation sites are not always visually apparent. However, this objection is easily overcome with the simple analogue reduction system described above.

Inherently, the method can also be used for

determining diffusivity as a function of height over this wide range of altitude.

The mechanism for vaporizing the sodium is relatively simple and very inexpensive compared with general rocket equipment. The altitudes of greatest interest are easily attained with small, inexpensive rockets which may be fired from portable launchers, requiring a minimum of auxiliary equipment.

Acknowledgments—The authors wish to express their sincere appreciation for the contributions of Robert Lynch and Robert Jenkins during both the taking and the analysis of the data.

REFERENCES

BEDINGER, J. F., S. N. GHOSH, AND E. R. MANRING, Emission from sodium ejected from rockets, *Threshold of space*, M. Zelikoff, ed., Pergamon Press, London and New York, 225-231, 1957.

BEDINGER, J. F., E. R. MANRING, AND S. N. GHOSH, Study of sodium vapor ejected into the upper atmosphere, *J. Geophys. Research*, 63, 19-29, 1958.

CHAPMAN, S., AND T. G. COWLING, *The mathematical theory of non-uniform gases*, Cambridge University Press, p. 245, 1939.

EDWARDS, H. D., J. F. BEDINGER, E. R. MANRING, AND C. D. COOPER, Emission from a sodium cloud artificially produced by means of a rocket, *The airglow and aurorae*, Pergamon Press, London and New York, 122-134, 1956.

MINZNER, R. A. AND W. S. RIPLEY, The ARDC model atmosphere, 1956, *Air force surveys in geophysics*, AFCRC TN-56-204 (ASTIA Doc. 110233), Bedford, Mass., 1956.

(Manuscript received February 10, 1959.)

The Propagation of World-Wide Sudden Commencements of Magnetic Storms

V. B. GERARD

*Magnetic Survey, Geophysics Division
Department of Scientific and Industrial Research
Christchurch, New Zealand*

Abstract—A study of the times of three sudden commencements, recorded on August 3, September 21, and November 6, 1957, respectively, at ten widely-separated magnetic observatories, indicates that when main and preliminary impulses are both recorded at one place (as in the typical SC*) they really begin approximately simultaneously. Therefore, it would appear that in nontropical regions the rate of growth of the so-called preliminary impulse is usually greater than that of the main impulse, so that the latter is obscured until the former begins to decay.

Differences around the earth between recorded times of the first impulse, whether the sudden commencement is an SC or SC* type, are only a few seconds, and the evidence suggests that the position of the sun controls the hemisphere in which the sudden commencement first occurs. This finding is interpreted in terms of the Singer shock-wave theory to mean that, as would be expected, the shock wave enters the auroral zone nearest the sun first and produces the sudden commencement a few seconds earlier in that hemisphere. At the equinox the sudden commencement times are roughly symmetrically distributed with respect to the geomagnetic equator.

It is often stated in the literature that sudden commencements occur simultaneously over the earth (within a minute or so). Apparently the most recent data are *Tanakadate's* [1934] who collected information from 29 magnetic observatories for three sudden commencements during the Second Polar Year. The times from some observatories agreed within just a few seconds, but others only within one or two minutes. It seems likely that in this study some of the apparent conflict in the data is the result of confusion, which was not recognized at the time, between the main impulse and the preliminary reverse impulse characterizing SC*. In a recent paper *Dessler* [1958] presents a model in which a longitudinal hydromagnetic wave carries the magnetic effect around the geomagnetic equator. This model gives a travel time of two minutes for the sudden commencement to be propagated around the earth.

To try to resolve this contradictory evidence we have collected copies of quick-run magnetograms from various magnetic observatories for four sudden commencements which occurred on August 3, September 21 and 22, and November 6, 1957, respectively. The observatories are:

Apia, College, Fredericksburg, Hartland, Hermanus, Honolulu, Koror, Tamanrasset, Scott Base, and Watheroo. The global distribution is by no means perfect but is considered to be reasonably satisfactory for this preliminary study. It was found necessary to reject the sudden commencement of September 22 from the analysis because the magnetograms were still too disturbed by the magnetic storm which commenced the previous day.

It is difficult to determine the exact time of the start of a sudden commencement impulse because on the quick-run magnetograms it never has the appearance of being 'sudden,' as on normal-rate magnetograms. Actually, it emerges slowly over a period of 5 to 10 seconds, with the result that different observers may put the start at quite different times. In this study, observer error was kept to a minimum because the starting times were all determined by the same observer. Measurements were confined to *H* and *D* (or *X* and *Y*) variometers only, because it has been observed that *Z* variometers are sometimes unreliable because of imperfect or dirty knife edges.

It was soon evident that the times of the

main impulses did not agree particularly well, and that high latitude observatories tended to record them about a minute after those in low latitudes. It became clear that it was the time of the first impulse that was significant; and whether this first impulse was the so-called preliminary reverse impulse or the main impulse, its time agreed within a few seconds at all observatories. As an example of this, Figure 1 shows reproductions made from the quick-run magnetograms from Scott Base and Apia, typical auroral and equatorial stations, respectively, for the sudden commencement of August 3, 1957. The comparative simultaneity of the first impulse at the two observatories can be easily seen although the type of sudden commencement is clearly SC* at Scott Base and SC at Apia. Table 1 is a tabulation of the times of the first impulse recorded at the various observatories. The maximum time difference recorded is 32 seconds between Fredericksburg and Koror for the sudden commencement of September 21. However, the mean time difference for all pairs of observatories, for all three sudden commencements, is 9 seconds.

It seems reasonable to interpret the relative simultaneity of the first impulses to mean that both the preliminary and main impulses begin more or less simultaneously, but in the middle and high latitudes the preliminary impulse has

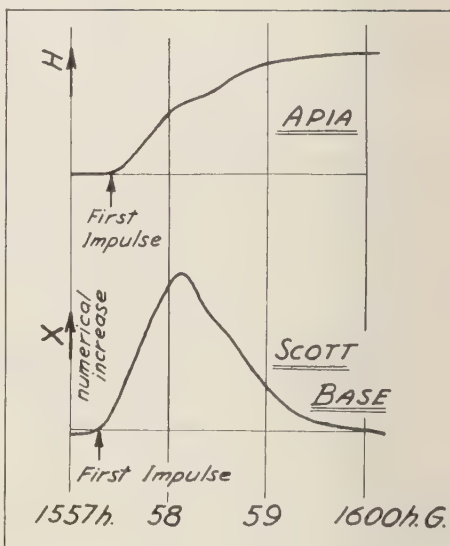


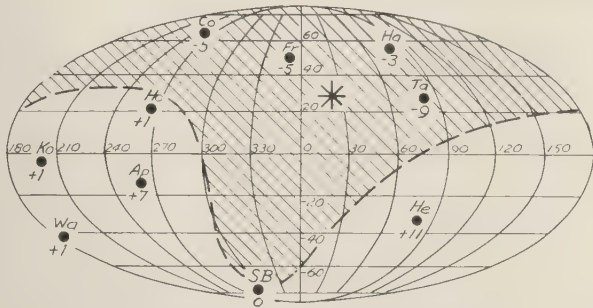
FIG. 1.—The sudden commencement of August 3, 1957, as recorded at Apia and Scott Base. The vertical scales are not the same

an initial rate of change which is greater than that of the main one and thus obscures the latter impulse. After about a minute the preliminary impulse begins to decay and the main impulse shows on the magnetogram. In equatorial

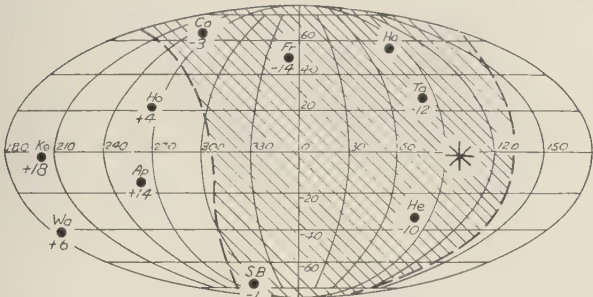
TABLE 1—Times of first impulse of three sudden commencements

Magnetic observatory	Geographic		Geomagnetic		First impulse (GMT)		
	Lat.	Long.	Lat.	Long.	Aug. 3 h m s	Sept. 21 h m s	Nov. 6 h m s
Apia	13°48'S	188°13'E	-16.0°	+260.2°	15 57 24	10 05 11	18 20 39
College	64°52'N	212°10'E	+64.5°	+255.4°	15 57 12	10 04 54	18 20 48
Fredericksburg	38°12'N	282°38'E	+49.6°	+349.8°	15 57 12	10 04 43	18 20 45
Hartland	50°59'N	4°29'W	+54.6°	+79.0°	15 57 14	no record	no record
Hermanus	34°25'S	19°14'E	-33.3°	+80.5°	15 57 28	10 04 47	18 20 40
Honolulu	21°18'N	201°54'E	+21.1°	+266.5°	15 57 18	10 05 01	18 20 40
Koror	7°16'N	134°32'E	-3.3°	+203.5°	15 57 18	10 05 15	18 20 43
Tamandasset*	22°47'N	5°32'E	+26.0°	+81.5°	15 57 08	10 04 45	18 20 44
Scott Base	77°51'S	166°47'E	-78.8°	+294.6°	15 57 17	10 04 56	18 20 35
Watheroo	30°19'S	115°53'E	-41.8°	+185.6°	15 57 18	10 05 03	no record
Mean Time							
15 57 17							
10 04 57							
18 20 42							

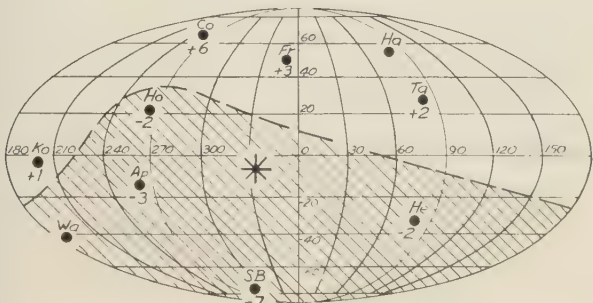
* This observatory supplied rate of change records.



August 3 1957, $t_0 = 15h.57m.17s. G.$



September 21 1957, $t_0 = 10h.04m.57s. G.$



November 6 1957, $t_0 = 18h.20m42s. G.$
Sub-Solar Point: *

FIG. 2—Departures, in seconds, from the mean (t_0) of the first impulse of each sudden commencement, at each observatory. The coordinates are geomagnetic. The shaded portion is the area where the first impulse occurred before t_0 .

regions SC* is seldom recorded. The regional character of SC* has been studied by several workers; for example, *Nagata and Fukushima* [1954]. They have clearly shown how the ratio of the amplitude of the preliminary impulse to that of the main impulse increases with geomagnetic latitude and has a maximum in the local afternoon. However, in the past it seems to have been tacitly assumed that the preliminary impulse commenced before the main one.

It is difficult to decide the probable errors to be assigned to the times shown in Table 1, and undoubtedly they are influenced by several factors such as paper rate (usually 3 mm/min, but occasionally 6 mm/min), variometer constants, quality of magnetogram and its copy, timing accuracy, and measurement errors (discussed above). However, we have assumed that the scatter in observed times contains real systematic differences and is not entirely due to the various inherent inaccuracies. The main justification for this assumption lies in the very reasonable picture obtained, as described in the next paragraphs.

The departures, in seconds, from the mean time of the first impulse of the sudden commencement have been plotted on a world map in terms of the geomagnetic coordinates of the observatory. Figure 2 shows this for all three commencements, together with the subsolar point and an isochronal line passing through points with zero time departure. This is, in effect, a primitive contour map with one isochronal, but no attempt has been made to draw more contour lines because the scatter in observed times does not warrant it.

It is immediately obvious that in all three cases the subsolar point lies in the area of the earth's surface where the first impulse occurred before the mean time. This area, shown shaded, is roughly half the earth's surface and its location varies according to the sun's position. Thus, for the sudden commencement of August 3, the shaded area is predominately confined to the Northern Hemisphere, although it does extend as far south as Scott Base. The commencement of November 6 shows an approximately inverse picture; the first impulse occurred earli-

est over an area which lies mainly in the Southern Hemisphere. At the equinox, on September 21, the first impulse first occurred over an area extending roughly an equal amount into both hemispheres.

If we accept the *Singer* [1957] shock-wave theory for the origin of sudden commencements, then these findings appear quite reasonable, for one would expect the shock-wave, traveling from the sun, to enter the auroral zone nearest the sun first, and so produce the resulting sudden commencement effects in that hemisphere a short time before the other. At the equinoxes one would expect a roughly symmetrical distribution with respect to the geomagnetic equator. The experimental results agree reasonably well with this explanation. There is no evidence for the comparatively slow propagation velocity derived by *Dessler* [1958] and based on a model in which a longitudinal hydromagnetic wave carries the magnetic effect of the sudden commencement around the geomagnetic equator.

This investigation is being extended to other sudden commencements recorded at a wider selection of observatories.

Acknowledgments—Thanks are due to the agencies and staff members of the following observatories that kindly supplied copies of the original magnetograms: College, Fredericksburg, Honolulu, Koror (U. S. Coast and Geodetic Survey); Harland (Royal Greenwich Observatory); Hermanus (Trigonometrical Survey Office); Tamanrasset (Institut de Météorologie et de Physique du Globe de l'Algérie); and Watheroo (Bureau of Mineral Resources, Geology, and Geophysics).

REFERENCES

DESSLER, A. J., The propagation velocity of worldwide sudden commencements, *J. Geophys. Research*, 63, 405-408, 1958.
NAGATA, T., AND N. FUKUSHIMA, Characteristics of Polar magnetic storms, *Indian J. Meteorol. and Geophys.*, 5 (spl. no.), 75-88, 1954.
SINGER, S. F., A new model of magnetic storm and aurorae, *Trans. Am. Geophys. Union*, 38, 175-190, 1957.
TANAKADE, A., Short preliminary report on the sudden commencements of magnetic storm, *Compt. rend. L'Assemblée Lisbone, 1933, UG*, Assoc. Magnetisme et Elec., Bull. 9, 149-154, 1934.

Auroral X-Rays, Cosmic Rays, and Related Phenomena during the Storm of February 10-11, 1958

J. R. WINCKLER, L. PETERSON, R. HOFFMAN, AND R. ARNOLDY

*School of Physics
University of Minnesota
Minneapolis, Minnesota*

Abstract—Balloon observations were made during the auroral storm of February 10-11, 1958, at Minneapolis. Strong x-ray bursts in two groups were detected. The groups appeared coincident with two large magnetic bays, with strong radio noise absorption, and with the passage across the zenith of a very large amount of auroral luminosity. From the x-ray intensity and measured energies, an electron current of 0.6×10^8 electrons/cm²/sec was present. These electrons ionizing the upper D layer accounted for the increased cosmic noise absorption. The x-rays themselves carried 1000 times less energy than the electrons and could not provide sufficient ionization for the observed radio absorption. Visual auroral forms during this storm are reported to have lower borders at the 200 to 300 km level. There is thus a difficulty in bringing the electrons to the D layer without an accompanying visible aurora. A cosmic-ray decrease accompanied the storm and was observed to be from 4 to 6 per cent at sea level, 21 per cent in the balloon altitude ionization, and 15 per cent in total energy influx at 55° geomagnetic latitude. Compared with the great intensity of the magnetic and auroral phenomena in this storm, the cosmic-ray modulation was not exceptionally large.

Introduction—During the course of high-altitude balloon measurements in the IGY period, we made observations at Minneapolis during the great storm of February 10-11, 1958. Because of the close connection in this case between the cosmic-ray changes, geomagnetic effects, and auroral and ionospheric phenomena, in this paper we will discuss not only the balloon observations but also data from many other sources in an attempt to document the storm as completely as possible.

Following the discovery of x-rays penetrating to balloon altitudes at Minneapolis during auroral storms on three occasions in 1957 [Winckler and others, 1958], attempts are routinely made to prepare a launching if a strong storm is forecast. On the basis of the WASHAGI summary on February 10th reporting a major flare on February 9th, near central meridian and with strong associated radio bursts, a flight was prepared. An IGY alert extended from February 9 to February 13. This balloon was launched on the evening of February 10, CST, in very unfavorable weather conditions. The geomagnetic storm, aurora, and other phenomena had already begun, and x-ray bursts were

detected when the balloon reached high altitude. A cosmic-ray decrease was also recorded at high altitude.

Related solar phenomena [*Solar Reports*, 1958]—Considerable solar activity was present several days prior to the terrestrial storm, and one therefore cannot be completely certain of the solar-terrestrial relationship. However, the outstanding event of the period was a flare with position coordinates S13-W14 reported by Honolulu Observatory as importance 2, starting at 2108 UT February 9 and ending at 2302 UT with maximum phase at 2140. This flare was also observed by Sacramento Peak Observatory from 2139 UT to 2204 UT with maximum phase at 2142 and was classified as importance 2+. The flare emitted strong radio bursts, as inferred from the time correlation with the visual observations, and some of these observations are summarized in Table 1. Large radio noise fluxes were reported by several stations during the flare. Of particular interest is the Type IV noise storm continuum observed by the dynamic type recorder at Fort Davis from 2140 to 2246 UT. This continuum began coincident with the optical maximum

phase of the flare. Examples of Type I bursts and Type III fast drift bursts were recorded during the flare, but Type II slow drift bursts, which are sometimes associated with the emission of matter at auroral transit speeds, were not reported.

Magnetic storm phenomena—The terrestrial effects of this storm began at $0125.7 \pm .2$ UT on February 11, according to the rapid-run magnetogram of Fredericksburg Observatory. Figure 1 shows the first phase of the storm from the record of this instrument. The horizontal field component immediately showed an excursion of $+117\gamma$ lasting 2.5 minutes. The recorded dH/dt was greater than $2.1\gamma/\text{sec}$ in the initial part of the excursion. A second sharp positive excursion, larger than the first, appeared at $0159.0 \pm .1$, following a disturbed period. This excursion which lasted for about five minutes could be followed completely only on the insensitive regular speed magnetogram. The initial rise rate was greater than the first excursion and exceeded the writing speed of the recorder, but the peak value could be estimated and was about $+500\gamma$. This sudden in-

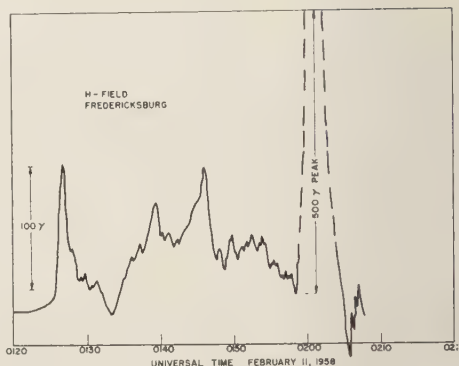


FIG. 1.—Rapid-run magnetogram trace of the first part of the storm of February 11, 1958. The 500γ peak was accompanied by large earth current disturbances.

crease in H was accompanied by sharp drops of about 150γ in Z and 30γ in D . We assume that these pulses represent the initial encounter of the solar gas cloud with the earth's dipole field; that is, the first phase of a storm as discussed by Chapman and Bartels [1940],

TABLE 1—Radio emission time associated with the flare of February 9, 2108 UT

Place	Frequency (Mc/s)	Start (UT)	End (UT)	Peak flux in 10^{-22} $\text{wm}^{-2} (\text{c/s})^{-1}$	Remarks
Boulder	470	2112	2204.3	2300	Boulder Type 9
Boulder	167	2115	2410	1900	Boulder Type 9
Ottawa	2800	2105	1 hr dur.	>70	Type 3 Simple 3 in sunset oscillation
Ft. Davis	100-580	2105 2116 2133 2133	2106 2133 2140	>100 5-30 30-100	{} Type 1 continuum
		2140	2246	>100	Type IV continuum
		2151 2246	2246 2246	>100 5-30	{ Type I noise storm
		2246 2253	2253 2302	30-100 5-30	{ Type I continuum
		2119 2120 2159		5-30 >100 >100	{ Single Group Group Type III fast drift bursts
Cornell	200		No outstanding disturbances reported during this flare.		

prompt ionospheric current systems, or both. If one assumes a relative speed between the earth and the solar stream of 1400 km/sec, then the time for an appreciable change in H to occur (0.1 min) corresponds to a relative movement of about two earth radii.

If the sudden commencement was associated with the solar flare occurring at 2108 on February 9 with maximum phase at 2140, then the transit time was approximately 28 hours, or a speed of 1400 km/sec. This speed lies in the range of values often postulated for solar corpuscular streams.

The over-all strength of the storm field with excursions of 1000γ would classify this storm as an extreme one.

Large earth currents were observed coincident with the H peak at 0159. The following is quoted from a personal communication of Dr. T. E. Talpey of Bell Telephone Laboratory, Murray Hill, New Jersey, in which he describes voltage changes on the North Atlantic telephone cable.

"... at 0200 GMT on February 11th, the voltage at the western end of the cable started down. At 0202 the earth potential reached a maximum of about 2650 volts. The polarity was such as to drive a current from west to east through the cable. At about 0207 it passed through zero and at about 0209 it reached a peak in the opposite direction. The magnitude of this peak will not be known precisely until the records from the eastern end have been received. Conditions settled down again at about 0220 with no more major swings. However, there were slight disturbances until about 1200 GMT on the 11th.

"... The section of cable between Clarenville and Sydney Mines, Nova Scotia, which is about 350 miles in length, exhibited a peak of 1450 volts (driving current from Sydney Mines to Clarenville) followed by a peak of 1100 volts in the opposite direction at about the same time as the peaks which I mentioned above for the trans-atlantic section. The cable from the northern part of the state of Washington to Alaska, which is about 1/3 the length of the trans-atlantic cable, exhibited a maximum peak

of about 250 volts. The cable to Hawaii which originates about 140 miles north of San Francisco exhibited no major voltage swings."

The observed earth-current peak seems to be an induction effect associated with the second, and largest, of the two magnetic peaks. According to the observations, the recorded current flow was from west to east, H increased, and Z decreased. The storm field is a north vector increasing initially. The circuit loop of the earth current, if considered to lie in a vertical east-west plane, therefore requires a return path through the sea *above* the cable. However, the cross-sectional area of the water with the observed dH/dt gives only about 15 volts around the circuit, compared with the measured 2650 volts maximum. The circuit cannot be closed *under* the cable, as the polarity would be wrong for an induction effect associated with the H excursion. The earth current, therefore, is apparently part of a system flowing in the earth's surface, associated with changes in Z in an unexplained way, and for which the fragmentary evidence given here is insufficient for complete analysis. The current system seems to be centered over Eastern United States.

The magnetic storm was characterized by two large negative bays in H . The first began at 0530 UT; H decreased 1000γ and recovered 860γ by 0700 UT. The second began at 0830 UT; H decreased to the same low value and recovered by 0930. These bays were accompanied by strong x-ray bursts observed at balloon levels (Fig. 2). The H field returned to approximately pre-storm values at 2200 UT but remained disturbed. These bays were closely associated with the sudden appearance of intense auroral activity passing the zenith in the neighborhood of Minneapolis.

The planetary magnetic indices K_p during the storm period were exceptionally high, ranging from 8 to 9 until 1500 on February 11.

Aurora—The aurora observed in North America during this storm was one of the most spectacular in recent years. At Minneapolis it was visually observed simultaneously with the sudden commencement at 0126 UT February 11. The all-sky camera record from Hanover,

New Hampshire, shows the appearance of aurora within a few minutes of the sudden commencement. (The all-sky camera records of this storm for a number of stations have been obtained through the Auroral Data Center at the Geophysical Institute, University of Alaska, College, Alaska.) At Minneapolis from 0130 to 0330 UT a very intense diffuse green arc covered an angular region from 20° to the zenith and from horizon to horizon in longitude. The outstanding feature, however, was the red color, also very intense, in diffuse patches at high angles, and at 0200 UT covering the northern sky from 15° to 30° elevation as a diffuse arc. The progression of events frequently seen in aurorae, in which an arc increases in elevation angle, breaks into rays, and subsides, was not followed in this case, at least prior to 0500 UT at Minneapolis. Due to overcast conditions after 0500 UT, no details could be observed at Minneapolis, but the intense red could still be seen scattered through the overcast.

The following two items have been supplied by the IGY Auroral Data Center at Cornell (C. W. Gartlein, private communication). The first is designated as Table 2 of this paper and

shows the southward advance and recession of the aurora in quantitative time correlation with data shown in Figures 2 and 3.

"1. (TABLE 2) Southern limit of arc forms:

Geomagnetic Latitude UT February 11

58	00
54	01
50	02
49	03
51	04
48	05
47	06
52	07
50	08
50	09
46	10
48	11
53	12
54	13

"2. An aurora was visible in the U. S. prior to the magnetic storm outbreak on February 11, and for the three preceding days. An outstanding feature of the February 11 aurora was the large amount of red color reported. Due to a perspective effect, many reports were received of red spots at 20° to

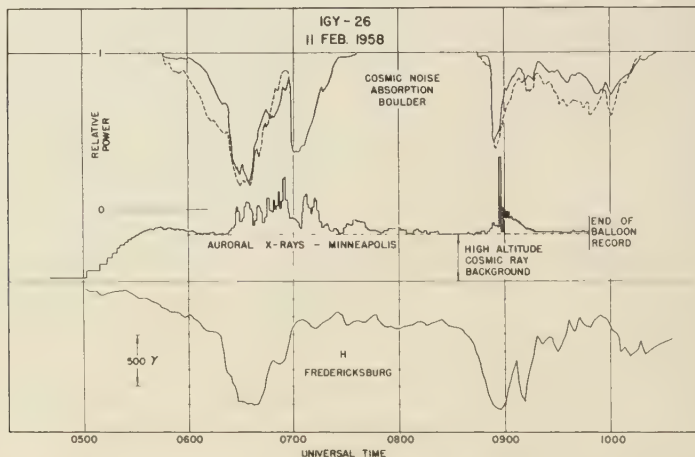


FIG. 2—Comparison of the horizontal magnetic field at Fredericksburg, auroral x-rays measured at Minneapolis, and cosmic noise absorption measured at Boulder. Two cases of intense ionospheric ionization apparently occurred, reaching maxima at approximately 0630 and 0900 UT. The ionization was very widespread as shown by this correlation and by the all-sky camera photographs (Fig. 3). The dotted Boulder curve refers to the total interferometer power and the solid curve to the vertical beam power. The balloon curve shows the x-rays compared with the normal high-altitude cosmic ray background.

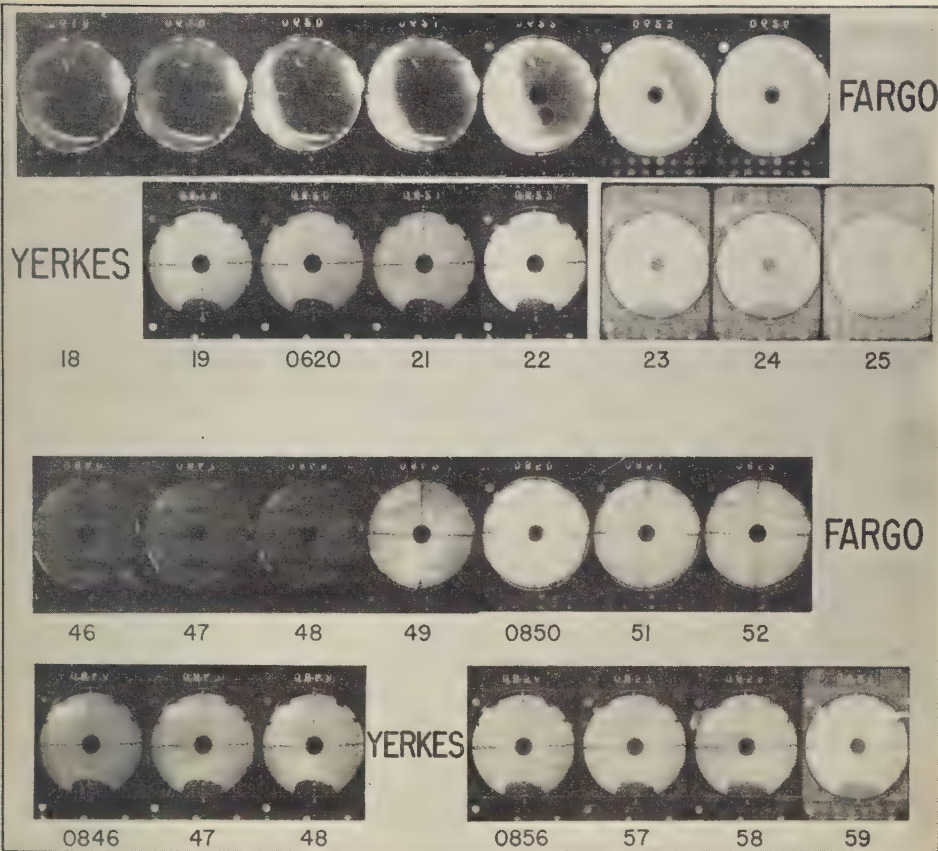


FIG. 3—All-sky camera records of the aurora of February 11, 1958 from stations adjacent to Minneapolis. Both the Fargo, North Dakota, and Williams Bay, Wisconsin, stations recorded intense auroral luminosity reaching a maximum at the times at which the magnetic bays, x-ray bursts, and cosmic noise absorption were observed. Note that the intensity through the clouds at Williams Bay was enough to illuminate the base plate of the all-sky camera.

30° altitude in the NW and NE. These reports, together with other information, suggest that the aurora was high, deep and wide. The lower border is estimated at 200 km altitude with the top extending to 800. The E-W extent is 9600 km and N-S extent 400 km."

The most impressive features of this aurora, when compared with others seen at Minneapolis, were the very high intensity of both the red and green spectral lines, the diffuseness and

extent of the luminescence, and its persistence for long periods of time without major changes in form.

Clouds prevented visual observation of the sky at Minneapolis during the time the balloon was at ceiling, but the auroral forms coincident with the x-ray bursts have been identified from all-sky camera films from Fargo, North Dakota, and Yerkes Observatory, Williams Bay, Wisconsin. In Figure 3 is shown a portion of the films from 0617 to 0625 UT and from 0846 to 0852 UT at both stations. It can be seen that at

0620 at Fargo the southern sky brightened, and the luminosity rapidly moved northward, spread across the zenith, and covered the entire sky by 0623. This is exactly coincident with the appearance of the first x-ray bursts at 0621 UT (Figs. 2 and 4) and the magnetic bay and cosmic noise absorption at Boulder (Fig. 2). The luminosity was so high that the base plate of the all-sky camera was illuminated and can be seen at 0623 in the photograph. At Yerkes the sky was cloudy, but the passage of the aurora is easily followed by the illumination of the sky and of the camera mounting at 0623.

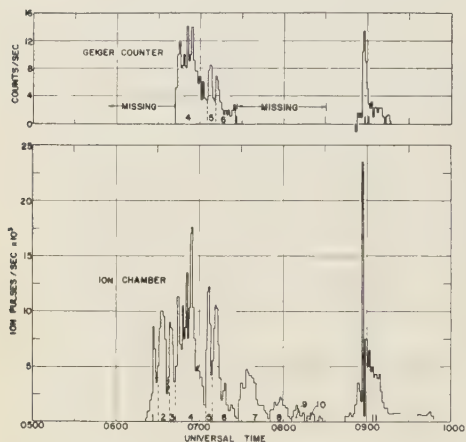


FIG. 4—Normalized ionization and counter records representing the x-ray effect at approximately 10 gm/cm² atmospheric depth with cosmic-ray background subtracted. See Table 3 for numerical values of bursts.

The second maximum began between 0848 and 0849 in the Fargo photographs (Fig. 3), and at Yerkes the intensity increased from 0845 to 0856, with an abrupt increase between 0858 and 0859. The auroral forms in this case are not clear, but the high intensity is shown by the illumination of sky and camera. This second maximum again coincides with the appearance of more x-rays, the second magnetic bay, and cosmic noise absorption at Boulder (Figs. 2 and 4).

Arguments are given below for attributing the magnetic and radio absorption effects to the auroral electrons, which also produced the

x-rays. It does not seem possible in this case to attribute the D- and E-layer effects to the x-rays alone.

Observation of auroral x-rays at balloon level— The equipment used on the standard IGY cosmic-ray monitoring balloon flights is described elsewhere [Winckler and others, 1958; Ney and Winckler, 1958; Peterson and others, 1958]. Figure 2 reproduces the ionization chamber current during the balloon flight for correlation with magnetic and ionospheric data. The balloon was launched at 0445 UT, reached a floating altitude of 11 gm/cm² at 0612, and encountered the first detectable x-ray bursts at 0622, coincident with the major decrease in the first large magnetic bay referred to earlier, and extending to 0730. A second large period of bursts occurred at 0850, coincident with the second magnetic bay. Both these major bursts and intermediate intensity changes follow very closely the inverted form of the Fredericksburg *H*-field. Such close correlation between x-ray intensity and magnetic intensity has not been generally observed when magnetic records coincident with auroral x-rays are compared. It is reasonable to assume that both the changes in conductivity of the ionospheric E layer associated with the magnetic bays and the observed x-rays have a common origin in electrons produced by the solar gas stream. These electrons, as suggested earlier [Winckler and others, 1958], may be accelerated at distances from the earth of several earth radii by an interaction between the earth's dipole field and the neutral plasma from the sun. Their energies would lie in the range of from 40 to 100 kv or higher, and most of their energy would be lost in the atmosphere as ionization and visible auroral light. About 1/1000 of the energy would be radiated as bremsstrahlung x-rays, the higher energy components of which are detected at the balloon level. On other occasions it was noted that the auroral x-rays were most intense when auroral ray structure was building up. Figure 4 shows the normalized ionization and counter records representing the x-ray effect with cosmic-ray background subtracted. The bursts have been numbered in an arbitrary way, and in Table 3 we summarize the x-ray burst data in the manner outlined in our previous paper [Winckler and others, 1958]. For an identifica-

TABLE 3—Analysis of x-ray bursts, February 10-11, 1958, IGY Flight 26

Burst No.	Integrated intensity		Peak intensity		Ratio: Ion pulses/count		X-ray ratio/cosmic-ray ratio	
	Ion pulses	Counts	Ion pulses/sec	Counts/sec	Integrated	Peak	Integrated	Peak
1	1.25		6.4×10^{-3}					
2	2.35		7.4×10^{-3}					
3	1.49		6.6×10^{-3}					
4	6.98	0.105×10^6	13.0×10^{-3}	14.4	$.66 \times 10^{-3}$	0.90×10^{-3}	2.17	2.95
5	2.36	0.019×10^6	9.0×10^{-3}	8.4	1.23×10^{-3}	1.07×10^{-3}	4.02	3.49
6	2.49	0.023×10^6	8.5×10^{-3}	6.9	1.10×10^{-3}	1.23×10^{-3}	3.59	4.02
7	2.34		3.5×10^{-3}					
8	0.90		1.6×10^{-3}					
9	0.35		1.1×10^{-3}					
10	0.14		0.6×10^{-3}					
11	4.40	0.0409×10^6	17.3×10^{-3}	13.4	1.08×10^{-3}	1.29×10^{-3}	3.53	4.22

tion of the burst numbers, see Figure 4. Due to a malfunction, part of the Geiger counter record is missing. An x-ray energy estimate can be made for several bursts, however. These energies are similar to others we have measured.

In Table 4 the bursts have been converted to R units. The intensities are intermediate between the largest and smallest effects observed on other occasions and, as in those cases, vary over wide extremes.

TABLE 4—Summary of x-ray data, February 10-11, 1958, Flight 26

Flight total integrated intensity	
Ion pairs in chamber	1.89×10^{11}
R units	3.01×10^{-6}
Time of observation (hrs)	3.5
Peak intensity	
Ion pairs/sec in chamber	1.30×10^7
MR/hr	7.45×10^{-2}
Weighted mean	
x-ray ratio	2.81
Cosmic ray ratio	
Mean measured x-ray energy (kv) . . .	~100 kv
Mass absorption coeff. in atmosphere	
cm ² /gm	0.15
Atmosphere depth gm/cm ²	13
Chamber characteristics: Chamber No. 25	
2.41 $\times 10^{-10}$ coulombs/pulse	
Filling 95 lbs gage press. argon.	

Cosmic noise absorption—In Figure 2 is shown also a record of cosmic noise obtained at 18 Mc/s at Boulder by Warwick [1958]. The striking effect is the large absorption observed exactly coincident with the magnetic bays and the x-ray bursts. The absorption was observed both with a vertically beamed antenna and an interferometer directed at an elevation angle of 35° to the northeast. The similarity of the records is good evidence for a very widespread increase in ionospheric electron density extending for at least 150 km in the north-south direction. Heavy overcast at Boulder prevented direct observations of the aurora, but the correspondence even in fine details of the fluctuations of the output of the two antennas implies simultaneous fluctuation of the primary phenomena over distances of the order of hundreds of kilometers. Furthermore, the correspondence between Fredericksburg, Minneapolis, and Boulder, although with different manifestations, shows that the major primary fluctuations were simultaneous over distances of the order of thousands of kilometers. Striking visual evidence for the reality of this situation is obtained from the all-sky camera records discussed above and shown in Figure 3.

Quantitative correlation between x-rays, magnetic bays, and cosmic radio noise absorption—The large changes in the magnetic H component, the strong cosmic noise absorption, the auroral

x-rays, and the general presence of the aurora itself are all consistent with a very intensified ionospheric bombardment by high energy electrons between the times 0530-0700 UT and 0830-0930 UT on February 11 at the latitudes of Central United States.

For comparing the x-ray and cosmic noise absorption measurements, we assume as usual that the radio absorption is proportional to the value of $\int Nv \, dS$, the integrated product of the ionospheric electron density times collision frequency. We assume that the absorption occurs mainly in the upper D layer of the ionosphere, at altitudes of 80 to 90 km, and is proportional to the electron density there. The measured cosmic noise absorption at Boulder [Warwick, 1958] during the two sets of x-ray bursts has peak values between 60 and 90 per cent of totality, or 10 db maximum.

Chapman and Little [1957] give electron densities at night at College, Alaska, at 80 to 90 km during aurora of $6.4 \times 10^4 \text{ cm}^{-3}$,* corresponding to 2.5 db of the attenuation at 30 Mc/s. Converting this to 10 db of absorption at 18 Mc/s one obtains $1.4 \times 10^6 \text{ electrons/cm}^3$.

Since the electrons are in equilibrium,

$$\frac{dN}{dt} = P - \frac{N}{t} = 0$$

where P is the production rate, N the electron density, and t the lifetime against absorption. We may also write

$$P = \text{flux} \cdot \frac{dE}{dx} \rho \frac{1}{w} = \frac{N}{t}$$

The flux refers to the ionizing agent; for example, auroral electrons or x-rays at night; ρ the atmospheric density; dE/dx , the rate of energy loss by the ionizing agent; and w , the energy required to produce one ion pair in air.

The auroral electron flux given in Table 3, inferred from the x-ray intensity and energy, is

* One should revise the Chapman-Little electron densities by a factor of approximately 1.5 on the basis of recent rocket measurements of collision frequencies (See *IGY Rocket Report Series 1*, July 30, 1958, National Academy of Science). We are indebted to Dr. Little for discussions of the interpretation of the cosmic noise absorption data.

$0.6 \times 10^6 \text{ electrons/cm}^2/\text{sec}$. The electrons are a much more efficient ionizing agent than x-rays and we assume that these electrons can reach to the upper D layer, where the radio absorption occurred, because of their observed energy of 100 kv or higher.

Using the following values for the factors,

flux = $0.6 \times 10^6 \text{ electrons/cm}^2/\text{sec}$ (Burst 11, Flight 26)

$$\frac{dE}{dx} = 6 \times 10^6 \text{ e.v. cm}^2/\text{gm}$$

$$\rho = 10^{-7} \text{ gm/cm}^3 \text{ at } 85 \text{ km}$$

$$w = 30 \text{ ev/ion pair}$$

$$t = 1 \text{ sec (lifetime of electron at } 85 \text{ km against attachment to O}_2 \text{ [Hill, to be published])}$$

gives $N = 1.2 \times 10^6 \text{ electrons/cm}^3$. Of course only the high energy part of the x-ray spectrum is retained at balloon depths, and the much more abundant low energy quanta are lost above the balloon. In terms of energy this may be estimated from the work of J. E. Kasper (unpublished data, State University of Iowa). For 100 kv primary electrons 7 per cent of the x-ray energy reaches the balloon at 10 mb, and 15 per cent for 300 kv primary electrons. This factor therefore is about 10. Considering the many approximations used, the resulting figure of $10^6 \text{ electrons/cm}^3$ is in reasonable agreement with the cosmic noise absorption values of $1.4 \times 10^6 \text{ electrons/cm}^3$. This agreement may reflect the wide-scale distribution of the aurora ionization, as we are comparing radio absorption near Boulder, Colorado, with x-rays observed at Minneapolis. If the ionization consists of patches which are very dense, separated by relatively transparent regions, then it is impossible to infer electron densities from radio absorption information. This aurora, however, was characterized by structureless regions of luminosity on an unusually large scale, and apparently the Boulder measurements arose from just this sort of distribution [Warwick, 1958] rather than from patchiness.

The visual estimates of this aurora placed the lower limit of luminosity at about 200 kn (see above). If the lower border of the luminescence marks the greatest depth of penetration of the electrons or other primary ionizing agent then the radio absorption can only arise from

the x-rays as a secondary ionizing agent which penetrates to much greater depths, ionizes the E and D layers, and appears at balloon heights. This possibility was first pointed out by Chapman and Little [1957]. Since only 10^{-3} to 10^{-4} of the electron energy appears as bremsstrahlung x-rays, replacement of the electron ionization by x-ray ionization would require x-radiation 10^3 to 10^4 times more intense than that observed. We seem to have a major discrepancy at this point. Either the visual height estimates were too high, and the frequently-observed auroral lower border of 75 to 100 km actually existed in this case also, or electrons or other particles carried considerable energy downward below the point of observed luminescence in the aurora. It is possible that the visual luminescence is associated with protons which stop at higher levels; and the high energy electrons, constituting somewhat smaller current, penetrate to lower levels and produce the ionospheric effects without large amounts of visual luminosity.

The large magnetic bays observed at Fredericksburg coincident with the x-ray bursts may be attributed to an increased conductivity of the ionospheric E layer, due probably to the same ionizing agent which produced the cosmic noise absorption phenomena. We assume in the dynamo process which produces the H component that H varies as the conductivity σ , and that this is proportional in turn to the ion production rate P as outlined above. The storm effect on H may be compared to the quiet-day diurnal effect on H , and we find that the ratio $(\Delta H \text{ storm bay})/(\Delta H \text{ diurnal}) \sim 20$. Considering a 100-km daytime electron density of 10^8 [Chapman and Little, 1957] we obtain approximately 2×10^8 electrons/cm 3 during the storm. The electron current inferred from the x-rays recorded at the balloon can produce 5×10^5 electrons/cm 2 in equilibrium at 100 km, one-quarter the number needed according to these crude computations. Perhaps another shorter-ranged component (protons?) may account for the excess ion ratio at the 100-km level.

Cosmic ray phenomena—The storm was accompanied by a world-wide modulation of galactic cosmic rays. The effect is demonstrated by Figures 5 and 6, which show the recordings of two groups of ground-level neutron monitors

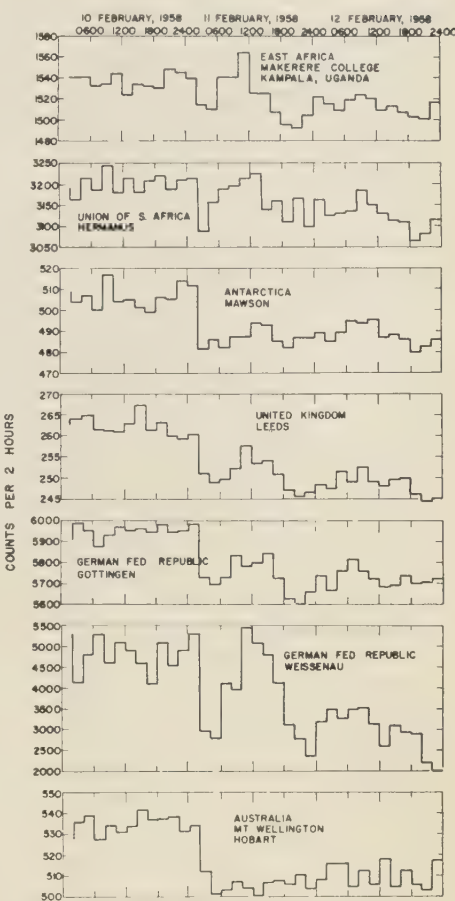


FIG. 5.—Ground-level cosmic-ray neutron records showing the Forbush-type decrease accompanying the auroral storm of February 11, 1958. The above group of stations covers Europe and Antarctica.

[IGY Data Center A for Cosmic Rays; see references]. The stations in Figure 5 are in Europe and Africa, close to the longitude of Greenwich. Also shown in Figure 5 is one station at Hobart, Tasmania, at longitude 145° E. In Figure 6 are grouped stations in the Western Hemisphere, extending from Northern Canada to the Antarctic at longitude approximately 90° W. All stations show an initial drop at the same time, 0200 UT on February 11, of roughly the same amount, from 4 to 6 per cent. This is

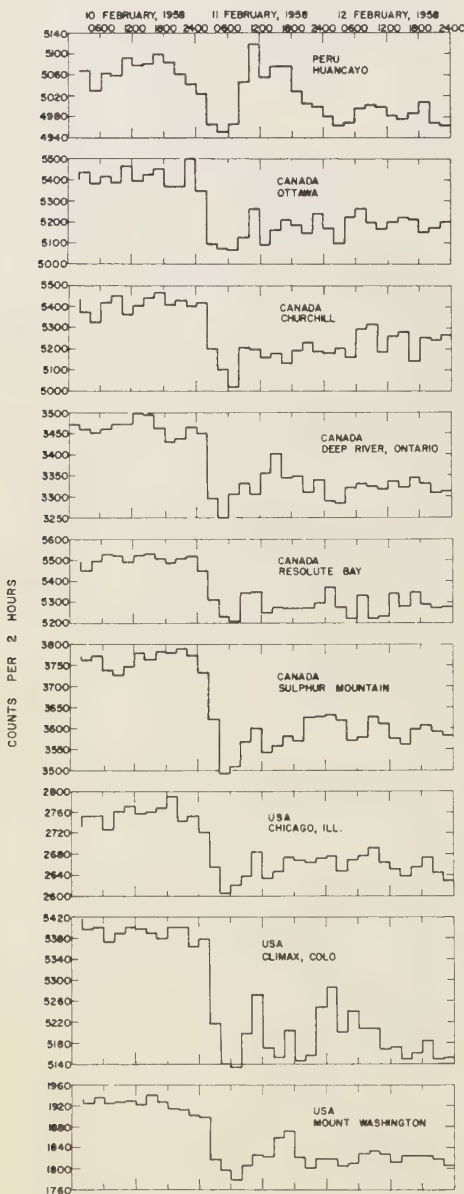


FIG. 6—Cosmic-ray neutron monitors in the Western Hemisphere showing the Forbush decrease of February 11, 1958

considered to be a well-documented case of a phenomenon [Forbush, 1954] now very familiar

to cosmic-ray investigators. The modulation is usually characterized by a sudden decrease and a slow recovery requiring several days, and frequently much longer periods. It has been shown by Simpson that the modulation affects all energies of primary cosmic rays, but the low-energy part of the spectrum is affected to a larger extent than the high. This effect is present in this case if one compares, in Figure 5, Huancayo, Peru (latitude -2° geomagnetic, cutoff rigidity 14 BV) where the initial effect is about 2 per cent, with a high latitude station such as Ottawa (geomagnetic latitude 57° , cutoff rigidity 1.3 BV) where the initial effect is 6 per cent. Another real difference between stations is the temporary recovery which follows the initial decrease by about 10 hours and is evident most strongly in the European chain of stations, but also at Huancayo, Peru.

Another feature of the decrease which may be very significant, and which seems to have been reported for the first time in this event, is a precursor, occurring closely time-coincident with the sudden commencement of the magnetic storm at 0127 UT. This is shown in Figure 7 by two stations with high counting rate monitors, the Deep River neutron monitor (H.

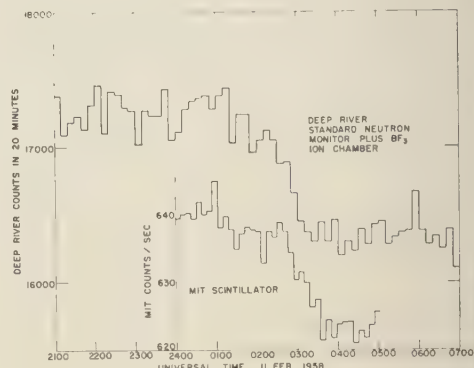


FIG. 7—High counting rate record of cosmic rays showing details of the Forbush decrease. Upper: neutron monitor at Deep River, Canada, responding to energies down to 1 Bev. Lower: Scintillation detector responding to energies in the 10 Bev region at Massachusetts Institute of Technology. There is evidence for an effect at the time of the sudden commencement (0127) followed by the major decrease beginning at approximately 0230 UT.

Carmichael and J. F. Steljes, private communication) and the MIT meson scintillator telescope [Palmeira and Williams, 1958]. The latter instrument detects mesons and responds to primary energies of 10 Bev and higher (for primary protons). The neutron monitor is sensitive to primaries as low as 1 Bev; it shows a larger relative effect for the various changes, but with somewhat lower counting rates. The precursor drop amounts to about 0.5 per cent on the meson telescope and 1 per cent on the neutron monitor. There is an apparent difference of up to 18 minutes in the appearance of this precursor in the two instruments, but in neither case is it well resolved statistically. Both records show an apparent increase in intensity just ahead of the precursor.

The major decrease in Figure 7 occurred between 0200 and 0330 UT and was completed by the end of the 'first phase' of the magnetic storm, when Fredericksburg H (Figs. 1 and 2) decreased below the pre-storm level. The Deep River monitor reached its floor at 0310, 20 to 30 minutes earlier than the MIT meson telescope. This may be a significant effect.

In Figure 8 are shown three high-altitude soundings with the standard ion chamber and counter before, during, and after the decrease. The instruments have been normalized between the three sets of curves. Unfortunately the counter on IGY-26 malfunctioned at the beginning of the flight, so that counter data from the parachute descent was used in Figure 8.

Due to the ensuing time interval of 13 hours between the ion chamber on ascent and counter on descent, possible geographic and temporal effects on the cosmic-ray intensity and the known malfunction in the counter may render this counter value unsatisfactory for comparison. Ion chamber data was not available on parachute descent due to mechanical vibration effects. The ion chamber at 10 mb pressure recorded a decrease of 21 per cent between February 9 and February 11, and a recovery by February 16 to 15 per cent below the February 9 value. The ion chamber and counter rates at 10 mb, the atmospheric integral of the ion chamber, and for comparison, the Deep River, Canada, neutron monitor rates for the same time are tabulated in Table 5. The total influx of cosmic-ray energy obtained by integrating the ion chamber rates throughout the atmosphere dropped 14.9 per cent and recovered to within 8.4 per cent of the February 8 value by February 16.

One feature of the high altitude data which has been noted on earlier flights is the change of the ratio of counting rates of ion chamber and counter. The lowered intensity decreases this ratio, as can be seen in Figure 8. This ratio measures the mean ionization rate per particle in the atmosphere. At least two-thirds of the particles measured by the ion chamber and counter are secondaries, but studies of the response of these instruments at various latitudes show that the mean ionization of the total

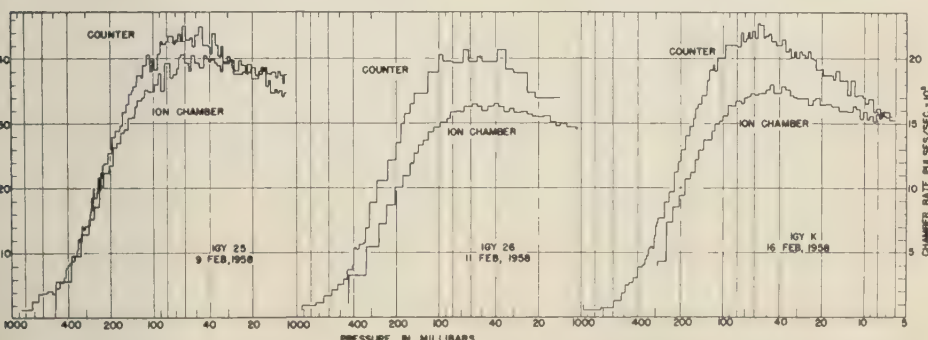


FIG. 8.—Normalized high altitude balloon soundings utilizing the standard University of Minnesota apparatus. Relative values before, during, and after the initial stages of the Forbush decrease are shown. Note the change in ratio of the ion chamber and counter on February 11 and 16 compared with that of February 9.

TABLE 5—Comparison of cosmic-ray intensities during a Forbush decrease

Flight No.	Date (UT)	Time at ceiling (UT)	Ion chamber rate (10 mb c/sec)	Counter rate (10 mb c/sec unnormalized)	Relative integrated value-ion chamber	Deep River neutron rates (c/2 hr)
25	Feb. 9	0344	18.4×10^{-3}	33.4	5.37	3498
26	Feb. 11	0620 1924	14.5×10^{-3}	=32	4.57	3310
K	Feb. 16	1633	15.6×10^{-3}	33.8	4.92	3447

measured particle flux at high altitude is sensitive to primary energy. The ratio decreases with increasing energy. The lower ratio on February 10 and February 16, compared with that of February 8, is consistent with an increase of the average primary energy during this period. This fact is also consistent with the three-times-larger effect observed at high altitude compared with the effect at sea level. This implies that a large part of the decrease occurs in the lower-energy end of the spectrum. The greater effect observed at high latitude compared with that at the equator in the neutron monitors discussed above is also in agreement with this character of the change. The daily average neutron rate at Deep River, Canada, for the period February 8 to 16 is shown in Figure 9. The ion chamber 10-mb values and the 2-hour average neutron values covering the time at which the balloon reached ceiling are also shown. The ground-level neutrons show a more complete recovery and considerably smaller change during the decrease than are shown by the high-altitude values.

Summary and discussion—The magnetic record of this storm shows a very strong sudden commencement followed by several sharp increases in H . The second of these, approximately 500 γ in amplitude, was accompanied by large earth currents which were maximum at longitudes of Eastern United States and were small in the Pacific. It does not seem possible to find an emf loop in a vertical plane to account for these currents by an electromagnetic induction process, and either the current circuit is in the horizontal plane or the currents are not the result of an induced emf.

Two very large magnetic bays in H are correlated with strong cosmic noise absorption, x-ray bursts recorded at balloon altitude, and visually observed intense auroral luminosity moving rapidly past the zenith and covering very large part of the United States. The magnetic bays and cosmic noise absorption seem too strong to be caused by the observed x-rays and must be accounted for by direct ionization of the D and E layers by the auroral electrons. The visually observed luminosity apparently did not extend down to these heights, and one is left with a contradiction which at present is not resolved.

The major world-wide decrease in cosmic rays accompanying the storm occurred several hours after the sudden commencement, but there is evidence for a small effect accompanying the sudden commencement. The decrease was observed to be from 4 to 6 per cent at sea level, 21 per cent in the balloon altitude ionization, and 15 per cent in total energy influx at 5

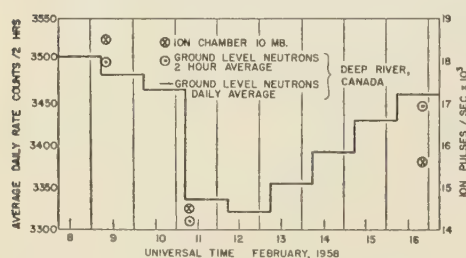


FIG. 9—Comparison of cosmic-ray ground-level neutron monitor at Deep River, Canada, with the balloon ionization chamber. The two-hour average of the ground-level neutrons during the period of the balloon flight is plotted. The high altitude effect seems to recover more slowly than the sea-level neutron effect.

geomagnetic latitude. The low energy part of the primary spectrum was depressed most. No clear, detailed correlation is evident between the occurrence of the major cosmic-ray decrease and any other observable geomagnetic phenomenon.

All the above phenomena together are consistent with the passage of the earth into a remarkably intense solar cloud. This cloud may have originated in the solar flare of 2108 UT February 9, with position coordinates S13 W14, and ending 2302 UT February 9. According to the magnetic records, the terrestrial disturbances began at 0127 February 11 and 24 hours later had decreased to a low level. One may assume that by that time the earth was clear of the cloud, which then continued to move out into the solar system. If the cloud originated within the 2-hour interval of the flare and required 24 hours to pass the earth, considerable velocity dispersion must have been present in the solar gas. The velocity limits must have been about 700 and 1400 km/sec and the radial extent of the cloud when passing the earth about 0.5 astronomical units. The minimum lateral extent near the earth, estimated from the flare angular position with respect to the sun-earth line, is about 0.25 astronomical units. The velocity dispersion requires that the slower solar particles would predominate later in the storm. Compared with these dimensions, the leading edge of the cloud must have been exceedingly well defined and of the order of an earth radius, in view of the sharpness of the first phase phenomena discussed earlier. The cloud, furthermore, must have contained considerable internal structure, as revealed by the 'spikes' in the first phase and the two large 'spikes' accompanying the x-ray bursts later in the storms. These structural features must have persisted in the sun-earth passage despite the large velocity dispersion. However, the process of tracing these features back to a specific series of events in the flare (as revealed by the radio noise bursts, for example) seems impossible. One must conclude that either the flare emitted considerable matter in very discrete velocity groups, or a non-linear propagation effect intensified certain portions of the stream, in particular the leading edge and several internal regions.

This storm was unique for the great intensity of the ionospheric phenomena, and it is reasonable to attribute this to an exceptionally high density of the solar gas enveloping the earth. In contrast, the modulation of galactic cosmic rays, while appreciable, was in no way exceptional when compared with other Forbush-type decreases. If the cosmic-ray decrease is to be attributed to magnetic fields in the cloud, the effectiveness of these fields in producing the Forbush decrease does not seem to be related to the amount of ionized matter in which the fields are contained.

Acknowledgments—The authors gratefully acknowledge the cooperation of many individuals who sent private information or preprints and contributed discussion. The sources of the information have been cited in the references.

We also acknowledge with admiration the expert handling of the balloon, which was launched by W. Huch and R. Maas on the evening of February 10 in extremely high winds and sub-zero cold.

REFERENCES

CHAPMAN, S., AND J. BARTELS, *Geomagnetism*, Oxford-Clarendon Press, p. 859, 1940.
CHAPMAN, S., AND C. G. LITTLE, The Nondeviative absorption of high-frequency radio waves in auroral latitudes, *J. Atmospheric and Terrest. Phys.*, 10, 20-31 (see p. 29), 1957.
FORBUSH, S. E., World-wide cosmic-ray variations, 1937-1952, *J. Geophys. Research*, 59, 525-542, 1954.
HILL, E. L., Second Wentworth Conference on Atmospheric Electricity, May 1958, Pergamon Press (to be published).
IGY DATA CENTER A FOR COSMIC RAYS—Neutron Monitor Data furnished from the following stations and investigators:
Makere College, Kampala, Uganda—Dr. D. M. Thomson; Hermanus, Union of South Africa—Mr. A. M. van Wijk; Mawson, Antarctica—Dr. N. R. Parsons; Leeds, United Kingdom—Dr. P. L. Marsden; Göttingen, German Fed. Republic—Prof. Dr. Heisenberg; Weissenau, German Fed. Republic—Prof. A. Ehmert; Hobart (Mt. Wellington), Australia—Dr. N. R. Parsons; Huancayo, Peru—Dr. J. A. Simpson; Ottawa, Canada—Dr. D. C. Rose; Deep River, Canada—Dr. Hugh Carmichael/Dr. J. F. Steljes; Resolute Bay, Canada, Churchill, and Sulphur Mountain, Canada—also Dr. D. C. Rose; Chicago, Illinois, and Climax, Colorado, U.S.A.—Dr. J. A. Simpson; Mount Washington, N. H., U.S.A.—Dr. J. A. Lockwood.

NEY, E. P., AND J. R. WINCKLER, High altitude cosmic ray measurements during the IGY, *Geophys. Monograph 2*, Am. Geophys. Union, 81-91, 1958.

PALMEIRA, R. A. R., AND R. W. WILLIAMS, Rapid decrease of cosmic-ray intensity, *Nuovo cimento*, 8, 352-355, 1958.

PETERSON, L., R. HOWARD, AND J. R. WINCKLER, Balloon gear monitors cosmic rays, *Electronics*, 31, 76-79, 1958.

SOLAR REPORT—Obtained from *Summary of Solar-geophysical data*, pt. B, CRPL F163 and CRPL F164, March and April 1958, Natl. Bur. Standards, Boulder, Colo.

SOLAR REPORT—Obtained from *Spectral classification of solar radio activity*, Harvard Univ. Radio Astron. Sta., Ft. Davis, Texas, A. Maxwell and Mrs. A. Williams, ARDC Contract AF19 (604)-1394, Jan.-Mar., 1958.

WARWICK, J. W., Absorption of cosmic radio noise during the great aurora of February 11, 1958, High Alt. Observatory, Univ. of Colorado, (available in preprint form, July 1958).

WINCKLER, J. R., L. PETERSON, R. ARNOLDY, AND R. HOFFMAN, X-rays from visible aurorae at Minneapolis, *Phys. Rev.*, 110, 1221-1231, 1958.

(Manuscript received December 8, 1958.)

On the Excitation Rates and Intensities of OH in the Airglow*

JOSEPH W. CHAMBERLAIN AND CLAYTON A. SMITH

*Yerkes Observatory
University of Chicago
Williams Bay, Wisconsin*

Abstract—Published photometric observations of several OH bands are analyzed with the aid of available transition probabilities. The rate of excitation of the vibrational levels with $v \leq 9$ by the excitation mechanism seems to be nearly independent of v . The relative populations of the vibrational levels are computed, and the predicted absolute intensities of all the OH bands are given.

In his original analysis of the OH bands in the airglow, Meinel [1950] suggested that the intensity distribution of the bands might be explained by primary excitation (from a photochemical reaction) into $v = 9$ only, with lower vibrational levels being populated entirely by cascading from above. The idea seemed consistent at the time with the ozone-hydrogen reaction Bates and Nicolet, 1950; Herzberg, 1951, which has just enough energy to excite $v = 9$, but not higher levels. In the absence of a detailed theory for the distribution of the energy produced in a chemical reaction, it is impossible to predict how the various levels will be excited. But the idea that resonance would be important, that is, that a chemical reaction would proceed with a high rate coefficient because nearly all the excess chemical energy could be picked up by a particular molecular level, has been largely discredited by Oldenberg [1952]. There seems to be no valid reason to expect highly preferential excitation to the ninth or any other level.

With the existing data one can obtain an empirical estimate of the rates of population of the OH levels and thence the intensities of bands still unobserved. Observations in the middle latitudes of spectrophotometric intensities for a number of OH bands in the near infrared have been published recently by various authors.

Fedorova announced, at the meetings of the International Astronomical Union in Moscow, August 1958, intensities for 7 different bands at Burokan. These intensities are between 5 and 8 times larger than those previously published by Fedorova [1958]. Dufay [1958] has measured relative intensities for a number of bands; we have normalized these by adopting Fedorova's value of 2.7 kR for the 7-3 band. This is close to the 2.5 kR reported by Onaka and Nakamura [1957]. In addition to these measurements, which we adopted for our computations, Harrison and Vallance Jones [1957] have measured 175 kR for 4-2. This is about twice the value expected from the lower-latitude data. Also the total intensity for the three bands, 9-5, 4-1, and 5-2, obtained by Roach and others [1950] is in fair accord with our adopted intensities. Night-to-night fluctuations are known to be important, so these data may be somewhat inhomogeneous.

In addition, approximate relative values of the transition probabilities $A_{v'v''}$ have been computed. We have adopted the calculations, based on a Morse potential and with the electrical anharmonicity neglected, of Heaps and Herzberg [1952]. These relative values are quite similar to those computed in the same fashion by Shklovskii [1950]. Heaps and Herzberg's calculations with a quadratic term included in the dipole-moment expansion do not cover a sufficient number of bands to be useful. It is likely that this refinement as well as the use of a less restrictive potential function will prove important, especially for the larger values of v . So far, the number of

* The research reported in this paper was supported in part by the Geophysics Research Directorate of the Air Force Cambridge Research Center, Air Research and Development Command, under Contract AF 19(604)-3044.

measurements of the relative intensities of bands in a progression with $v' = \text{constant}$ has been insufficient for one to evaluate with confidence the accuracy of the relative $A_{v''v''}$'s.

Let \mathfrak{N}_v be the population of the v th vibrational level along an entire vertical column 1 cm² in cross section and q_v the net rate of population excluding radiative cascading from higher levels (that is, the rate of excitation less the rate of collisional deactivation) of the v th level along the same column. Then the populations are governed by equations of statistical equilibrium, in which the total rate of population of a level is set equal to the rate of emission from that level

$$\begin{aligned} q_v + \sum_{v''=v+1}^9 \mathfrak{N}_{v''} A_{v''v} \\ = \mathfrak{N}_v \sum_{v'''=0}^{v-1} A_{v'''v}, \quad v = 1, 2, \dots, 9 \end{aligned} \quad (1)$$

If $g_{v''v''}$ is the photon intensity referred to the zenith, then $4\pi g_{v''v''} = \mathfrak{N}_{v''} A_{v''v''}$. [Here we shall express $4\pi g$ in rayleighs (R) where 1 R is the equivalent of 10^6 photons (or transitions) per cm² (column) sec.] A knowledge of the absolute transition probabilities is not necessary to derive values of q_v , although absolute values are required if \mathfrak{N}_v itself is to be computed. The OH abundance in the ground vibrational level may be sufficiently high [Bates and Nicolet, 1950] so that reabsorption of emitted radiation in the $v'' = 0$ progression is appreciable. However, being without definite knowledge of the absolute transition probabilities and abundance, we have not considered the radiative-transfer problem that would be pertinent. For higher levels, reabsorption is almost certainly negligible.

Population rates—Equation (1) may be solved for q_v (first for $v = 9$, then $v = 8$, and so on for all levels down to $v = 3$) since the adopted data yield the relative populations \mathfrak{N}_v for all these levels. We find $q_v \approx 1.2 \times 10^{11}$ molecules/cm² (column) sec nearly independent of v . Actual values determined for q_v varied from this average value by 40 per cent at most. If we assume that the same q_v holds also for $v = 0, 1$, and 2 as well, the total rate of OH formation is about 1.2×10^{12} molecules/cm² (column) sec.

Relative populations—Adopting $q_v = 1.2 \times 10^{11}$ for each level and putting the transition probabilities on an absolute scale of $A_{1-0} = 10^2$

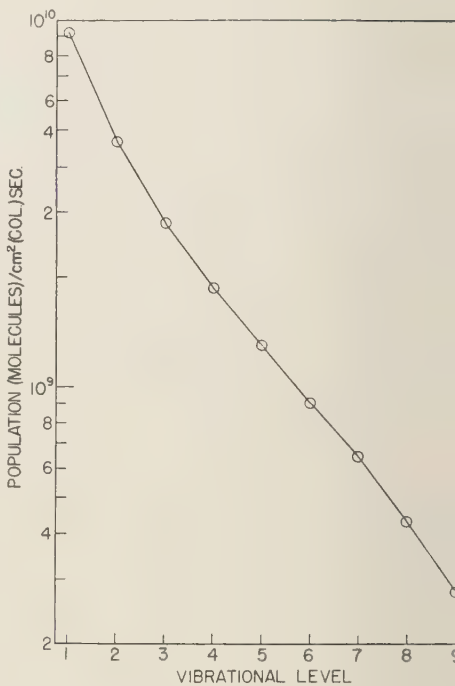


FIG. 1—Total populations \mathfrak{N}_v . The relative populations depend on relative values of the transition probabilities. The absolute populations quoted assume, with Heaps and Herzberg [1952], that $A_{1-0} = 10^2 \text{ sec}^{-1}$, which may be considerably in error

sec^{-1} , we may recompute the populations, \mathfrak{N}_v . The results are shown in Figure 1. To a first approximation the relative populations between $v = 4$ and 9 may be represented by $\mathfrak{N}_v = \text{const.} \exp[-hc G(v)/k T_{\text{vib}}]$ where G is the vibrational energy [Chamberlain and Roesler, 1955] and $T_{\text{vib}} = 10,000^\circ\text{K}$. Between $v = 1$ and 2, $T_{\text{vib}} = 7,200^\circ\text{K}$. Needless to add, the vibrational temperature is merely a convenient parameter; it is not to be construed as a measure of the atmospheric temperature.

Emission rate—Again with $q_v = 1.2 \times 10^{11}$ for each level we may compute $4\pi g_{v''v''}$ for all bands from equation (1). The results are shown in Table 1 and Figure 2, expressed both in rayleighs and in energy units, and do not include any correction for absorption by the lower atmosphere. The total rate of emission from OH

TABLE I—Meinel Bands of OH

$v' - v''$	Band origins		Predicted emission		Observed emission		
	λ_{air} (Å)	v_{vao} (cm $^{-1}$)	(erg/cm 2 (column) sec)		(rayleighs)	(rayleighs)	
			(rayleighs)	Misc.		Dufay	Fedorova
9-0	3,816.6	26,193.9	1.2×10^{-7}	0.023			
8-0	4,172.9	23,957.5	5.7×10^{-7}	0.12			
9-1	4,418.8	22,624.3	3.3×10^{-6}	0.73			
7-0	4,640.6	21,543.2	3.0×10^{-6}	0.71			
8-1	4,903.5	20,387.9	1.5×10^{-5}	3.8			
9-2	5,201.4	19,220.3	4.2×10^{-5}	11.0			
6-0	5,273.3	18,958.2	1.6×10^{-5}	4.4			
7-1	5,562.2	17,973.6	7.7×10^{-5}	22			
8-2	5,886.3	16,983.9	1.9×10^{-4}	57			
5-0	6,168.6	16,206.7	1.4×10^{-4}	33			
9-3	6,256.0	15,980.1	3.4×10^{-4}	110			
6-1	6,496.5	15,388.6	4.0×10^{-4}	130			
7-2	6,861.7	14,569.6	9.0×10^{-4}	310			
8-3	7,274.5	13,743.7	1.4×10^{-3}	520		1,000	
4-0	7,521.5	13,291.5	7.4×10^{-4}	280		850	
9-4	7,748.3	12,902.4	1.8×10^{-3}	710			
5-1	7,911.0	12,637.1	2.3×10^{-3}	930		1,700	
6-2	8,341.7	11,984.6	4.3×10^{-3}	1,800		2,150	1,700
7-3	8,824.1	11,329.4	6.2×10^{-3}	2,800	2,500*	2,700	2,700
8-4	9,373.0	10,666.0	7.2×10^{-3}	3,400		2,800	3,200
3-0	9,788.0	10,213.8	6.3×10^{-3}	3,100			1,500
9-5	10,010.1	9,987.2	7.0×10^{-3}	3,600	†	3,400	3,600
4-1	10,273.3	9,721.9	0.014	7,600	†		8,000
5-2	10,827.7	9,233.1	0.022	12,000	†		12,000
6-3	11,432.8	8,744.4	0.026	15,000			
7-4	12,115.4	8,251.7	0.027	17,000			
8-5	12,898.4	7,750.8	0.024	16,000			
9-6	13,816.7	7,235.7	0.019	13,000			
2-0	14,335.9	6,973.6	0.062	46,000			
3-1	15,046.6	6,644.2	0.096	74,000			
4-2	15,823.7	6,317.9	0.11	88,000	175,000†		
5-3	16,681.9	5,992.9	0.10	90,000			
6-4	17,642.2	5,666.7	0.091	82,000			
7-5	18,733.8	5,336.5	0.074	71,000			
8-6	19,997.3	4,999.3	0.052	54,000			
9-7	21,496.3	4,650.7	0.034	37,000			
1-0	28,006.7	3,569.6	0.64	920,000			
2-1	29,369.2	3,404.0	0.54	820,000			
3-2	30,853.9	3,240.2	0.40	640,000			
4-3	32,482.9	3,077.7	0.29	490,000			
5-4	34,293.6	2,915.2	0.20	360,000			
6-5	36,333.9	2,751.5	0.14	260,000			
7-6	38,674.2	2,585.0	0.089	180,000			
8-7	41,408.6	2,414.3	0.052	110,000			
9-8	44,702.5	2,236.4	0.028	65,000			

* Onaka and Nakamura [1957]

† Roach and others [1950] find 33,000 R for these three bands together.

‡ Harrison and Vallance Jones [1957] at high latitude.

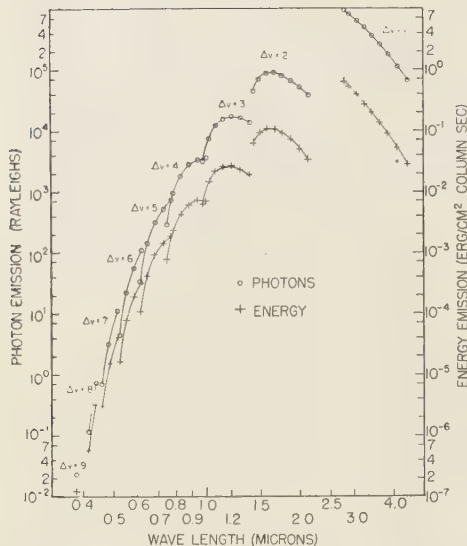


FIG. 2—Predicted photon emission rates in Rayleighs and energy emission rates in erg/cm^2 (column) sec for the OH Meinel bands. Predictions are based on Heaps and Herzberg's [1952] transition probabilities and observed intensities of several bands as explained in the text. Within each sequence ($\Delta v = \text{constant}$) the band with $v' = 9$ is on the right; decreasing v' and v'' run to the left

is estimated to be about 4500 kR. Thus on the average nearly 4 quanta are emitted for every OH molecule formed. The high quantum yield is due to the fact that $A_{v''}$ is much higher for $\Delta v = 1$ than for other transitions. The total radiant energy liberated through the Meinel bands is about $3.2 \text{ erg}/\text{cm}^2$ (column) sec. These values may be compared with $250 \text{ R} = 10^{-3} \text{ erg}/\text{cm}^2$ (column) sec for the green [OI] airglow line, $\lambda 5577$, and $30 \text{ kR} = 0.07 \text{ erg}/\text{cm}^2$ (column) sec for the Atmospheric O₂ system (mostly

reabsorbed in the lower atmosphere in the A band at 7619 Å).

We wish to emphasize the tentative nature of these conclusions and the importance of having more accurate transition probabilities as well as further photometric data.

REFERENCES

- BATES, D. R., AND M. NICOLET, The photochemistry of atmospheric water vapor, *J. Geophys. Research*, **55**, 301–327, 1950.
- CHAMBERLAIN, J. W., AND F. L. ROESLER, The OI bands in the infrared airglow, *Astrophys. J.*, **12**, 541–547, 1955.
- DUFAY, M., Sur les intensités bandes d'émission du ciel nocturne dans le proche infrarouge, *Compt. rend.*, **246**, 2281–2283, 1958.
- FEDOROV, N. I., Hydroxyl emission from observations at Burokan (Armenia), *Ann. géophys.*, **1**, 365–366, 1958.
- HARRISON, A. W., AND A. VALLANCE JONES, Measurements of the absolute intensity of the auroral and night airglow in the 0.9–2.0 μ region, *J. Atmospheric and Terrest. Phys.*, **11**, 192–199, 1955.
- HEAPS, H. S., AND G. HERZBERG, Intensity distribution in the rotation-vibration spectrum of the OH molecule, *Z. Physik*, **133**, 48–64, 1952.
- HERZBERG, G., The atmospheres of the planet *J. Roy. Astron. Soc. Can.*, **45**, 100–123, 1951.
- MEINEL, A. B., OH emission bands in the spectrum of the night sky, *Astrophys. J.*, **111**, 551–564, 1950; **112**, 120–130, 1950.
- OLDENBERG, O., Resonance in collision processes, *Phys. Rev.*, **87**, 786–789, 1952.
- ONAKA, R., AND M. NAKAMURA, Photoelectric studies of near infrared OH emissions of night sky, II. Measurement of absolute intensity as brightness standard, *Sci. of Light Tokyo*, **6**, 910, 1957.
- ROACH, F. E., H. B. PETTIT, AND D. R. WILLIAMSON, The height of the atmospheric OH emission, *J. Geophys. Research*, **55**, 183–190, 1950.
- SHKLOVSKII, I. S., Quantitative analysis of the intensity of the hydroxyl emission of the night sky (translated title), *Doklady Akad. Nauk SSSR*, **75**, 789–792, 1950.

(Manuscript received February 20, 1959.)

A Preliminary Model Atmosphere Based on Rocket and Satellite Data

H. KORF KALLMANN

The RAND Corporation, Santa Monica, California

Abstract—The scientific results obtained from rocket and satellite observations have been studied in order to determine the physical properties of the atmosphere at high altitudes. A preliminary model atmosphere is presented for the region between 100 and 800 km. The paper contains numerical tables of density, pressure, and scale height as functions of altitude.

Due to solar effects these physical parameters may vary from day to night and from latitude to latitude. However, preliminary studies have indicated that average densities and pressures might vary by at most a factor of two, the variations being larger at high than at medium latitudes. Densities presented by Russian scientists, which were also obtained from rocket and satellite data, agree with the model density presented here reasonably well. The densities derived by American and Russian scientists from satellite observations agree within less than a factor of two. The densities derived from rocket data are lower than the ones derived from satellite data for the same altitude. The maximum difference between the densities derived by Michnevich [1958] from rocket data and the average densities presented here occur around 150 km, where the values differ by a factor of 3.8; above and below these altitudes the differences are much less. It is estimated that these differences then are within the limits of the variations to be expected and also within the limits of the uncertainties of the experimental data available at present.

INTRODUCTION

During the last year more than 100 research rockets probed the atmosphere for scientific information. During that same period seven artificial satellites and three satellite carriers circled the earth at various times and at various locations.

Since the density data obtained from satellites are the first experimental results which have been obtained at these great heights, a model based on this information may be justified, even though it is realized that it will be revised and improved when more and better data become available.

The upper air densities which have been obtained from these observations have been collected and will be discussed in the following section. In general, the densities obtained from satellite data are higher than was previously assumed, and are more nearly in agreement with early theoretical findings [Grimminger, 1948] and extrapolated data from observations of meteors at lower altitudes [Whipple, 1951]. The rocket data show large latitude and daytime and nighttime variation above 100 km. At present, however, the satellite densities do not indicate such a prominent latitude effect.

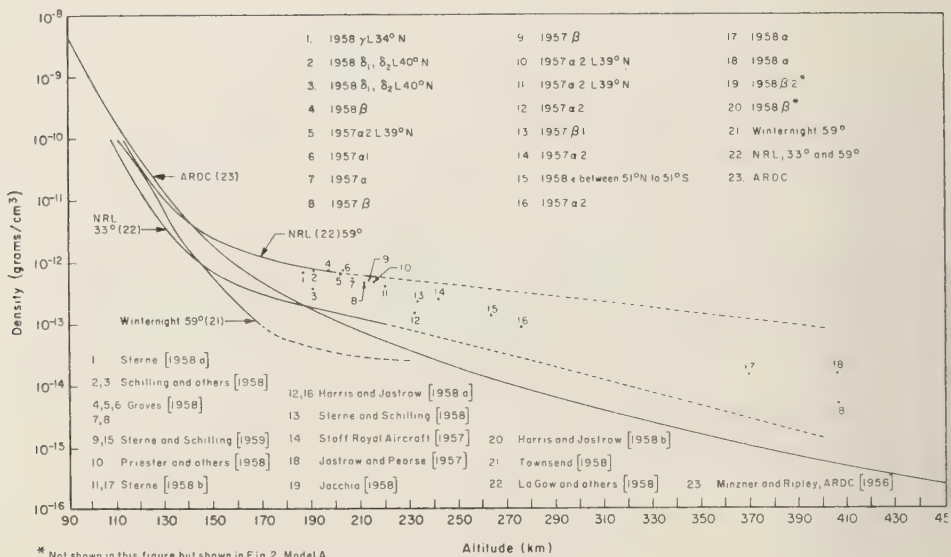
The analysis made by Schilling and Whitney [1958] failed to show a significant latitude effect. Also the diurnal effect, studied by Jacchia [1959], was found to be relatively small.

The method used here in deriving atmospheric properties is based, in principle, on the perfect gas law and the hydrostatic equation, which relate density, pressure, temperature, and molecular weight as functions of altitude. In order to obtain these physical parameters, it has been customary to assume a temperature or scale height gradient. In this investigation the variation of pressure with height was derived from the variation of density with height by numerical integration without assuming a scale height or temperature gradient.

It might be possible that the perfect gas law is not applicable at very high altitudes where the ion or electron density is comparable to or higher than the neutral particle density. However, this altitude probably would not be reached much below 1000 km.

AIR DENSITIES DERIVED FROM ROCKET AND SATELLITE DATA

Figure 1 shows a composite picture of the variation of air densities with altitude between



* Not shown in this figure but shown in Fig. 2, Model A

FIG. 1—Experimental results from rocket and satellite data

100 and 500 km as deduced from rocket and satellite data. The *Rocket Panel* [1952], *Townsend* [1958], *Horowitz* and *LaGow* [1957], and *LaGow* and others [1958] have obtained densities by means of rockets at various latitudes, seasons, and times of day. The summarized results and their extrapolation are also shown in Figure 1. The ARDC model atmosphere [*Minzner* and *Ripley*, 1956] is shown for comparison. The spread in experimental values in the region between 100 and 200 km is very great indeed. The densities at northern latitudes (59°N) are higher during the day than at temperate latitudes (33°N) by a factor of about 4.8 at 200 km. However, due to the possible experimental error involved in the measurements, the densities at these different altitudes may vary by as little as a factor of 2.5 or as much as a factor of 9.7 [*LaGow* and others, 1958]. The greatest difference in densities at one place, deduced from rocket observations, occurs at Fort Churchill (59°N) between summer days and winter nights. The results differ by more than a factor of 10 at 200 km. The satellite data do not show this large latitude effect. In fact, densities observed at various locations for approximately the same altitude at medium latitudes differ by less than a factor of 1.5. In discussing

the possible errors involved in densities derived from satellite observations, *Schilling* and *Stern* [1959] point out that the uncertainties in the mass area ratio are still numerically larger than any density variation with latitude or season. *Jacchia* [1959] found that the density between day and night varies at most by 25 per cent.

Because of these differences in the experimental results, some of the factors which enter into the evaluation of the satellite and rocket data will be discussed briefly. This also will give an indication of the possible errors involved in arriving at the results.

Sterne [1958c, 1958d] has described a method of determining densities from orbital elements. The accuracy of a density determination depends upon the accuracy with which the perigee altitude can be determined from the orbital elements, upon the effective mass to area ratio of the satellite, and upon the drag coefficient which itself is a function of the air density. *Jastrow* and *Pearse* [1957] have discussed the problem of atmospheric drag on the satellite.

I am indebted to Dr. S. A. Schaaf (private communication, 1958) for his estimates of the drag coefficient. Assuming continuous flow, the coefficient is probably less than 1 (0.9) in the region between 80 and 100 km; it increases

out 2.3 and may reach a maximum value of about 2.5 in the region where nitrogen dissociates. For deriving the density from orbit data, usually a drag coefficient of 2 or 2.3 is assumed. Thus the maximum error in density due to the uncertainty in this parameter is about 20 per cent. The drag due to charged particles might become comparable to the neutral drag at altitudes where the neutral particle density is comparable to the ion or electron density. These altitudes are probably higher than the ones considered here. Therefore, the charge drag will not affect the densities derived from neutral drag coefficients which are presented in Figure 1 and which are used in this paper for the proposed variation of density with altitude.

The maximum error due to the uncertainty in the mass-area ratio varies from satellite to satellite. The estimates made vary by a factor from 2 to 4. For Satellites 1958-1 and 1958-2 (Sputnik III), Schilling and others [1958] calculated the error to be not more than a factor of 2. For Satellite 1958e (Explorer IV), Schilling and Whitney [1958] show that uncertainties in the orientation at perigee are covered by a factor of only 1.48. Harris and Jasnow [1958b] estimated the projected area of 1958a (Explorer I) to be uncertain by a factor of 2, but they point out that the maximum and

minimum projected areas may vary by a factor of 20 due to the cylindrical shape of the satellite (203 cm long, 7.3 cm radius). Densities deduced from 1957a-2 (Sputnik I) are probably rather accurate because of the spherical shape of the satellite.

The densities derived from rocket data have been obtained from the stagnation pressure, measured at the nose cone, and from the velocity of the vehicle. Ionization-type pressure gauges have been used above 100 km. Around 200 km the experimental error involved varies from 20 to 35 per cent on the average [LaGow and others, 1958]. Townsend and Meadows [1958], who have discussed the possible errors in the evaluation of the mass spectrometer rocket data, however, estimate the maximum error to be a factor of 2 or 3 at 200 km. The same authors also point out that the error due to dynamic effects is very difficult to estimate.

At higher altitudes more weight is given to the densities derived from satellite observations.

ADOPTED DISTRIBUTION OF AIR DENSITY WITH ALTITUDE

An attempt was made to combine the air densities obtained from rockets with those obtained from satellite data. Because of the spread in data and the uncertainties involved in the

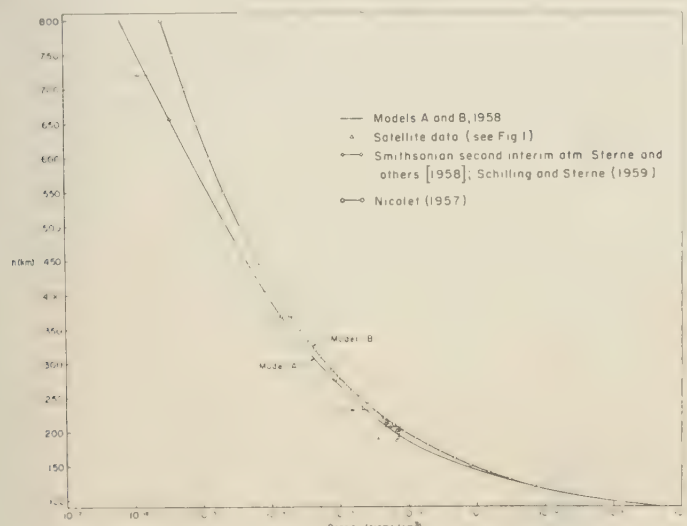


FIG. 2—Variation of density with altitude for Models A and B

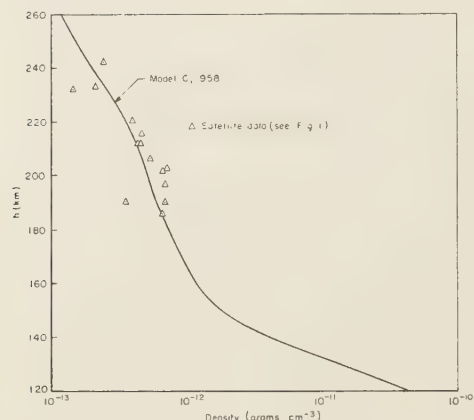


FIG. 3—Variation of density with altitude for Model C

experimental results, various density curves have been studied. They are shown in Figures 2 and 3 and are labeled Models A, B, and C.

Model A presents a smooth density curve in the region between 90 and 800 km. In the lower regions, around 120 km, the densities are essentially the same as in the model proposed by Kallmann and others [1956] and the ARDC model atmosphere [Minzner and Ripley, 1956]. Above that altitude, up to 200 km, the densities are slightly higher than the more recent results obtained for latitude 59°N by LaGow and others [1958]. Above 200 km the curve presents a smooth fit of the satellite data.

Model B was constructed from the Smithsonian interim atmosphere Model 2, derived by Sterne and others [1958b] and from theoretical estimates. Below about 400 km the curve is

identical with the density curve labeled (2a) by Schilling and Sterne [1959] in their recent study of densities inferred from satellite observations. Theoretical studies made by Nicolet and Mang [1952], in the region between 500 and 1000 km, are comparable to those made by Bates [1954] and are lower than the satellite data indicate. More recently Nicolet [1957] has re-evaluated the problem on the basis of the heat conduction theory and has arrived at higher densities for these altitudes. His computed values [1957] have been used above 500 km. The densities are somewhat higher than the ones obtained from satellite observations. However, they are probably within the limit of the uncertainties involved in the experimental data and also within the limit of the fluctuations to be expected from solar influences.

In Model C, shown in Figure 3, the density presented by Minzner in the ARDC model atmosphere was adopted, up to 150 km, as representative for medium latitudes. This curve was based entirely on rocket data. Above that altitude the satellite data have been used.

It will be seen from Figure 3 that a close combination of rocket and satellite data lead to a density curve which changes its slope in the region of the ionosphere. If physical reasons can be found to explain why the change in density with altitude in the ionosphere should deviate from the simple exponential form, the a change in the slope, as indicated by present observations, might not be impossible. It is interesting to note that in the stratosphere and thermosphere the density curve shows such changing slopes, which correspond to temperature inversions at around 50 km and 90 km.

TABLE 1—Comparison of atmospheric densities derived from various sources

Height h (km)	Air densities (gm cm^{-3})				
	USSR rocket τ	USSR satellite	Model A	Model B	Model C
100	4×10^{-10}		6.9×10^{-10}	6.9×10^{-10}	5.0×10^{-10}
150	1.7×10^{-12}		6.1×10^{-12}	8.1×10^{-12}	1.7×10^{-12}
200	2.7×10^{-13}		5.9×10^{-13}	8.5×10^{-13}	5.0×10^{-13}
220	1.6×10^{-13}		3.2×10^{-13}	4.5×10^{-13}	3.8×10^{-13}
228	1.3×10^{-13}	$(2.4-3.2) \times 10^{-13}$	2.7×10^{-13}	3.5×10^{-13}	3.0×10^{-13}
260	6.9×10^{-14}	1×10^{-13}	1.2×10^{-13}	1.5×10^{-13}	1.2×10^{-13}
355		8.8×10^{-15}	1.8×10^{-14}	2.5×10^{-14}	1.9×10^{-14}
370			1.4×10^{-14}	1.9×10^{-14}	

These temperature inversions are now adequately explained by the chemical reactions and the absorption and emission of energy which take place at these altitudes. Something similar might happen in the ionosphere, a region where absorption, dissociation, and recombination play predominant roles.

Soviet studies of atmospheric densities by rockets and satellites were presented by Michalich (USSR) at the Fifth Meeting of the SAGI (*Comité Spéciale de l'Année Géophysique Internationale*) in Moscow, early in August 1958. The results are given in Table 1 and are compared with the densities shown in Figures 1 and 3.

From the data presented above it will be seen that the densities for Model A agree fairly well with the region between 100 and 350 km with the results obtained by the Russian scientists. The satellite data are consistent to within a factor of two, a difference which might be due to the difference in location and the time of day of observation. Schilling and Whitney [1958] found that the density at 250 km may vary by a factor of two at high latitudes above about 50 degrees. The densities in Model B based on the Smithsonian Institution atmosphere are somewhat higher than the ones presented in Model A. If the effective mass-to-area ratio for Vanguard I and for Explorers I and III could be assumed smaller, as they might very well be, the air densities between about 200 km and 400 km would be smaller.

The atmospheric properties presented in Table 2 are based on the density curve, labeled

TABLE 2—Average density, pressure, and scale height derived from rocket and satellite data—(Continued)

Height <i>h</i> (km)	Density <i>p</i> (gm/cm ³)	Pressure <i>p</i> (dynes/cm ²)	Scale height <i>H</i> (km)	Acceleration of gravity <i>g</i> (cm/sec ²)
200	5.906×10^{-13}	2.059×10^{-3}	37.8	921.8
210	4.314×10^{-13}	1.594×10^{-3}	40.2	919.8
220	3.220×10^{-13}	1.215×10^{-3}	42.4	916.2
230	2.447×10^{-13}	9.939×10^{-4}	44.5	913.4
240	1.886×10^{-13}	7.977×10^{-4}	46.4	910.6
250	1.472×10^{-13}	6.459×10^{-4}	48.3	907.9
260	1.160×10^{-13}	5.273×10^{-4}	50.2	905.1
270	9.218×10^{-14}	4.338×10^{-4}	52.1	902.4
280	7.383×10^{-14}	3.593×10^{-4}	54.1	899.7
290	5.957×10^{-14}	2.996×10^{-4}	56.1	897.0
300	4.841×10^{-14}	2.515×10^{-4}	58.1	894.3
310	3.963×10^{-14}	2.123×10^{-4}	60.1	891.6
320	3.266×10^{-14}	1.802×10^{-4}	62.1	888.9
330	2.710×10^{-14}	1.538×10^{-4}	64.0	886.3
340	2.263×10^{-14}	1.319×10^{-4}	66.0	883.6
350	1.902×10^{-14}	1.136×10^{-4}	67.8	881.0
360	1.609×10^{-14}	9.816×10^{-5}	69.4	878.4
370	1.370×10^{-14}	8.513×10^{-5}	71.0	875.8
380	1.173×10^{-14}	7.404×10^{-5}	72.3	873.2
390	1.012×10^{-14}	6.454×10^{-5}	73.3	870.6
400	8.745×10^{-15}	5.635×10^{-5}	74.2	868.0
410	7.562×10^{-15}	4.930×10^{-5}	75.3	865.4
420	6.553×10^{-15}	4.321×10^{-5}	76.4	862.9
430	5.696×10^{-15}	3.795×10^{-5}	77.4	860.3
440	4.970×10^{-15}	3.337×10^{-5}	78.3	857.8
450	4.352×10^{-15}	2.939×10^{-5}	79.0	855.3
460	3.823×10^{-15}	2.590×10^{-5}	79.5	852.8
470	3.364×10^{-15}	2.285×10^{-5}	79.9	850.3
480	2.961×10^{-15}	2.016×10^{-5}	80.3	847.8
490	2.601×10^{-15}	1.781×10^{-5}	81.0	845.3
500	2.281×10^{-15}	1.576×10^{-5}	81.9	842.9
510	2.003×10^{-15}	1.396×10^{-5}	82.9	840.4
520	1.761×10^{-15}	1.238×10^{-5}	83.9	838.0
530	1.550×10^{-15}	1.100×10^{-5}	84.9	835.5
540	1.367×10^{-15}	9.780×10^{-6}	85.9	833.1
550	1.207×10^{-15}	8.711×10^{-6}	86.9	830.7
560	1.068×10^{-15}	7.769×10^{-6}	87.8	828.3
570	9.471×10^{-16}	6.937×10^{-6}	88.7	825.9
580	8.418×10^{-16}	6.200×10^{-6}	89.4	823.5
590	7.500×10^{-16}	5.547×10^{-6}	90.0	821.2
600	6.683×10^{-16}	4.966×10^{-6}	90.8	818.8
610	6.045×10^{-16}	4.450×10^{-6}	91.7	816.5
620	5.284×10^{-16}	3.993×10^{-6}	92.8	814.1
630	4.696×10^{-16}	3.587×10^{-6}	94.1	811.8
640	4.174×10^{-16}	3.228×10^{-6}	95.6	809.5
650	3.710×10^{-16}	2.910×10^{-6}	97.2	807.2
660	3.297×10^{-16}	2.628×10^{-6}	99.0	804.9
670	2.929×10^{-16}	2.378×10^{-6}	101	802.6
680	2.599×10^{-16}	2.157×10^{-6}	104	800.3
690	2.301×10^{-16}	1.961×10^{-6}	107	798.0
700	2.039×10^{-16}	1.789×10^{-6}	110	795.8
710	1.811×10^{-16}	1.636×10^{-6}	114	793.5
720	1.613×10^{-16}	1.500×10^{-6}	118	791.3
730	1.439×10^{-16}	1.380×10^{-6}	122	789.0
740	1.286×10^{-16}	1.273×10^{-6}	126	786.8
750	1.150×10^{-16}	1.177×10^{-6}	130	784.6
760	1.029×10^{-16}	1.092×10^{-6}	136	782.4
770	9.214×10^{-17}	1.016×10^{-6}	141	780.2
780	8.253×10^{-17}	9.477×10^{-7}	148	778.0
790	7.396×10^{-17}	8.869×10^{-7}	154	775.8
800	6.632×10^{-17}	8.327×10^{-7}	162	773.7

TABLE 2—Average density, pressure, and scale height derived from rocket and satellite data

height <i>h</i> (km)	Density <i>p</i> (gm/cm ³)	Pressure <i>p</i> (dynes/cm ²)	Scale height <i>H</i> (km)	Acceleration of gravity <i>g</i> (cm/sec ²)
90	3.994×10^{-9}	2.262×10^6	5.9	953.5
100	6.933×10^{-10}	5.339×10^{-1}	8.1	950.5
110	1.818×10^{-10}	1.811×10^{-1}	10.5	947.6
120	6.339×10^{-11}	7.867×10^{-2}	12.8	944.7
130	2.655×10^{-11}	3.719×10^{-2}	14.9	941.8
140	1.237×10^{-11}	1.984×10^{-2}	17.1	938.9
150	6.108×10^{-12}	1.155×10^{-2}	20.2	936.0
160	3.240×10^{-13}	7.355×10^{-3}	24.3	933.1
170	1.888×10^{-13}	5.041×10^{-3}	28.7	930.2
180	1.208×10^{-13}	3.636×10^{-3}	32.4	927.4
190	8.295×10^{-13}	2.707×10^{-3}	35.3	924.6

Model A, in Figure 2. At present this curve seems to represent the best smooth fit of the experimental data available to this writer.

THE FUNDAMENTAL RELATION BETWEEN PHYSICAL PROPERTIES OF THE UPPER ATMOSPHERE

The variation of pressure p , density ρ , temperature T , and molecular weight M with altitude is determined by the ideal gas law and the hydrostatic equation; thus

$$\rho = \frac{pM}{RT} \quad (1)$$

and

$$dp = -g\rho dh \quad (2)$$

where R is the gas constant (8.314×10^7 erg/ $^{\circ}\text{K}/\text{mole}$) and g is the acceleration of gravity. Substituting (1) into (2) gives

$$\frac{dp}{p} = -\frac{gM}{RT} dh \quad (3)$$

which relates the pressure to the scale height H , defined as follows

$$H = \frac{RT}{Mg} = \frac{p}{\rho g} \quad (4)$$

This implies that if the pressure can be obtained from observed densities, the value of T/M or the scale height can be obtained. The numerical results will be discussed later. In order to determine T and M separately more assumptions have to be made.

Below 90 km, where the molecular weight does not change appreciably, the temperature can be determined from pressure and/or density measurements. Above this altitude both T and M vary and they cannot be deduced from density measurements alone. If the height and degree of dissociation of molecular oxygen and nitrogen were known, the true kinetic temperature could be calculated. However, they are not known. The problem becomes still more complicated because of the dynamic effects which take place at high altitudes, effects which also influence the temperature and molecular weight. In order to calculate the pressure from the density as functions of altitude, a variation with altitude of temperature, molecular weight, or scale height is generally assumed. To avoid this, an attempt has been made to integrate (2) numerically.

VARIATION OF ATMOSPHERIC PARAMETERS WITH ALTITUDE

Integration of the differential equation for pressure—The pressure $p(h)$ at altitude h can be obtained from the differential equation (2) by numerical quadrature of the integral in the equation

$$p(h) = P(h_0) - \int_{h_0}^h \rho(h) g(h) dh \quad (5)$$

However, in the cases where $h > h_0$, very small errors either in $p(h_0)$ or in the evaluation of the integral result in very large relative errors in $p(h)$ as h becomes large. Hence it was desirable to integrate (2) in the reverse direction. With an initial pressure value at 800 km, (2) was solved for values of $h < 800$ km by integrating numerically

$$p(h) = P(800) + \int_h^{h_0} \rho(h) g(h) dh \quad (6)$$

The numerical quadrature formula used to approximately evaluate the integral of the right-hand side was that recommended by Kallmann and others [1956]; namely, for two nearby points, h_1 and h_2

$$\int_{h_1}^{h_2} F(h) dh \simeq \frac{F(h_2) - F(h_1)}{\ln F(h_2) - \ln F(h_1)} (h_2 - h_1) \quad (7)$$

where $F(h)$ is nearly an exponential and, in fact, is exact when $F(h)$ is an exponential $e^{\alpha h + \beta}$. In view of the fact that the use of (7) leads to truncation errors in the evaluation of (6), which are of the order of the step size Δh , and because the use of a method such as Simpson's Rule leads to errors in the evaluation of (6) of the order of $(\Delta h)^4$, a comparison of these two methods was made on a pressure evaluation at a step size of $\Delta h = 4$ km. The results were in such agreement that it was felt that at steps of $\Delta h = 1$ km no significant difference would result, and (7) was used at steps of $\Delta h = 1$ for the pressure calculations in this paper.

Numerical results—In order to integrate (6) a pressure value at 800 km must be known. At any altitude, p is a function of T/M and ρ . Knowing ρ , one has to estimate the kinetic temperature and the molecular weight at 800 km to determine p at 800 km.

Theoretical studies by Chapman [1957] have shown that the temperature in the upper region of the atmosphere might increase steadily and might be 2000°K at 520 km and 7920°K at 1000 km. Nicolet [1958] has calculated possible temperatures ranging from 1000°K to 3000°K above 500 km. He finds a temperature of not less than 2250°K necessary to account for a calculated density of 4×10^{-15} gm/cm², assuming no dissociation of nitrogen. Thus, the kinetic temperature at 800 km must be less than 5000°K and higher than 2000°K.

From Byram and others' [1955] analysis of their rocket data, one may assume that molecular oxygen is dissociated well below 800 km; probably it is already dissociated around 300 km. Thus, the molecular weight at 800 km cannot be greater than 24. Molecular nitrogen may or may not be completely dissociated at 800 km; however, one might assume that it is partially dissociated. If, on the other hand, nitrogen is completely dissociated, the molecular weight of air decreases to 14.7.

On the basis of these arguments, the pressure was calculated at 800 km for $T/M = 100, 150, 200$. The corresponding pressures are 5.4×10^{-7} , 1.1×10^{-7} , and 1.1×10^{-6} dynes/cm². For $T/M = 150$, the true kinetic temperature is 600°K if no nitrogen is dissociated and 2200°K if nitrogen is completely dissociated.

Figure 4 shows the variation of pressure with altitude for Models A and B, assuming $T/M = 50$ at 800 km. Calculations made for $T/M = 100$ and 200 give very similar pressure values; in fact, below about 600 km the pressures are the same. This is due to the fact that the pressure at 800 km is very small and the integration of (6) is carried out in the direction of increasing pressures. Figure 5 shows the variation of scale eight with altitude.

DISCUSSION OF THE RESULTS AND CONCLUSIONS

The proposed model and the method used to construct it might provide the best estimates which can be made at present. However, the preceding discussions have indicated the difficulties and uncertainties involved in deriving a model atmosphere from the data available now.

Model A is based entirely on rocket and satel-

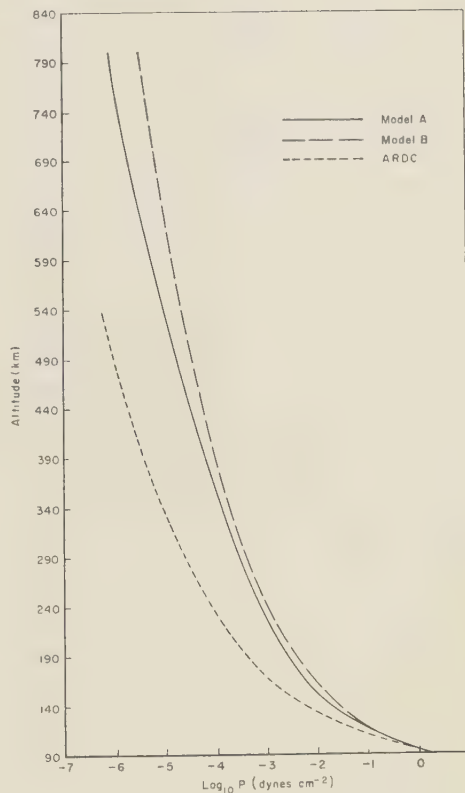


FIG. 4—Variation of pressure with altitude for Models A and B

lite data, whereas Model B, above 500 km, is based on theoretical considerations. At high altitudes, between 500 and 800 km, only two experimental results are available. Furthermore, the observational data are uncertain by at least a factor of two; also, the density may vary, because of the position of the sun and its activity, by more than a factor of two. Thus, Model B, which shows higher densities and pressures, might well be possible. Below 500 km the two models differ by less than a factor of 1.5. In Table 3 a comparison of density, pressure, and true kinetic temperature for Models A and B is shown. The temperature is based on the assumption that oxygen is completely dissociated.

It must be pointed out that the pressure and kinetic temperature values given for Model B

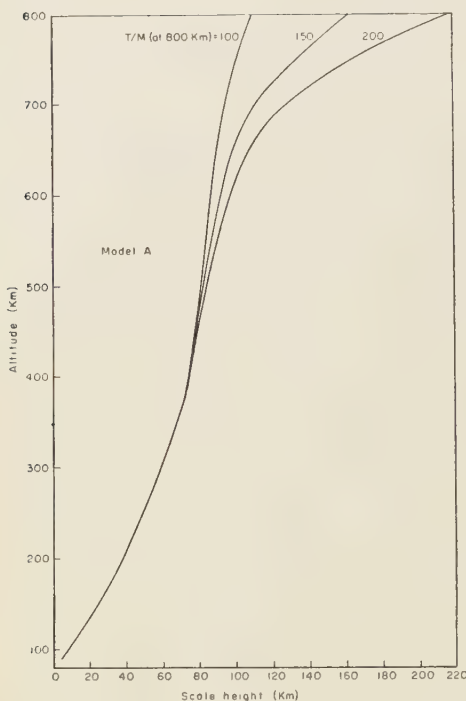


FIG. 5—Variation of scale height with altitude for Model A

have been calculated by the author by the method outlined in this paper. Using an independent approach, Nicolet [1958] estimates the temperature at 500 km to be 2225°K.

The method described above was used to avoid assuming a variation of temperature or scale height with altitude throughout the region of investigation. However, an assumption had to be made at the datum level, $h = 800$ km. This assumption affects the pressure values less than the T/M values. The maximum uncertainty in pressure is a factor of 2 at 800 km. Below about 700 km the pressures depend on the density curve and are not influenced by the assumption made at 800 km. Therefore, it is concluded that the pressures at lower altitudes correspond fairly accurately to the densities at these altitudes.

The uncertainties in the ratio of T/M at high altitudes can be rather large, since this ratio is determined from the ratio of p to ρ ;

these latter quantities differ by many powers of 10 and also vary by several powers of 10 over the range of altitude considered here. A study of the data shows that the T/M or scale height values are independent of the assumed pressure at 800 km below an altitude of about 600 km. On the other hand, it is interesting to note that T/M increases steadily with altitude and does not approach a constant value, as has been assumed previously. This is a finding which could have been obtained only by the integration method and not by assuming an

TABLE 3—Comparison of Models A and B

h (km)	ρ (gm/cm ³)	p (dynes/cm ²)	Temperature (°K)
Model A			
800	6.632×10^{-17}	8.327×10^{-7}	3624
500	2.281×10^{-15}	1.576×10^{-5}	1993
300	4.841×10^{-14}	2.515×10^{-4}	1499
100	6.933×10^{-10}	5.339×10^{-1}	222
Model B			
800	2.683×10^{-16}	3.241×10^{-6}	
500	3.598×10^{-15}	3.177×10^{-5}	2548
300	6.312×10^{-14}	3.510×10^{-4}	1605
100	6.942×10^{-10}	5.438×10^{-1}	226

^aBased on $M = 24$

priori temperature gradient. The increase in temperature is in agreement with Chapman [1957] theory and predictions of an increasing temperature up to great altitudes.

Accepting the densities derived from rocket and satellite data, we conclude that the 'upper atmosphere working tables' are fairly accurate and consistent up to an altitude of 500 to 600 km. Above that height the uncertainties in the values increase with altitude.

Acknowledgments—It is a pleasure to acknowledge the help and assistance received from a great number of colleagues. I want to thank G. E. Schilling, Smithsonian Institution and Harvard University, for the many fruitful discussions on the subject, especially with regard to the satellite data. I am indebted to H. E. LaGow, Naval Research Laboratory, for his advice on the rocket data. The work of calculating atmospheric properties was performed by W. L. Sibley, RAN.

'corporation, and his computer staff. Patricia Walers' technical aid was also greatly appreciated.

REFERENCES

BATES, D. R., *Rocket exploration of the upper atmosphere*, Pergamon Press, London, 1954.

BYRAM, E. T., T. A. CHUBB, AND H. FRIEDMAN, Dissociation of oxygen in the upper atmosphere, *Phys. Rev.*, **98**, 1594-1597, 1955.

CHAPMAN, S., Speculations on the atomic hydrogen and the thermal economy of upper ionosphere, *Threshold of space*, Pergamon Press, London, 65-72, 1957.

GRIMMINGER, G., Analysis of temperature, pressure, and density of the atmosphere to extreme altitudes, *RAND Corp., Rept. R-105*, (ASTIA Doc. 43648), 149 pp. 1948.

GROVES, G. V., Effect of the earth's equatorial bulge on the life-time of artificial satellites and its use in determining atmospheric scale heights, *Nature*, **181**, 1055, 1958.

HARRIS, I., AND R. JASTROW, Upper atmosphere densities from minitrack observations on Sputnik I, *Science*, **127**, 471-473, 1958a.

HARRIS, I., AND R. JASTROW, An interim atmosphere derived from rocket and satellite data, presented at the Fifth CSAGI Assembly, Moscow, July 1958b.

HOROWITZ, R., AND H. E. LAGOW, Upper air pressure and density measurements from 90 to 220 kilometers with the Viking 7 Rocket, *J. Geophys. Research*, **62**, 57-78, 1957.

JACCHIA, L. G., The secular perturbations and the orbital acceleration of Satellite 1958 Beta Two, *Smithsonian Astrophys. Observatory, Spec. Rept.* **12**, 30-33, 1958.

JACCHIA, L. G., The diurnal effect in the orbital acceleration of Satellite Beta One, *Smithsonian Astrophys. Observatory, Rept. 20*, 5, 1959.

JASTROW, R., AND C. A. PEARSE, Atmospheric drag on the satellite, *J. Geophys. Research*, **62**, 413-423, 1957.

KALLMANN, H. K., W. B. WHITE, AND H. E. NEWELL, Physical properties of the atmosphere from 90 to 300 kilometers, *J. Geophys. Research*, **61**, 513-524, 1956.

LAGOW, H. E., R. HOROWITZ, AND J. AINSWORTH, Rocket measurements of the upper Arctic atmosphere, *World Data Center A, IGY Rocket Rept. Ser. 1*, 26-37, 1958.

MICHNEVICH, V. V., On pressure and density of atmosphere, paper presented during Fifth Réunion of the Comité Spéciale de l'Année Géophysique Internationale held in Moscow, July 30-August 9, 1958. (Reproduced by the National Academy of Sciences, Washington).

MINZNER, R. A., AND W. S. RIPLEY, The ARDC model atmosphere, 1956, Air Force surveys in geophysics, AFCRC TN-56-204, (ASTIA Doc. 110233) Bedford, Mass., 1956.

NICOLET, M., AND P. MANGE, An introduction of the physical constitution and chemical composition of the high atmosphere, *Ionospheric Research, Sci. Rept. 35*, Pennsylvania State Univ., 1952.

NICOLET, M., La thermosphere, presented at a meeting of the IUGG, Toronto, September 1957.

NICOLET, M., High atmosphere densities, *Science*, **127**, 1317-1320, 1958.

PRIESTER, W., H. G. BENNEWITZ, AND P. LENGRUSSER, *Radiobeobachtungen des ersten künstlichen Erdsatelliten*, Westdeutscher Verlag, Köln und Opladen, 38 pp., 1958.

ROCKET PANEL, Pressures, densities, and temperatures in the upper atmosphere, *Phys. Rev.*, **88**, 1027-1032, 1952.

ROYAL AIRCRAFT ESTABLISHMENT, Observations on the orbit of the first Russian earth satellite, *Nature*, **180**, 937-941, 1957.

SCHILLING, G. F., AND C. A. WHITNEY, Atmospheric densities from Explorer IV, *Smithsonian Astrophys. Observatory, Spec. Rept. 18*, 13-22, 1958.

SCHILLING, G. F., C. A. WHITNEY, AND B. M. FOLKART, Preliminary note on the mass-area ratio of Satellites 195881 and 195882, *Smithsonian Astrophys. Observatory, Spec. Rept. 14*, 32-34, 1958.

SCHILLING, G. F., AND T. E. STERNE, Densities and temperatures of the upper atmosphere inferred from satellite observations, *J. Geophys. Research*, **64**, 1-4, 1959.

STERNE, T. E., The density of the upper atmosphere, *Smithsonian Astrophys. Observatory, Spec. Rept. 11*, chap. 3, 1958a.

STERNE, T. E., B. M. FOLKART, AND G. F. SCHILLING, An interim model atmosphere fitted to preliminary densities inferred from USSR satellites, *Smithsonian Contrib. Astrophys.* **2**, 275-280, 1958b.

STERNE, T. E., High-altitude atmospheric density, *Phys. Fluids*, **1**, 165-170, 1958c.

STERNE, T. E., An atmosphere model, and some remarks on the inference of density from the orbit of a close earth satellite, *Annals IGY*, Pergamon Press, London, vol. VI, 133-142, 1958d.

STERNE, T. E., AND G. F. SCHILLING, Some preliminary values of upper atmosphere density from observations of USSR satellites, *Smithsonian Contrib. Astrophys.*, **2**, 207-210, 1958e.

TOWNSEND, J. W., Atmospheric structure above Ft. Churchill, *World Data Center A, IGY Rocket Rept. Ser. 1*, 11-25, 1958.

TOWNSEND, J. W., JR., AND E. B. MEADOWS, Density of the winter night time arctic upper atmosphere 110 to 170 km, *Ann. géophys.*, **14**, 117-130, 1958.

WHIPPLE, F. L., Meteors as probes of the upper atmosphere, *Compendium Meteorol.*, T. F. Malone, ed., Am. Meteorol. Soc., 356-365, 1951.

(Manuscript received January 17, 1959.)

Cosmic-Ray Intensities and Liquid-Water Content in the Atmosphere

H. ARAKAWA

*Meteorological Research Institute
Tokyo, Japan*

Abstract—Cosmic-ray intensity data have been studied in Japan, and it has been found that passages of cold fronts do not produce a pronounced variation in cosmic-ray intensities. Warm fronts produce a gradual but pronounced decrease. Further evidence from the decrease in neutron counts accompanied by little change in ionization chamber records substantiates the conclusion that the variations are due to liquid-water content of the atmosphere. Estimates of as much as 50 to 70 mm of liquid water in the atmosphere are supported by records of tremendous rainfall during the passages of typhoons.

Blackett [1938] has suggested that the "temperature effect" of cosmic rays is due to the vertical shift of the layer in which mesons are formed, and he has further suggested that it may be possible to correlate cosmic-ray data with the structure of depressions. Loughridge and Gast [1939] have pointed out that cosmic-ray data in the United States indicate a marked change in intensity during front passage. The late Dr. Y. Nishina and the present author [1940 a, b, c, d] have pointed out (1) that statistical air-mass effect on the cosmic-ray intensities can also be found under different air-mass conditions; (2) that positive changes of cosmic rays are associated with the passages of air masses of polar origin and negative changes with the passages of air masses of tropical origin (this can be statistically detected in the area of cyclones and anticyclones); and (3) that the cosmic-ray intensity (after reduction to the normal pressure) is generally almost constant, at least within the accuracy of observation, on the passages of individual cold fronts, but it decidedly decreases on the passages of marked warm fronts.

First, the cosmic-ray data obtained at the Institute of Physical and Chemical Research, Tokyo, during the period 1937–1939 with a Steinke apparatus and an IPCR cosmic-ray meter (both inside 10 cm Pb) have been studied. Hourly means of observed cosmic-ray intensities were reduced to the values at a standard pressure 755 mm Hg using a true absorption co-

efficient $\mu = 9.5 \times 10^{-3}/\text{cm Hg}$ for air. On plotting cosmic-ray intensities as ordinate and time as abscissa, we found that the approach and passage of any cold front did not indicate pronounced variation in cosmic-ray intensities within the accuracy of observation as shown by Figure 1; whereas Figure 2 illustrates that the approach and passage of a marked warm front produced a gradual but pronounced decrease in cosmic-ray intensities, possibly due to the increase of the effective thickness of the air column. It must be noted that a heavy thunderstorm with excessive rainfalls (over 100 mm of depth) over the wide district surrounding Tokyo was experienced during the passage of a warm front which occurred at about midnight on September 20–21, 1939. Other warm front

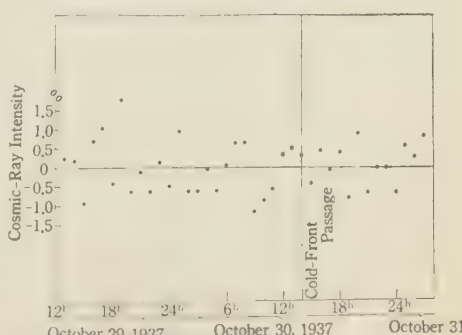


FIG. 1.—Effect on cosmic-ray intensities of the passage of a marked cold front

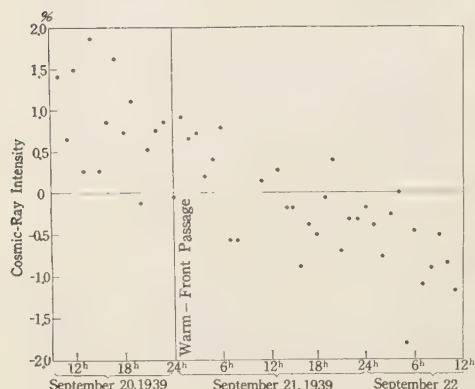


FIG. 2.—Effect on cosmic-ray intensities of the passage of a marked warm front

passages studied gave a similar change (*Nishina* and others, 1940b, Fig. 1). In Japan, a marked warm front is known to consist of warm tropical moist air which overrides a shallow cold wedge of air underlying it. The warm front extends to a height of from 10 to 15 km and is associated with heavy rainfall from the overcast sky. (Throughout the present study, the Japanese Standard Time or 135th meridian civil time is used.)

Similarly, cosmic-ray intensities in different quadrants of typhoons were studied. The conclusions stated below are based on the examination of a number of similar examples which are not reproduced here.

A tropical disturbance of typhoon intensity appeared on September 11, 1939, in the southern sea far away from Japan proper. The center crossed the sea to the southeast of Tokyo on September 23. Later, on October 2, 1939, a second typhoon crossed the sea to the southeast of Tokyo, following a path quite similar to that of the former one. The observations showed that the cosmic-ray intensities were fairly constant during these periods.

In the south quadrant of a typhoon fresh tropical air advances rapidly to the north under the influence of the typhoon. On September 11, 1937, a typhoon crossed the Sea of Japan moving northeastwards (Fig. 3). The cosmic-ray observations on that day (Fig. 4) showed that the intensity decreased beyond



FIG. 3.—Path of typhoon across Sea of Japan September 11, 1937

doubt during the passage of the typhoon. However, the intensities at the stage of full violence of the typhoon were uncertain (owing to the vibration of the building itself under severe southerly gales). Amount of rainfall was about 40 mm. We have considered that the cosmic

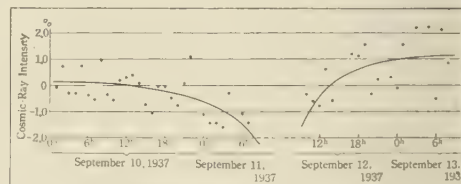


FIG. 4.—Cosmic-ray observations, September 11, 1937

ray variations in the typhoon area as shown in Figure 4 can be safely attributed to the so-called temperature effects.

During the International Geophysical Year, two cosmic-ray meters, a Standard Neutron Monitor N-3 (Simpson's neutron pile) and a Nishina Ionization Chamber (10 cm Pb shielded), were established on Mount Norikura (36.1°N , 137.5°E , 2840 m above msl). The variation of cosmic-ray intensities during the passages of three typhoons in 1957, whose tracks are illustrated in Figure 5, will be the subject of another paper.

Bihourly values of cosmic-ray intensities measured by the Nishina Ionization Chamber at Itabashi, Tokyo, as well as at Mount Norikura (after reduction to the normal pressure), were constant within the accuracy of observa-



FIG. 5.—Tracks of three typhoons; full lines represent observed paths, open circles the morning (3:00 a.m.) positions, and dots the critical positions

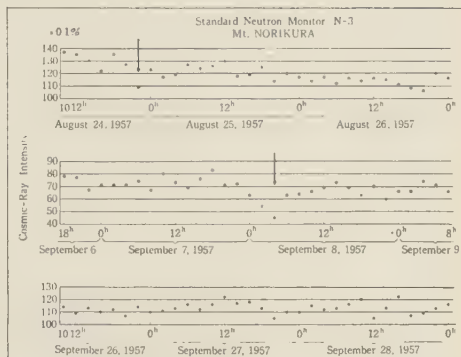


FIG. 6.—Bihourly values of cosmic-ray intensities measured by Standard Neutron Monitor N-3 at Mount Norikura

tions during the passages of these three degenerating typhoons. (In 1957, no typhoon of full intensity hit Japan proper.)

Bihourly values of cosmic-ray intensities on Mount Norikura measured by the Standard Neutron Monitor N-3 (after reduction to the normal pressure) show sharp depressions at the time just after the passages of two typhoons (Fig. 6). It should be noted that the cosmic-ray meter with a Nishina Ionization Chamber measures mainly the high-energy component (meson) of cosmic-ray intensity, and the Standard Neutron Monitor measures intensity of neutrons produced by primary protons.

To test the temperature effect, the author plotted the geopotential (in meters) of levels corresponding to 100-mb, 300-mb, and 500-mb constant pressure surfaces at Tateno Aerological Observatory ($36^{\circ}03'\text{N}$, $140^{\circ}08'\text{E}$). We can see no significant change in these constant pressure altitudes based on twice-a-day aerological observations.

As shown in Figure 6, cosmic-ray intensities measured by the Standard Neutron Monitor show sharp depressions during the passages of typhoons, whereas cosmic-ray intensities measured by the Nishina Ionization Chambers do not show any significant variation. So these sharp depressions in cosmic-ray intensities might be caused by the presence of abundant liquid-water content in the typhoon area. Note that precipitable-water content contributes to the surface barometric pressure, but the liquid-

water content does not contribute to the pressure as a primary factor. Therefore, we could not exclude the effect of the presence of the liquid-water content by taking the barometric effect only. As for the liquid-water content in the typhoon area, no reliable observations have been made, but torrential rainfall in the typhoon area suggests the existence of enormous amounts of liquid water.

As indirect proofs, two alternatives are proposed. First, precipitable-water contents during the passages of these three typhoons over the Tateno Aerological Observatory are calculated and illustrated in Figure 7. As much as some 60

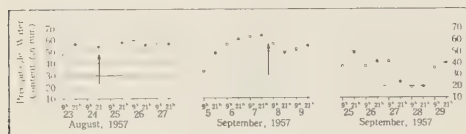


FIG. 7—Precipitable-water contents during passages of three typhoons; dots represent nighttime observations and open circles represent daytime observations

to 70 mm of precipitable water existed during the passages of the two typhoons; therefore existence of an immense liquid-water content seems to be a reasonable assumption. Dr. R. R. Braham informed me in private discussions that 50 mm of liquid-water content seems to be a reasonable estimate, based on the data obtained by the National Hurricane Research Project reconnaissance flights in the stormy areas of hurricanes.

Secondly, we have records of the tremendous rainfall during the passages of typhoons over lofty mountains. World records of heavy rainfall have been tabulated by Jennings [1950] and Fletcher [1950], and rainfall observations on the top of Mount Fuji ($35^{\circ}21'N$, $138^{\circ}44'E$, 3776 m above msl) show such heavy rainfall that almost all world records of precipitation come from Japan. It might be noted here that these rainfall values were obtained by means of a special rain gauge installed on the wind tower to give better exposure as shown in Figures 8 and 9. Under stormy conditions, rains at the summit of Mount Fuji move horizontally instead of falling vertically (Table 1). This special



FIG. 8—Photograph illustrating the exposure of the special rain gauge installed on the wind tower of the Mount Fuji weather station

rain gauge [Huzimura, 1948] has been designed to collect both (1) raindrops falling vertically into an ordinary rain gauge (horizontal receiver, marked as A), and (2) tremendous raindrops blowing nearly horizontally under wind of hurricane force (vertical receiver, marked as B), the component (2) being much greater than the component (1). The standard rain gauge

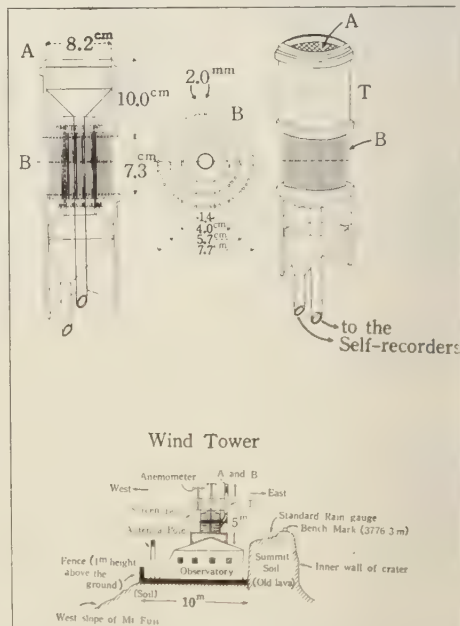


FIG. 9—Special rain gauge for mountain-use at the environment of the station

TABLE 1.—Rainfall at the summit of Mount Fuji (3776 m), obtained during passages of marked atmospheric depressions during the period of the last five years. Courtesy of Mr. I. Huzimura.

Date	Typhoon or front	Rainfall (in mm)		
		Gauge for mountain use		Standard rain gauge (on the green field, as shown in Fig. 9)
		Vertical receiver	Horizontal receiver	
1954		B	A	
Aug. 18-20	Typhoon Grace	4800	889	225
Sept. 25-26	Typhoon Marie	2827	118	158
1955				
July 3-7	Stationary front	1466	120	97
Sept. 26-28	Typhoon Louise	1585	215	178
1956				
Aug. 17-18	Typhoon Babs	1784	1913	78
Sept. 26-27	Typhoon Harriet	1467	512	179
1957				
Sept. 6-8	Extra-tropical cyclone with front	4125	302	261
1958				
July 22-23	Typhoon Susan	2961	263	144
Aug. 25-26	Typhoon Alice	2675	156	72
Sept. 17-18	Typhoon Helen	556	179	75
Sept. 25-27	Typhoon Ida	2050	642	43
1947*				
Sept. 12-15	Typhoon Kathleen	5932	5596	260.3

* Adding, for reference, this 96-hr. record value.

on the green field does not show such high values of rainfall as might be suggested by Figure 9.

Thus the depressions in the neutron component of the cosmic-ray intensities could be largely, if not wholly, due to the existence of abundant liquid-water content in the typhoon area. Conversely, it is possible to measure the total amount of liquid-water content in the atmosphere by constructing large cosmic-ray meters of the Standard Neutron Monitor type to reduce the present inevitable fluctuation of the measured cosmic-ray intensity by the ordinary monitors.

REFERENCES

BLACKETT, P. M. S., On the instability of the barytron and the temperature effect of cosmic rays, *Phys. Rev.*, **54**, 973-974, 1938.
 FLETCHER, R. D., A relation between maximum observed point and areal rainfall values, *Trans. Am. Geophys. Union*, **31**, 344-348, 1950.

HUZIMURA, I., On the relation between rainfall and altitude on Mt. Fuji and in the neighborhood of it, *Geophys. Mag., Tokyo*, **20**, 113-126, 1948.

JENNINGS, A. H., World's greatest observed point rainfalls, *Monthly Weather Rev.*, **78**, 4-5, 1950.

LOUGHridge, D. H., and PAUL GAST, Air mass effect on cosmic-ray intensity, *Phys. Rev.*, **56**, 1169-1170, 1939.

NISHINA, Y., Y. SEKIDO, H. SHIMAMURA, and H. ARAKAWA, Cosmic-ray intensities and air masses, *Phys. Rev.*, **57**, p. 663, 1940a.

NISHINA, Y., Y. SEKIDO, H. SHIMAMURA, and H. ARAKAWA, Air mass effect on cosmic-ray intensity, *Phys. Rev.*, **57**, 1050-1051, 1940b.

NISHINA, Y., Y. SEKIDO, H. SHIMAMURA, and H. ARAKAWA, Cosmic-ray intensities and cyclones, *Nature*, **145**, 703-704, 1940c.

NISHINA, Y., Y. SEKIDO, H. SHIMAMURA, and H. ARAKAWA, Cosmic-ray intensities in relation to cyclones and anticyclones, *Nature*, **146**, p. 95, 1940d.

Recent Seasonal Interactions between North Pacific Waters and the Overlying Atmospheric Circulation

JEROME NAMIAS

*Extended Forecast Section
U. S. Weather Bureau
Washington, D. C.*

Abstract—The recent pronounced anomalous warming of surface waters of the eastern North Pacific is related to prevailing abnormalities in the overlying atmospheric circulation. The gross features of the abnormalities in water temperature patterns during the cold season appear to be caused by abnormal wind components. The data suggest that a preponderant surface drift of water masses from warmer (or colder) sources is induced, and this may be augmented by divergence and upwelling factors. The summer surface-water temperature patterns suggest, in addition to surface advection, the possibility of heating through enhanced insolation combined with light wind.

An attempt is made to ascribe long-period continuity to the atmospheric mean seasonal circulations from summer 1957 through spring 1958 and to hypothesize that this continuity is the result of a certain interplay (involving feedback) between ocean and atmosphere against the slowly changing climatological background.

Introduction—The fact that temperatures of the surface layers of the oceans undergo substantial variations from month to month, season to season, and even year to year has been realized by many generations of oceanographers. A large part of the inter-monthly and inter-seasonal variations are, of course, expressions of normal climatological behavior. But even after removing the long-period normal there are sizeable anomalies of temperature which either persist or change from one month or season to another, so that the same month of different years may exhibit significantly different characteristics. Even in the open ocean differences of several degrees Fahrenheit between the same month of different years are not uncommon.

There seems to be general agreement that these anomalous variations in the ocean's surface layers are somehow associated with variations in the prevailing wind circulations. Moreover, if the normal oceanic thermal structure is related to the normal general atmospheric circulation, then anomalous air circulations must give rise to anomalous conditions in the ocean. However, as the periods considered become longer and longer, the resulting mean atmospheric circulation patterns depart less and less from one another, so that the fundamental

large-scale ocean temperature patterns are not apt to differ appreciably from one period to another. Furthermore, short-period fluctuations in air circulation, say from one day to the next, while producing substantial changes in the surface waters, are apt to be variable or even conflicting, and therefore transitory. Since 'regimes' where certain aberrant forms of atmospheric circulation persistently recur for periods of a month or even a season are well recognized [Namias, 1953], these could provide the sustained systematic abnormal wind distributions required to produce systematic anomalous surface-water transports, divergence, and hence anomalous temperatures. How deep these effects penetrate and how much they interfere with the planetary ocean current systems is at present largely a matter of conjecture. Some recent evidence presented by Schroeder and others [1959] suggests that, at least in the area off Bermuda, variations in temperature and salinity at about 200 meters are remarkably small in the same month of different years, in spite of the fact that relatively large surface variations there are common. While short-period and local responses of water to atmospheric behavior have been demonstrated over and over, it has been difficult to establish the nature of

interactions on a long-term (monthly, seasonal, or annual) basis. Perhaps some of this difficulty stems from the poor quality and quantity of records of sea-surface temperature. Again, the exploitation of meteorological data for longer time intervals has not attracted many meteorologists; and it is painfully clear that the systematic study of long-period atmospheric-oceanic interactions has not been pursued recently with such vigor as by *Helland-Hansen and Nansen* [1920] shortly after the turn of the century.

Currently there appears to be a revival, if not a spurt, of interest in this problem. For example, *Neumann* and his colleagues [1958] have recently published "Studies on the interaction between ocean and atmosphere with application to long-range weather forecasting"; the Fish and Wildlife Service has initiated routine preparation of 10-day mean charts (in the central ten days of each month) of Pacific sea-surface temperature anomalies; and the importance of these anomalies to fish migrations and other things has led to a conference of concerned specialists to explore the recent (1957-1958) climatic warming of the North Pacific [*California Cooperative Oceanic Fisheries Investigation*, 1957].

The author's interest in long-period ocean-atmosphere interactions stems indirectly from work in long-range weather forecasting, where the quest for conservative elements to explain certain observed long-period atmospheric persistence seems to lead either to anomalies in character of land and water surfaces or to things of extra-terrestrial origin, such as long-lasting departures from normal in solar emission. A few possible cases of impact of unusual surface characteristics on the general circulation have been described by the writer [*Namias and Dunn*, 1955; *Namias*, 1958].

In this report certain large-scale water temperature anomalies will be described and associated with time-averaged air pressure distributions and lower tropospheric temperature patterns. The water anomalies and upper-air height patterns suggest a subsequent feedback of the ocean to the overlaying atmospheric circulation. Such studies suggest that the time has arrived for synoptic oceanography to take its place alongside synoptic meteorology.

Recent ocean-surface temperature variations over the eastern North Pacific—Perhaps the most striking characteristic of the 1957-1958 period over the North Pacific was the presence of warmer than normal surface water over the eastern third and especially just along and off the west coast of North America. A fairly representative sample of the type of sea-surface temperature anomaly which has been observed there is shown in the record of monthly mean temperature anomalies for Santa Monica (Fig. 1) taken from a paper by *Stewart* and others

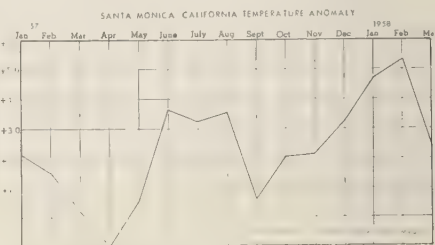


FIG. 1—Monthly mean sea-surface temperature anomaly at Santa Monica, California, January 1957 through March 1958 [from *Stewart* and others, 1958]

[1958]. In this report the authors give data from 10 stations along the west coast of North America from San Diego to Sitka which show anomalies similar to those in Figure 1. On a broader scale we refer to 10-day mean maps for the central 10 days of each month for the eastern Pacific prepared by the Fish and Wildlife Service, from U. S. Weather Bureau ship collections. One of these is reproduced in Figure 2. While the detail of these charts can naturally not be vouched for, the big picture of abnormal warmth off the west coast of North America is indisputable. In his description of the month-to-month series of these anomaly charts *McGary* [1958] stresses the month-to-month persistence of some of the large-scale features and also remarks on the occasional apparent eastward propagation of the anomaly areas.

Although one obtains the impression that the 10-day mean sea temperature anomalies are to some extent related to the contemporaneous monthly mean sea-level pressure anomalies, it

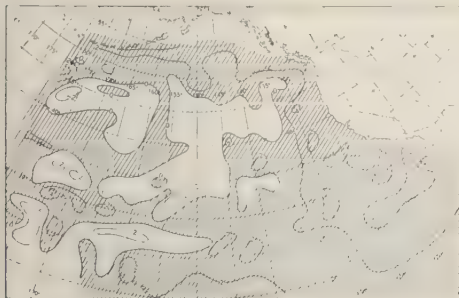


FIG. 2—Mean sea-surface temperature anomaly ($^{\circ}\text{F}$) for February 11-20, 1958. Shaded areas represent above-normal temperatures (copied from charts prepared by U. S. Fish and Wildlife Service [McGary, 1958])



FIG. 5—Mean sea-surface temperature anomaly ($^{\circ}\text{F}$) for winter 1957-58. Shading represents above normal temperatures

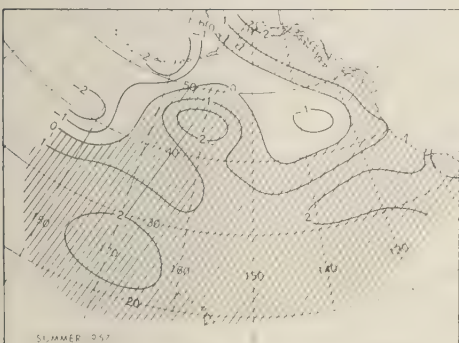


FIG. 3—Mean sea-surface temperature anomaly ($^{\circ}\text{F}$) for summer 1957. Shading represents above normal temperatures

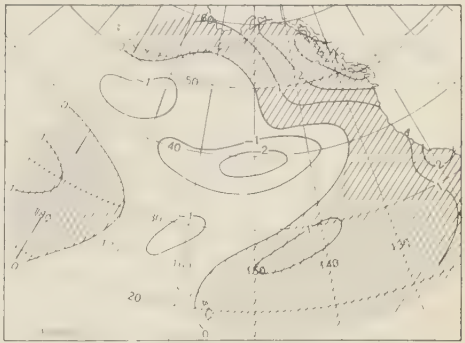


FIG. 6—Mean sea-surface temperature anomaly ($^{\circ}\text{F}$) for spring 1958. Shading represents above normal temperatures



FIG. 4—Mean sea-surface temperature anomaly ($^{\circ}\text{F}$) for fall 1957. Shading represents above normal temperatures

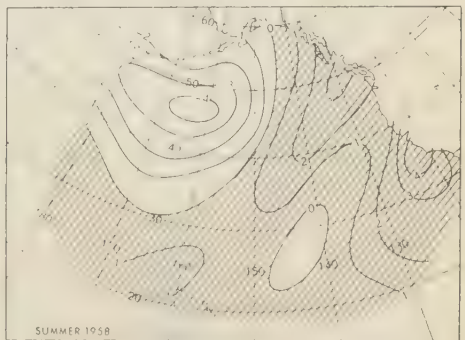


FIG. 7—Mean sea-surface temperature anomaly ($^{\circ}\text{F}$) for summer 1958. Shading represent above normal temperatures

is clear that this time interval of a month may be too short for a recurrent anomalous circulation to impress on the ocean surface a distinct pattern of temperature anomalies. Frequently there is considerable variability in the circulation patterns during one month. Furthermore, the initial state of abnormality of the sea surface must have a decided effect on the subsequent month's pattern. Whereas complications of this sort also arise for longer periods, it seems reasonable to suppose that a more balanced state between water temperature and air circulation patterns would arise after a longer period, especially if the monthly air circulation patterns exhibited some coherence. Partly for these reasons and partly because of ignorance of the response time of oceanic behavior to atmospheric circulation, seasonal means have been used in this study.

For purposes of treating seasonal characteristics the three 10-day means supposed to characterize individual months for a given season have been further averaged by using interpolations made at 5-degree intersections. The resulting charts have been analyzed in a reasonably smooth fashion and are reproduced in Figures 3 to 7. They are in no sense to be considered highly accurate for many reasons: for example, they are means of only 30 (not 90) days of observations; furthermore, this sample is undoubtedly rifled with many types of errors and frequent unrepresentativeness; the normals themselves may be suspect in some areas; the arithmetic mean of months whose individual characteristics vary considerably may in places give misleading pictures. All that may be said for these charts is that they afford a rough idea of the large-scale seasonal sea-surface temperature anomalies over the eastern North Pacific.

Attention is drawn especially to the prevailing warmth in eastern portions off the west coast of North America.

The character of the atmosphere's general circulation in 1957-1958—The most consistent abnormality of the Northern Hemisphere's general circulation during 1957 and early 1958 appears to be the prevalence of low zonal index (low strength of the prevailing westerlies of the temperate latitudes). In fact, from January

1957 through April 1958, the average monthly zonal index was above normal for only two months. Low index conditions are, however, not associated with the same displacements of the centers of action in both summer and winter. In the cold season, pressure distributions accompanying low index generally involve an excess of mass (with respect to normal) over northern latitudes with a somewhat compensatory deficit at lower latitudes. In cases of this kind the subtropical anticyclones are weak and are displaced south of their normal positions.

In the winter and spring seasons of 1958 the westerlies were much farther south than normal, a fact associated with great abnormalities in weather. Detailed reference to these and their relation to the atmospheric circulation may be found in a routinely prepared series of articles in the *Monthly Weather Review* [U. S. Weather Bureau, 1958].

The seasonal characteristics of the general circulation and its regional components are probably best illustrated with the help of mean maps at sea level and aloft. The anomalous nature of these circulations is clearly brought into focus by constructing isopleths of departure from normal; that is, by subtracting from a seasonal mean the long-period normal for the appropriate season and constructing a field of isopleths for the differences. Such charts for the period from summer 1957 through spring 1958 are shown in Figures 8 to 12. The isobars (or contours) on these charts give a measure of the total resultant or prevailing wind, whereas the isopleths of anomaly represent only the anomalous component. Thus an anomalous component from the south may represent an increased southerly prevailing wind or may imply a diminution of the northerly wind which is normally present. These anomalies of atmospheric circulation have been extremely helpful in extended forecasting practice [Namias, 1953], especially in estimating weather and climatic anomalies from circulation patterns. In an analogous fashion it is believed that they may be helpful in relating abnormalities in sea-surface temperature to wind circulation. This suggestion has also been made by Roden and Reid [in press] and formerly by Hanzawa and Inoue [1952].

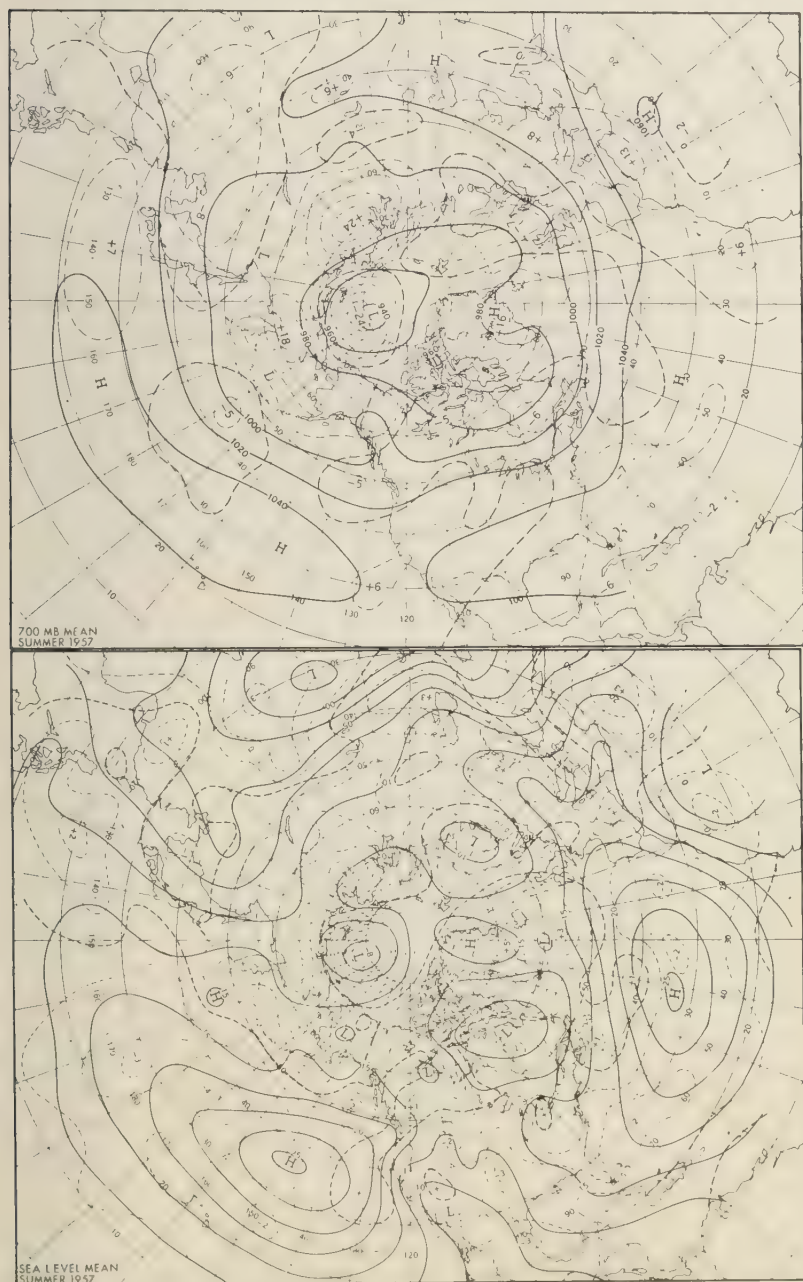


FIG. 8—700 mb (above) and sea-level seasonal means for summer 1957. Broken lines give departures from seasonal normal

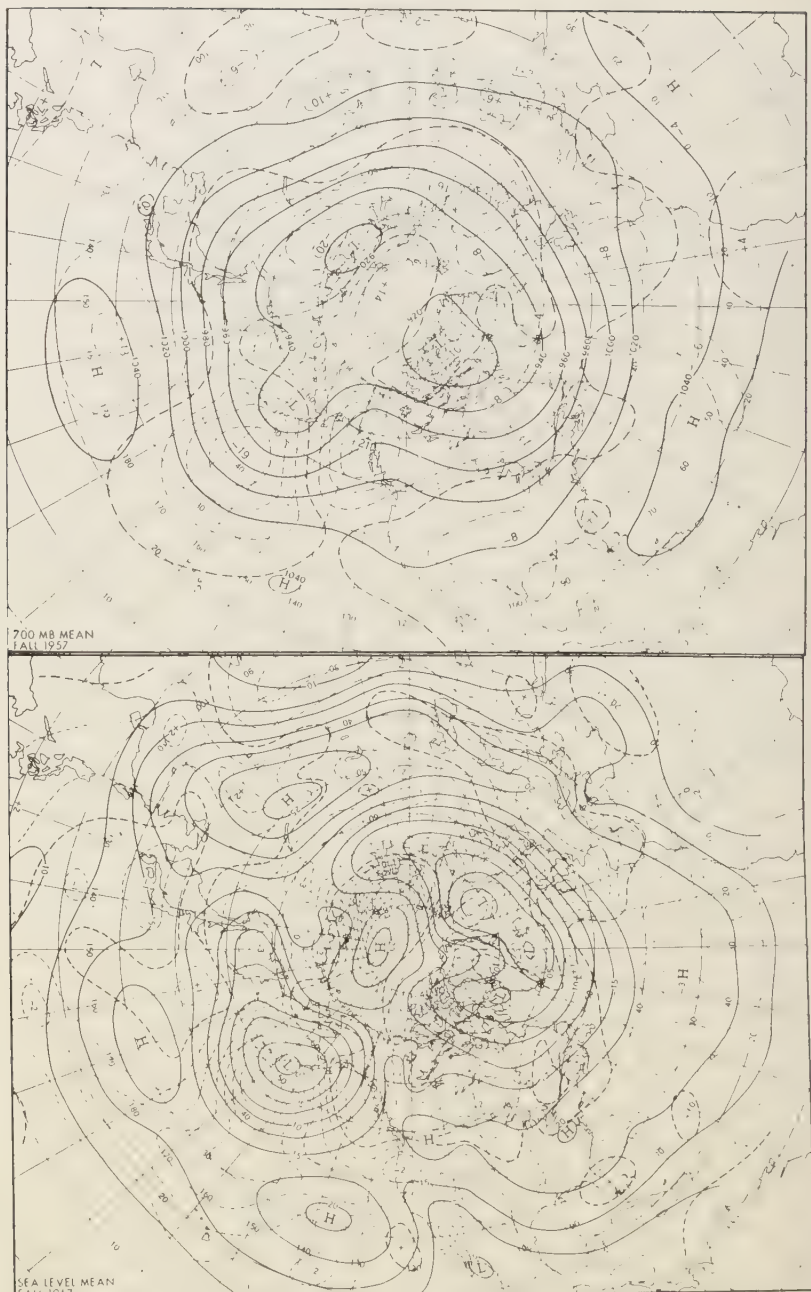


FIG. 9—700 mb (above) and sea-level seasonal means for fall 1957. Broken lines give departures from seasonal normal

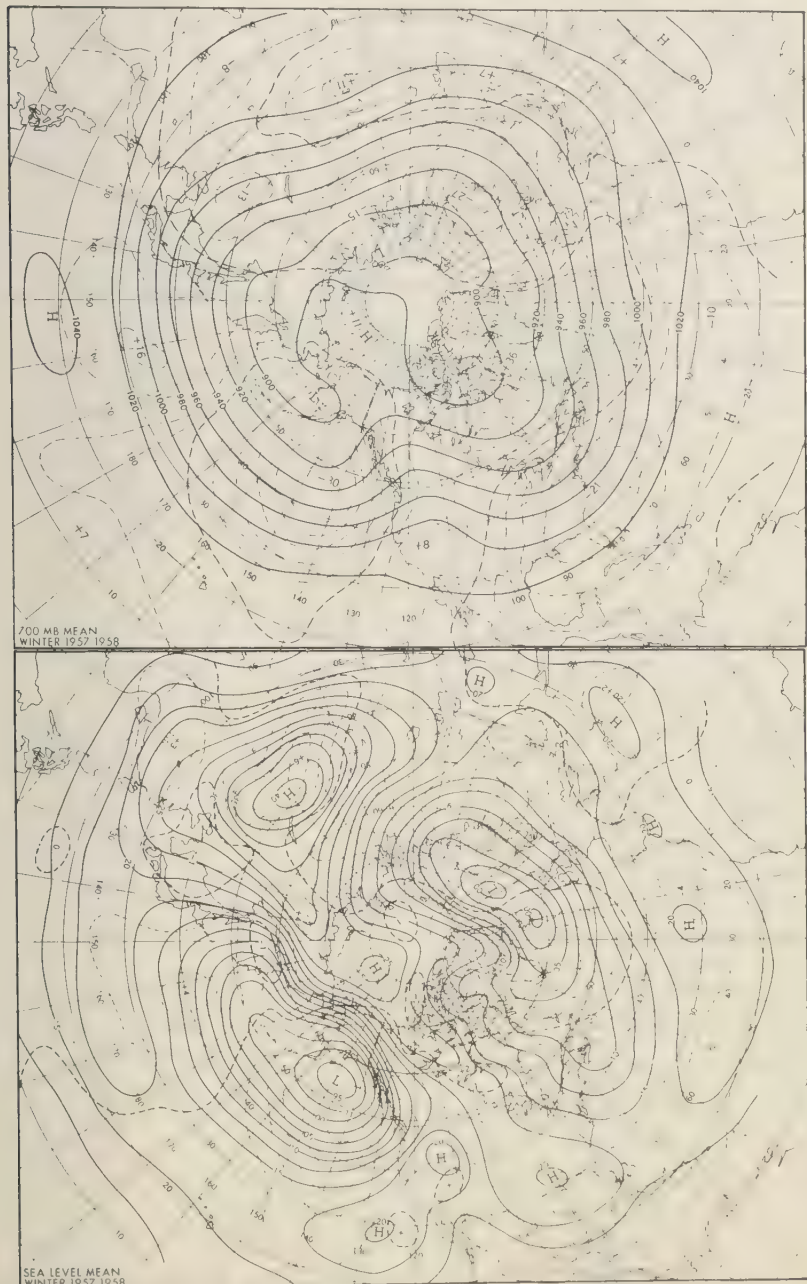


FIG. 10.—700 mb (above) and sea-level seasonal means for winter 1957-58. Broken lines give departures from seasonal normal

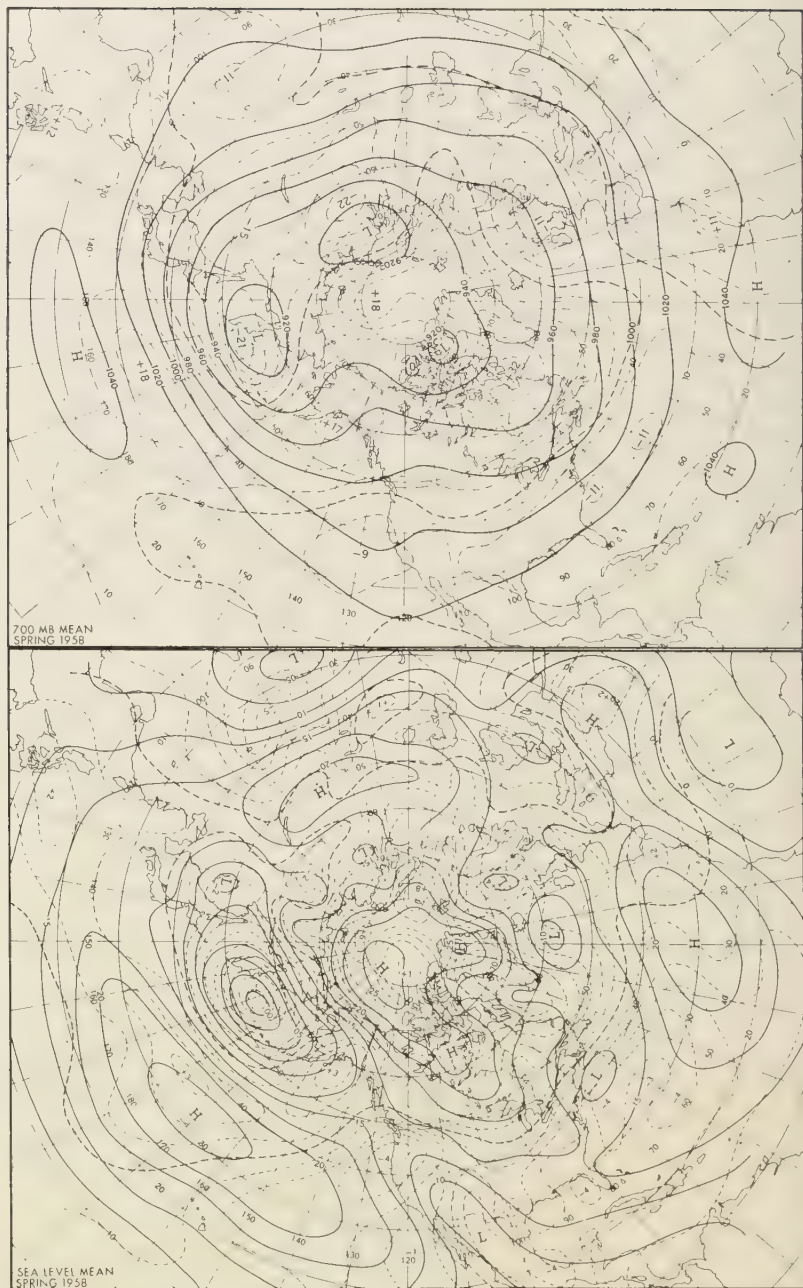


FIG. 11—700 mb (above) and sea-level seasonal means for spring 1958. Broken lines give departures from seasonal normal

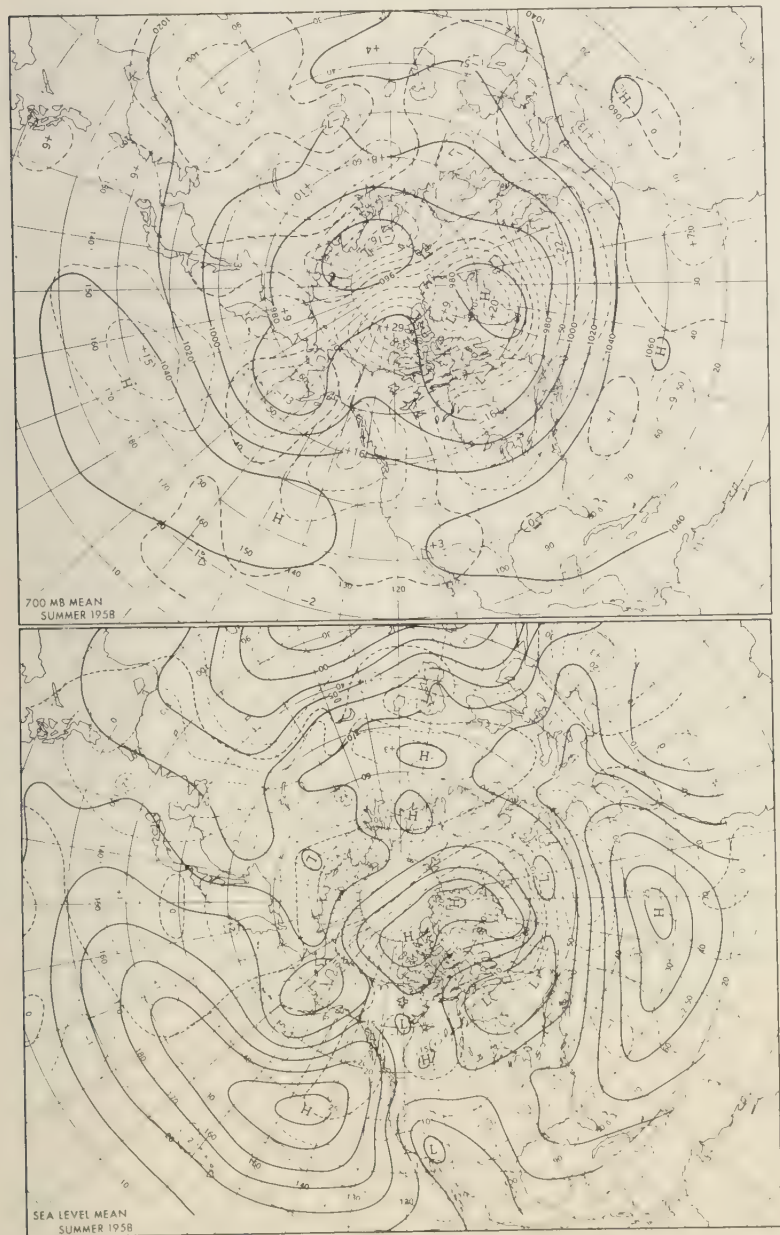


FIG. 12—700 mb (above) and sea-level seasonal means for summer 1958. Broken lines give departures from seasonal normal

With regard to the North Pacific, the most striking aberration involves negative anomalies which have dominated the central and eastern areas of the Pacific over the period extending from summer 1957 through spring 1958. These conditions on the whole were associated with an eastern Pacific anticyclone much weaker than normal at sea level. It is also noteworthy that the Atlantic anticyclone was also predominantly weak. During the winter and spring of 1958 both of these phenomena were associated with westerlies displaced much farther south than normal.

Relationship of large-scale surface water anomalies to the general circulation—Some of the largest surface-water temperature anomalies were observed in the fall and winter of 1958 (Figs. 4 and 5). At first glance the 10-day mean charts (not reproduced) appear to have little or no organization, and indeed close scrutiny reveals a scale of synoptic systems which appear to be smaller than the resolving power permitted by presently obtainable data. We shall not be concerned with these chaotic islands of anomalous warmth or cold but rather with the macro-scale features which embrace large portions of the ocean.

Scanning the gross features of the 10-day means for each month (not reproduced) we observe that during September, October, and November of 1957 the surface water temperature of the entire southern portion of the eastern Pacific (east of 170°W , south of 40°N) was above normal. North of here, the ocean remained characteristically warm over the eastern portions, but marked changes occurred over the west—from anomalously cold to warm from September to October and reverting to a more or less normal, though highly chaotic, situation in November. In December conditions not too dissimilar to those in September arose but were characterized by larger departures. In January a chaos with small departures began before the more organized February state (Fig. 2) when temperatures were relatively cool in central and western portions shown on the chart and warm in the east. The resultant seasonal means (Figs. 4 and 5) for fall and winter show the net warmth in the east and relative coolness in the west, with some suggested eastward displacement of the anomalies.

The seasonal meteorological picture for fall (Fig. 9) shows a deep trough with a -190 foot anomaly aloft over the central Pacific with adjacent ridges and positive anomalies in the western Pacific and Gulf of Alaska. This distribution of isopleths, and the corresponding lines at sea level, means that over much of the area east of 165°W the prevailing and resultant wind had a stronger south-to-north component than normal. West of here the reverse anomalous components are implied. These mean anomalous components are composed of persistently recurrent northward thrusts of air in advance of the trough (east of 165°W) and southward thrusts behind (west of 165°W) as rapidly developing cyclones move into a central Aleutian low. On each occasion when the southerly wind component sets in, surface water, perhaps limited to a shallow depth, is set in motion, and an eastward Ekman surface drift becomes established. However, this surface drift is at about 45° to the right of the wind, a conclusion from Ekman's theory borne out by observations made by Stommel [1954] of drifting buoys in the western Atlantic under varying wind conditions. Therefore, persistently recurrent southerly winds would bring about a net northeastward surface water transport.

It is possible to obtain a more quantitative estimate of sea-surface temperature anomalies which might be produced by the seasonal wind anomalies for these two seasons. In order to do this we employ a procedure used with some success in predicting weekly or monthly mean air temperature anomalies from anomalous wind components. The method is to superimpose the anomalous wind field onto a chart showing isotherms of *normal* temperature (or thickness) and thereby to obtain a measure of the extent to which the normal lines might be displaced. It is assumed that the major element in the displacement is systematic advection from predominantly warmer or colder air mass source regions. In an analogous manner, if advection from prevailingly warmer or colder source regions plays a major role in producing sea-surface temperature anomalies, we might superimpose the anomalies of the sea-level pressure distribution onto the normal sea-surface isotherms appropriate to the season. We could then make use of Ekman's empirical expressio-

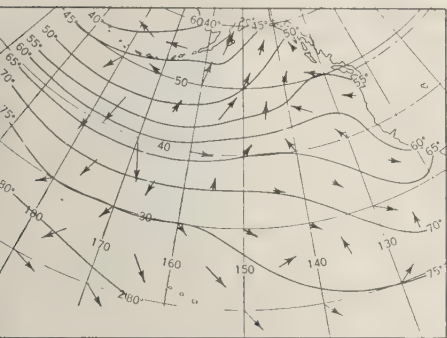


FIG. 13—Anomalous surface-water displacements (arrows) computed from mean seasonal sea-level pressure anomalies for fall 1957 (see text for method). Isotherms show normal sea-surface temperatures for October

or the transport of water due to wind stress to obtain an estimate of the anomalous water transport 45° to the right of the wind

$$\frac{v}{w} = \frac{0.0127}{\sqrt{\sin \phi}}$$

where v is the speed of the surface water current, w is the wind speed, and ϕ the latitude.

This enables us to compute surface-water displacement arrows like those in Figure 13 which, when superimposed on the normal sea-surface isotherms, permit computations of simple advective changes with respect to the normal for

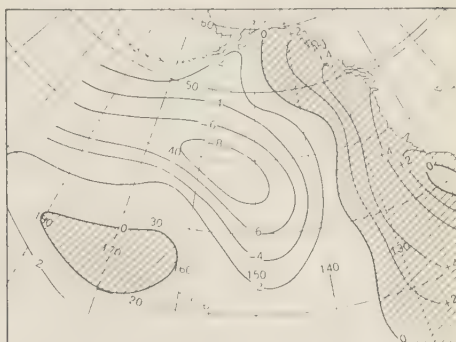


FIG. 15—Computed sea-surface temperature anomalies for winter 1957-1958 using advective method described in text. Shaded areas represent above-normal temperatures

a given season. Such computations of isopleths of anomaly for fall 1957 and winter 1957-1958, based on computations made for 5-degree latitude-longitude intersections, are reproduced in Figures 14 and 15.

When the advectively computed anomalies are compared with the observed seasonal anomalies (Figs. 14 and 15 with 4 and 5), it is quite apparent that there are large discrepancies. In the first place, the magnitudes of the computed anomalies are too large. Secondly, the correspondence in pattern is by no means striking and can be extracted only with effort. Nevertheless, there appears to be some agreement in

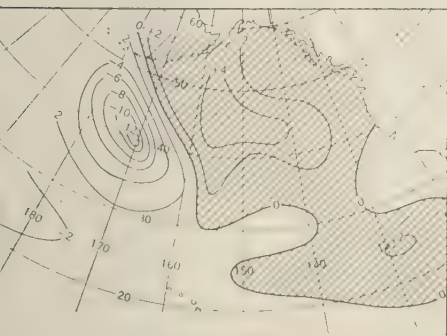


FIG. 14—Computed sea-surface temperature anomalies for fall 1957 using advective method described in text. Shaded areas represent above-normal temperatures



FIG. 16—Computed sea-surface temperature anomalies for summer 1958 using advective method described in text. Shaded areas represent above-normal temperatures

the northwestern and eastern portions in fall, and in winter the most striking correspondence lies in the anomalously warm areas just off the west coast of North America. In other areas the correspondence is not good.

When one considers the many factors opposing such a simple correlation, it is perhaps surprising that any agreement in computed and observed anomalies can be found. We have already cited the inadequacy of the oceanographic data. In addition, the computation is based on the assumption that the abnormal wind stresses apply to an ocean whose initial surface temperatures are everywhere normal, whereas in reality the initial temperature field is abnormal. Thus *abnormal* water may be persistently advected. It is not easy to devise a method of taking this into account without a better knowledge of the large ocean current systems. Again, the computation neglects all non-advective factors, not the least of which are divergence, upwelling, and vertical mixing.

In the open ocean it is difficult to consider these properly. However, one may estimate roughly from the transport arrows (Fig. 13) the divergence or convergence of surface water simply by noting the inflow and outflow indicated over various regions. Thus in fall (Fig. 13) it is suggested that strong surface-water divergence exists over the area from 35°N to 45°N and from 170°W to 160°W . However, it is not easy to decide whether the enhanced upwelling during the fall of 1957 in this area would result in heating or cooling. This involves the nature of the lapse of water temperatures down to the thermocline which in fall is in a transition stage between summer and winter conditions. But during winter, when the upper layer of the free ocean is practically isothermal to considerable depth, it is likely that the excess surface cooling computed at 40°N and 150° to 160°W is partially offset by vertical mixing. This area was so stormy during this winter (Fig. 10) that it is possible that enhanced vertical mixing also prevented the degree of cooling indicated by surface advection alone.

Upwelling is known to play an important role just off the West Coast, especially off California and Baja California where northerly wind components result in upwelling of colder water. This phenomenon, according to Sverdrup [1942], is

most prevalent in the warm season, but it may also play some role in winter. Stewart and others [1958] and the CCOFI report [1957] maintain that increased southerly wind components off the California coast have played a part in raising the water temperature by reducing or inhibiting the upwelling.

Computations of the anomalous transports have also been carried out for the summer of 1958, when pronounced water temperature anomalies were observed (Figs. 7 and 16). There is reasonable general agreement between computed and observed anomalies, with the greatest discrepancy over the central North American coast. Here again effects other than simple surface advection must contribute overwhelmingly. For some reason, the warm water regime established during the preceding several seasons off the west coast of North America persisted.

The above paragraphs imply that the water phenomenon established by the anomalous wind system is essentially a shallow one and that no density changes of consequence occur below. Therefore, no complicating major oceanic current dislocations need be introduced. An alternative explanation is that it is one of mutual adjustment between induced water current (induced by anomalous wind components) and mass, leading to a transport of surface water, convergence to the right of the induced current, and divergence to the left. The resulting upwelling of cooler water from deeper strata to the left would cause cooling there, whereas there would be some increase in temperature to the right if the water originally transported northward is warmer than the displaced original water. Again, it may be shown that the isothermal surfaces across an ocean current generated in this manner must be inclined so that the warmer water lies to the right and the cooler to the left when the observer is looking in the direction of the current. With an increase in current speed, brought about in this case by the southerly thrusts of wind, the slope of isothermal surfaces must increase. These processes of mutual adjustment of current and pressure field, which were first described by Rossby [1937, 1938], could well account for the fact that the major warmth is found east of the negative air pressure anomaly and the major cool area near its center. The above-described mechanisms

have been employed by Neumann and his colleagues [1958] to explain broad-scale water temperature anomalies in the North Atlantic. Whereas these abnormal atmospheric circulations appear to account in a general way for the broad-scale nature of the water temperature anomalies in fall and winter of 1957-1958 and the following summer, it is not so easy to account for the remarkable warming just off California which was observed during the summer of 1957 (Fig. 1). The associated mean circulations and wind anomalies for this summer are given in Figure 8. In the first place, the anomalies are characteristically weaker than those in fall and winter, and the anomalous gradients are rather weak, probably too weak to induce current changes responsible for such water temperature abnormalities as were observed.

Perhaps another factor is suggested by the marked weakness of the upper-level trough off the west coast as indicated in Figure 8 by the contours and by the +60 foot anomaly (a large positive value for a mean seasonal anomaly in this area). The failure of the west coast upper-level trough to develop in a normal fashion during the summer of 1957 was also associated with light winds, pronounced warmth along the California coast, and generally less cloud and more clear sky than normal, as may be seen in charts published in appropriate issues of the *Monthly Weather Review* [U. S. Weather Bureau, 1957]. Now with the observed mid-tropospheric contour pattern it is quite reasonable that the stratus over the sea was much less thick and intensive than normal because positive anomalies in a trough area imply less cyclonic vorticity and less ascent (more subsidence) than normal. In the area off California, lower inversion bases and hence thinner and more disintegrated stratus decks are probable. It is well known that especially during fairly calm conditions in summer the surface layers of the ocean respond to solar radiation, and since evaporation is not favored by light winds, these layers warm up. striking responses of surface temperatures up to a few degrees during calm clear days were found in the Gulf of Mexico by Stommel and Goodcock [1951]. However, a simple calculation shows that to increase the water temperature 1°C through a depth of 100 meters requires about 10,000 gram calories, or the ab-

sorption of about 333 calories per day for one month or about 110 per day over the entire summer season. This seems excessive when one considers that this area in summer normally receives about 700 cal/cm²/day.

In fact, during the summer (June, July, and August) of 1957 the total radiation from sun and sky recorded at Los Angeles averaged only 5 per cent above the average of the 5-year period 1951-1955. While the departure is in the direction of producing heating of the sea surface, it could account for a temperature increase of perhaps 1°C of only the uppermost 30 meters. Although the depth and extent of water partaking in the warming is not known, the preliminary CCOFI report [1957] indicates it was of the order of a few hundred meters. Thus the heat supplied by increased radiation plays only a small role, although lessened evaporation associated with less wind than normal must be added to this.

Thus the long period of warm water off California may result from a combination of different mechanisms: the summer and early fall warmth which is associated with diminished upwelling, increased absorption of solar radiation, and diminished evaporation; and the late fall and winter warmth which is mainly associated with the surface advection of warmer water and with somewhat reduced upwelling.

Relationship between sea-surface temperature anomalies and 1000-700 mb thickness anomalies—If one compares the mean seasonal fields of 1000-700 mb thickness anomaly (not reproduced) with the corresponding charts of sea surface temperature, it appears that a positive correlation exists. During winter the warm water off the entire west coast of North America was associated with warm air in the lower troposphere, whereas in the central Pacific cooler air than normal was found over relatively cool water. A similar positive correlation existed in fall, especially in the Gulf of Alaska and in the central and eastern Pacific. Seasonal averages of thickness anomaly and sea-surface temperature at La Jolla (Fig. 17) show the relationship. Some positive correlation might be anticipated because lower layers of air in contact with the sea are strongly and rapidly modified by the underlying supply of heat, especially in the open ocean after lengthy air trajectories.

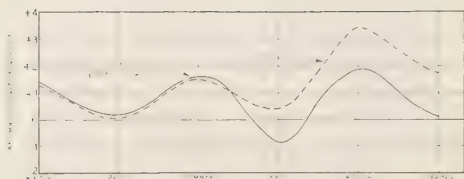


FIG. 17—Seasonal mean sea-surface temperatures at La Jolla, California (broken) and mean seasonal values of 1000-700 mb thickness (solid) over nearby ocean. Both curves expressed in units of °F

Furthermore, the patterns of thickness anomalies are related not only to the ocean surface but even more to the anomalous atmospheric flow. Hence, anomalous southerly currents not only drive water northward and eastward but also ordinarily reflect advection of warm air masses from the south. Positive air temperature anomalies result.

This three-way relationship between the anomalous patterns of mean height, mean thickness, and mean sea-surface temperature must be considered before conclusions are hastily drawn regarding coastal air temperature anomalies. For example, the abnormal warmth along the west coast of the United States during much of the cold season of 1957-1958 was primarily due to the anomalous character of the general atmospheric circulation there, although it was to some extent due to the fact that the offshore waters were warmer than normal. Both water and air temperatures responded to the abnormal winds, although the water, once warmed, certainly helped to keep the invading air masses warm along the coast. It is possible to obtain some quantitative estimate of how much the water temperatures may have contributed to the abnormal warmth along the west coast from the results of objective techniques developed for translating 700 mb circulations into associated surface-air temperature anomalies. This method is used a great deal in extended forecast practice in which it is necessary to interpret prognostic contour charts in terms of associated weather patterns. Data have been worked up for four West Coast cities: San Diego, San Francisco, Eureka, and Tatoosh Island. Those for San Diego and Tatoosh Island are based on work by Klein and others (to be pub-

lished), and the data for the other two are from work by Martin and Hawkins [1950]. In both methods two or more geographical locations are determined whose 700 mb heights (on a 5-day mean or monthly basis) account for the maximum variance of surface temperature anomalies at each station.

The observed anomalies and computed estimates for the months of September 1957 through March 1958 are compared in Figure 18. The estimates are predominantly too low. Examina-

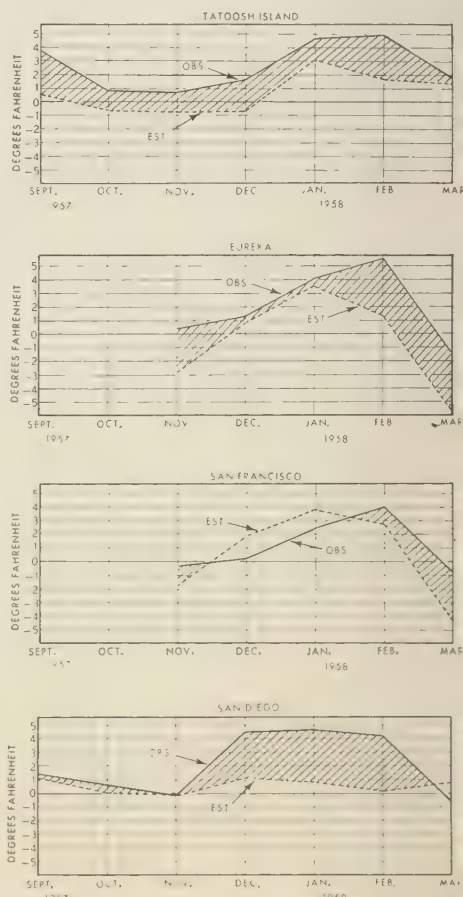


FIG. 18—Objectively estimated air temperature anomalies (broken) derived from anomalous air circulation, and observed temperature anomalies (solid) for four West Coast cities. Shaded area shows excess of observed over estimated temperature

on of the means for all months and stations indicates that perhaps only one half of the observed positive departure of about $+2.0^{\circ}\text{F}$ can be ascribed to the anomalous circulation pattern. The other half may very well be related to the presence of warmer waters over which the air was modified. O'Connor [1958], in describing the weather of June 1958, arrived at a similar conclusion from other considerations.

The existence of a three-way relationship between mean anomalies of height, thickness, and sea-surface temperature indicates that these fields ought to be considered mutually in analysis. However, since analysis of sea-surface temperature fields is much more difficult than analysis of either atmospheric thickness or contour patterns, largely because of inadequate and inferior data, it is suggested that analysts of mean sea-surface temperature can profit by the use of the mean atmospheric properties.

A possible cause of the evolution of the observed seasonal flow patterns—Although some success has been achieved in describing the continuity of mean circulations over periods of the order of a month [Namias, 1953], it is usually extremely difficult, if not impossible, to do this for mean patterns spanning seasons. Occasionally, however, there seems to be some suggestion of continuity in seasonal charts; and the present case, from summer 1957 through the following spring, seems to be one of these.

In the summer a trough with negative anomaly appears at 180° longitude (Fig. 8), implying somewhat stronger than normal cyclonic activity to the south of the Aleutians. In the subsequent fall we might interpret the strong trough at 170°W and the -19 anomaly as an eastward displacement of activity. In the following winter this zone of anomalous cyclonic activity appears to have shifted farther eastward to 145°W (-30 anomaly) and in spring to 130°W . However, only when physical understanding of the nature of anomalies is attained can one feel secure in implying continuity to such charts. Such understanding has so far evaded meteorologists. A possible hypothesis for this case is suggested.

As summer goes into fall two climatological phenomena are highly probable: (1) the westerlies over the Pacific increase in strength, and (2) the trough along the east coast of Asia becomes established. These phenomena are associ-

ated with increased cyclonic activity off the Asiatic coast, incident to the onset of the Asiatic cold-season monsoon, and with the increased baroclinic developments of these cyclones as they approach the Aleutians. Now if we assume that the negative anomaly and associated trough have long lifetimes, and if the pre-existing summer Asiatic trough (north of Korea) is fairly well locked into position along the coast in fall, then the climatologically probable increase in westerlies would favor a position farther to the east for the downstream trough. A similar trend in winter may explain the further progression as the westerlies increase. On the other hand, in the subsequent spring the eastward motion is more difficult to explain. Probably the establishment of a quasi-permanent block over the eastern Pacific downstream from the fast westerly flow has something to do with this eastward motion, for according to Rex [1950, 1951] this extreme eastern Pacific area is especially subject to such blocks in the spring.

Now if such a hypothesis contains a germ of truth, one might inquire why the anomaly centers and mean troughs should have such a long lifetime. This is a central question which has puzzled researchers in long-range weather forecasting for years [Namias, 1953.] In this case it is conceivable that the existence of warm water to the east of the negative anomaly and the general contrast between this water and the cooler water to the west might help to explain this long life. In the first place, the abnormally warm water provides an enhanced source of both heat and moisture for cyclonic development. The longitudinal water contrast, by influencing the overlying air masses, may also assist cyclonic development. In other words, cyclones moving over these abnormal waters might feed on the increased moisture, sensible heat, and temperature contrast imparted to the air and in this way provide a more or less geographically fixed area for cyclogenesis and prevailingly negative anomalies. However, the area of influence would also be affected by climatic conditions involving the general circulation (as indicated above) and thus might shift. That is, the air circulation responsible for the underlying oceanic temperature variations might change because of factors more potent than those produced solely by the water anomalies.

Of course, such a hypothesis requires more testing. But the history of meteorology indicates that imaginative hypotheses are initially required in such a complex field as the study of climatic anomalies (and long-range forecasting). Perhaps when reasonably complete general circulation models are programmed for electronic computers the above hypothesis can be evaluated quantitatively.

Meanwhile, in the quest for significant factors, students of longer-period weather phenomena might well pay more attention to anomalous oceanic temperatures.

REFERENCES

CALIFORNIA COOPERATIVE OCEANIC FISHERIES INVESTIGATION, 1957, *the year of warm weather and southern fish, prelim. rept.*, Dec. 19, 1957. (Mimeo. rept. in *Proc. Rancho Santa Fe Symposium*, June 2-4, 1958.)

HANZAWA, M., AND T. INOUE, Relation between oceanic and atmospheric states in the North Pacific Ocean for the year of bad and good rice crop (in Japanese), *Central Meteorol. Observatory, Oceanog. Repts.*, 2, (3), 1952.

HELLAND-HANSEN, B., AND F. NANSEN, Temperature variations in the North Atlantic Ocean and in the atmosphere. Introductory studies on the cause of climatological variations, *Smithsonian Inst. Publs., Misc. Collections*, 70, 408 pp., 1920.

KLEIN, W. H., B. M. LEWIS, AND ISADORE ENGER, Objective prediction of five-day mean temperatures during winter (to be published).

MARTIN, D., AND H. F. HAWKINS, JR., Forecasting the weather: the relationship of temperature and precipitation over the United States to the circulation aloft, *Weatherwise*, 3, 16-19, 40-43, 65-67, 89-92, 113-116, 138-141, 1950.

McGARY, J. W., *Surface temperature anomalies in the central North Pacific, January 1957-May 1958*, Pacific Oceanic Fishery Investigations, May 1958 (mimeo. rept.).

NAMIAS, J., Thirty-day forecasting: a review of a ten-year experiment, *Meteorol. Monographs*, Am. Meteorol. Soc., 2 (6), 1953.

NAMIAS, J., AND C. R. DUNN, The weather and circulation of August 1955—including the climatological background for Hurricanes Connie and Diane, *Monthly Weather Rev.*, 83, 163-170, 1955.

NAMIAS, J., Persistence of mid-tropospheric circulations between adjacent months and seasons 1958 (to be published in *Rossby Memorial Volume*, Stockholm).

NEUMANN, G., E. FISHER, J. PANDOLFO, AND W. PIERNON, JR., Studies on the interaction between ocean and atmosphere with application to long-range weather forecasting, *New York Univ. Dept. Meteorol. Oceanog., Final Rept.*, AFCRC TR-58-236, (ASTIA-AD-152 555), Air Force Cont. no. AF 19(604)-1284, 1958.

O'CONNOR, J. F., The weather and circulation of June 1958—record cold in northeast and warmth in northwest, *Monthly Weather Rev.*, 86, 229-236, 1958.

REX, D. F., Blocking action in the middle troposphere and its effects upon regional climate, *Tellus*, 2, 196-211 and 275-301, 1950; 3, 100-115, 1951.

RODEN, I., AND J. L. REID, JR., On a relation between atmospheric pressure and sea surface temperatures in the North Pacific Ocean, Scripps Inst. Oceanog., Univ. Calif. (to be published in new series).

ROSSBY, C. G., On the mutual adjustment of pressures and velocity distributions in certain simple current systems, I and II, *J. Marine Research, Sears Foundation*, 1 (1) and 1 (3), 1932 and 1938.

SCHROEDER, E., H. STOMMEL, D. MENZEL, AND W. SUTCLIFFE, JR., Climatic stability of eighteen-degree water at Bermuda, *J. Geophys. Research*, 64, 363-366, 1959.

STEWART, H. B., JR., S. B. ZETLER, AND C. B. TAYLOR, Recent increases in coastal water temperature and sea level—California to Alaska, *U. S. Coast and Geodetic Survey Tech. Bull.* 3, 1958.

STOMMEL, H., Serial observations of drift currents in the central North Atlantic Ocean, *Tellus*, 6, 203-214, 1954.

STOMMEL, H., AND A. H. WOODCOCK, Diurnal heating of the surface of the Gulf of Mexico in the spring of 1942, *Trans. Am. Geophys. Union*, 32, 565-571, 1951.

SVERDRUP, H. U., *Oceanography for meteorologists*, Prentice-Hall, New York, 235 pp., 1942.

U. S. WEATHER BUREAU, Monthly articles on the weather and circulation, *Monthly Weather Rev.* through 1958.

(Manuscript received March 3, 1959; presented at the annual meeting of the American Meteorological Society held in New York, January 26-29, 1959.)

A Practical Equal-Area Grid

EMANUEL M. BALLENZWEIG

*Extended Forecast Section
U. S. Weather Bureau
Washington, D. C.**

Abstract—The deficiencies of various methods used to date for mapping the geographical variation of geophysical quantities are discussed. A method for constructing a practical equal-area grid for use in such work is illustrated. It can be constructed for any scale or map projection and can also be used hemispherically. Its advantages over other methods are discussed. It is suggested that, in lieu of an equal-area grid, it is better to use the raw frequencies in n degree squares than to adjust them by proportionality factors designed to equate the size of the squares to that of the equal-area grid.

Introduction—Mapping the geographical distribution of certain physical quantities which show spatial and/or temporal variation is an important facet of many disciplines, both geophysical and non-geophysical. In meteorology, sopleths of many quantities are drawn. In certain studies of specific elements, an areal distribution is the best representation.

In the past, various methods have been used in meteorology for obtaining such a distribution. Use of n degree boxes is the oldest and most popular technique employed in this type of study, dating back at least to 1884 [Finley, 1884]. It consists of counting the frequency of occurrence of certain events in unit boxes, either squares with sides n degrees in length or, less commonly, rectangles n degrees in length and m degrees in height. The shortcoming of this method is the inequality of the unit areas, if the region studied has considerable latitudinal extent. A 5° square between 10° and 15° latitude is about double the size of a similar square between 55° and 60° latitude. Thus a distorted frequency distribution is created with undue weight given to boxes nearer the equator. Many researchers today still persist in using this method, despite this defect.

Kelsey [1925] devised a unique system for arriving at the geographical distribution of a geophysical quantity. He counted the frequency of cyclones crossing circles 200 miles in radius

whose centers were 200 miles apart. This method has two fine features, equal area and equal distance from the center of area to all boundaries; however, it has one major flaw—the circles have considerable overlap and are therefore unwieldy in actual practice. The use of tangent circles would retain the merits of this system but would result in areas where the frequency could not be counted due to the grid.

A method used by several other researchers consists of multiplying the frequency observed in each box by a proportionality factor (varying with the latitude) designed to make the density of observations at all latitudes apply to a unit box. Unfortunately, in getting rid of one bias this method introduces a new one which Klein [1957] pointed out: In latitudes where the adjusting coefficient is greater than one, the frequency is assumed to apply to a larger box than the one in which it was actually observed, and the artificial adjustments may intensify areas of local maximum and obliterate areas of local minimum. The opposite effect may occur in latitudes where the adjusting coefficient is less than one. Such results could be misleading, perhaps even more than the raw frequencies in n degree boxes.

To escape these difficulties, Klein [1957] devised another scheme. Frequencies were compiled in quadrangles, 5° latitude in length and with a varying width depending on the latitude (his Table 5). Complete equality was not attained because the choice of width was limited to integers and exact divisors of 360° . The aver-

* Present affiliation: Ship Routing Division, Fleet Weather Facility, Norfolk, Virginia.

age absolute areal deviation from the mean is approximately 8 per cent. This defect is magnified when cognizance is taken of the fact that large absolute errors of opposite sign are found in several adjacent latitude bands. In fact, in an extreme case the area of adjacent quadrangles differs by about 30 per cent.

In a recent article, *Bailey* [1956] suggested two equal-area grids. In one, the meridians were respaced; in the other, the parallels were respaced. The first of these methods is essentially the same as *Klein's* [1957] method, except that whole integers were not employed for obtaining the width of the quadrangles. *Bailey* [1956] states that areas in any zone of his grid fall within ± 3 per cent of the mean for the hemisphere. This accuracy is sufficient for most meteorological purposes. Furthermore, his technique can easily be applied on a hemispheric basis, and it provides quadrilaterals nearly alike in shape. He acknowledges the deficiency of this grid: north-south lines are not continuous. His second grid is both precise and continuous. Its sole defect is the pronounced latitudinal variation in the shape of its quadrilaterals; however, this is a serious defect for the type of sampling to be described in the following sections of this paper.

Other methods with obvious shortcomings

have been based on the use of n degree line segments and on the use of n degree segments multiplied by adjusting coefficients. A simple extension of these methods is to take line segments of equal length along latitude circles and connect them by pseudo-meridians to arrive at an equal-area grid. This method was used in the present study.

The equal-area grid—The orientation and size of the unit quadrilaterals were designed for a study of tropical storm frequencies in the North Atlantic. The grid (Fig. 1) was designed to fit the Lambert conformal base map used in Figure 3, as the data to be analyzed were plotted on this base. After choosing a reference meridian, line segments of equal length were then measured along latitude circles. (*Smithsonian Meteorological Tables* [1951] contain a table showing the value of one degree of longitude at each latitude.) The ends of these segments were connected by lines having a general north-south orientation. For this particular grid (Fig. 1) 60°W was used as a reference meridian, a distance of 2.5 degrees of longitude at 10°N as the east-west grid distance, and a distance of 2.5 degrees of latitude as the north-south grid distance. To simplify the construction, the 2.5-degrees longitudinal distance at 10° N (147.9 nautical miles) was approximated at 24°N .

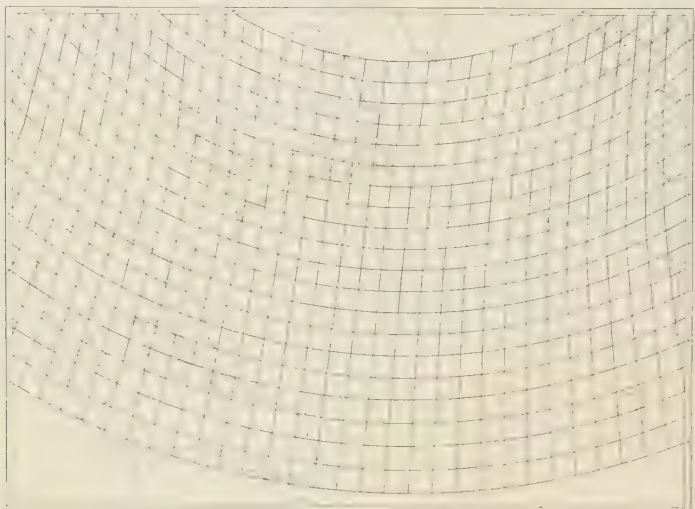


FIG. 1.—The equal-area grid designed for use on a Lambert conformal base map

TABLE 1—*East-west grid distance along selected latitude circles*

Latitude	Distance (deg. long.)	Distance (naut. mi.) ^a
10°N	2.5	147.90
24°N	2.75	150.99
34°N	3.0	149.55
45°N	3.5	148.91
60°N	5.0	150.55

^a Smithsonian Tables [1951]

(2.75° of longitude), 34°N (3.0°), 45°N (3.5°), and 60°N (5.0°). (The length of these arcs along each of these latitude circles is given in Table 1.) The 'equidistant' arcs, both east and west of the vertical reference meridian, were then connected by a series of straight lines: from 10°N to 24°N ; 24°N to 34°N ; 34°N to 45°N ; and 45°N to 60°N . These quadrilaterals are seen to assume the form of parallelograms on the earth's surface, although they are not parallelograms in the spherical sense (since the parallels of latitude are concentric circles, rather than parallel lines). The formula for measuring their areas will be derived and will be seen to be essentially that for a parallelogram. This formula will show that the areas are equal for all practical purposes.

In dealing with areas as small as these, the curvature of the earth can reasonably be neglected. Let us now consider Figure 2. In this figure, AB and CD represent arcs of two adjacent latitude circles. The arcs are of equal length, Q . The arc length Q can be expressed in polar coordinates and in this special case is defined as a constant

$$Q = R(\theta - \theta') = \text{a constant} \quad (1)$$

where R is the radial distance, in this case the distance from the pole (at zero) to the latitude circle, and θ is the polar angle. The unprimed symbol refers to points A and C , the primed to points B and D . (In Figure 2 subscript 1 refers to CD and subscript 2 to AB .)

The area of an infinitesimal curved strip is defined as

$$da = R(\theta - \theta') dR. \quad (2)$$

Substitute (1) in (2) and integrate. The total area of each quadrilateral is

$$a = Q(R_2 - R_1) \quad (3)$$

The arc length Q is not an exact constant due to approximations in constructing the grid. Also, the distance between the two adjacent latitude circles $R_2 - R_1$ is not invariant (range of 149.21 to 150.26). Thus the areas are not exactly equal. The deviation of any quadrilateral from the mean due to these factors is less than ± 1.3 per cent. Such a deviation is less than the thickness of the drafted grid-lines and is well within the realm of drafting error. Thus, for all practical purposes, this grid can be considered equal-area.

Applications of the grid—The grid described was used for counting the frequency of tropical storms in each month of the year to ascertain the geographical distribution of the occurrence of storms. After the count was made on the equal-area grid, isopleths were drawn and transferred to a standard base map. An example of the isopleth field for the month of August (1887–1956) is shown in Figure 3.

The frequency distribution obtained by use of the equal-area grid was then compared with that obtained by other common methods: the frequency in 2.5 degree squares, and the fre-

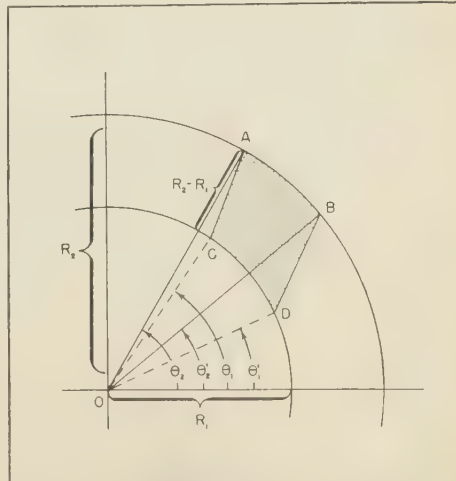


FIG. 2—Geometrical representation of one of the areas in the grid (the shaded area, $ABCD$)

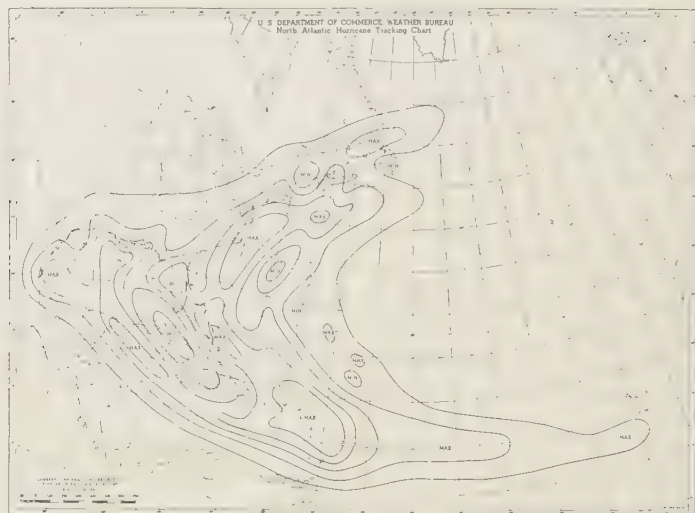


FIG. 3—Tropical storm frequency per unit box (equal-area grid) during August based on storm tracks for the years 1877–1956 as provided by the Office of Climatology, U. S. Weather Bureau

quency in those squares multiplied a proportionality factor varying with latitude. The isopleth fields were quite similar in all three cases. However, on the average, the 2.5 degree squares gave values lower than those given by the equal-area grid, whereas the values for the squares multiplied by a proportionality factor were higher. The magnitude of the errors was approximately equal, and in general, neither of the two methods showed superiority over the other.

From this small sample it is difficult to generalize; but it is safe to say that because of the discontinuous nature of such phenomena as storm tracks, any use of correction factors is to be discouraged as it may result in higher frequencies than are actually observed in the larger area to which it is being equated. The use of raw frequencies in n degree squares is therefore suggested as being the next best method. The results are as good as the corrected values and in no case are they fictional. But the equal-area grid is easy to use and it eliminates the uncertainties of the other two methods. Such a grid has other uses in meteorology. Godson [1957] maintains that, especially at high latitudes, such a grid is necessary in specifying atmospheric flow patterns from a

given array of 500-mb heights by fitting orthogonal polynomials (or other functions).

This type of grid is not restricted to the area for which it was drawn; it can be applied hemispherically by rotating the reference meridian. A rotation of 90 degrees has been found to be highly satisfactory; frequencies in all boxes up to 45 degrees on either side of the reference meridian are counted. The boxes used have little distortion and the field has little overlap (Fig. 4). This particular grid is on a polar stereographic projection rather than on the Lambert conformal base map discussed previously. In the polar area (north of 80°N) the parallelograms were replaced by triangles whose area is within 3 per cent of the mean area. In the Extended Forecast Section of the U. S. Weather Bureau a similar grid has been used in the routine preparation of cyclone and anticyclone statistics since January 1958. This particular grid has a north-south distance of 5° of latitude and an east-west distance equal to 5° of longitude at 44°N, a unit box area of approximately 66,000 n.mi.².

This is not the first time an equal-area grid has been suggested for use in geophysics, but it is hoped that this article will awaken scientists to the advantages of using such a grid. Further-

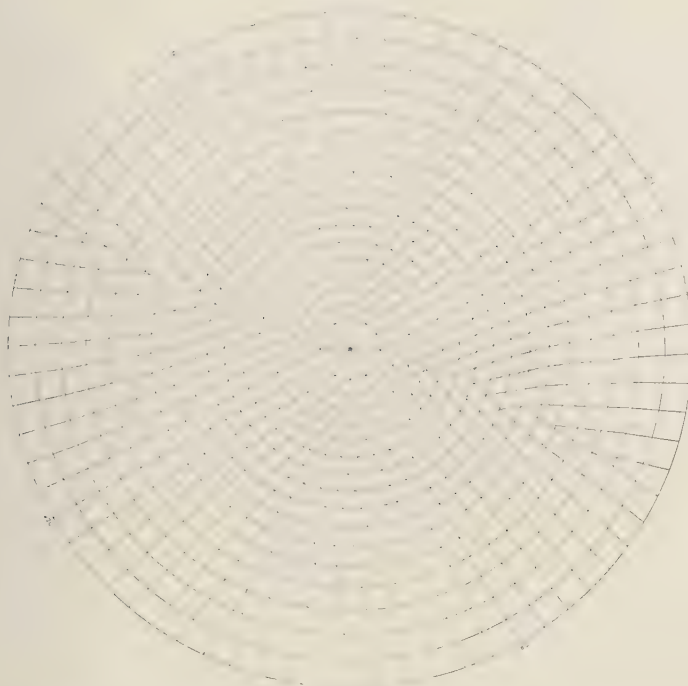


FIG. 4.—The hemispheric equal-area grid designed for use on a polar stereographic base map (north-south distance equal to 5° of latitude, east-west distance equal to 5° of longitude at the equator, reference lines at 0° , 90° , 180° , and 270°)

more, this type of grid can easily be constructed on any map projection and on any scale. It is not designed as an equal-area grid on the map base but is rather an equal-area grid on the surface of the earth.

Acknowledgments—I want to thank William H. Klein for indicating the need for an equal-area grid, Louis P. Harrison for a valuable discussion of the mathematical formulation, Carlos Bowne and Frederick Schaefer for constructing and drafting the equal-area grids, and the latter, as well, for suggesting its further application in counting the frequency of occurrence of cyclones and anticyclones.

REFERENCES

BAILEY, H. P., Two grid systems that divide the entire surface of the earth into quadrilaterals of equal area, *Trans. Am. Geophys. Union*, 37, 628-635, 1956.

FINLEY, J. P., Charts of relative storm frequency for a portion of the northern hemisphere, *U. S. War Depart., Prof. Pap. Signal Serv.* 14, 9 pp., 1884.

GONSON, W. L., The numerical representation of atmospheric flow patterns in polar areas, in *Sci. Rept. no. 3, Contract no. AF19 (604)-1141, Arctic Meteorol. Research Group Publ. Meteorol.*, no. 5, pp. 22-44, 1957.

KELSEY, K., A new method of charting storm frequency, *Monthly Weather Rev.*, 53, 251-252, 1925.

KLEIN, W. H., Principal tracks and mean frequencies of cyclones and anticyclones in the northern hemisphere, *U. S. Weather Bur. Research Pap.* 40, 60 pp., 1957.

SMITHSONIAN METEOROLOGICAL TABLES, 6th rev. ed., Smithsonian Inst., Washington, pp. 482-483, 1951.

(Manuscript received September 17, 1958;
revised January 17, 1959.)

The Experimental Fusion Curve of Iron to 96,000 Atmospheres

H. M. STRONG

General Electric Research Laboratory
Schenectady, New York

Abstract—The melting point of iron has been determined to 96,000 atmospheres, and the temperature for the α - γ transition to 76,000 atmospheres. Simon's fusion equation, $P/a = (T/T_0)^c - 1$, fits the experimental melting points with $a = 75,000$ atm and $c = 8$. Extrapolation of the melting points to 1.4×10^6 atm, the pressure at the boundary of the earth's core, gives $2340 \pm 200^\circ\text{C}$. The temperature for the α - γ transition decreased about 200°C at 76,000 atm.

A complete theory of metals must include an explanation of their melting-point variations with pressure. As a contribution to this problem, the fusion curves of iron and three other Group VIII metals have been determined to 10^6 atmospheres.

Of particular interest to geophysicists is the fusion curve of iron, since the accumulated evidence suggests that at least the outer part of the earth's core is composed of liquid iron, or iron-nickel alloy, [see discussions of this problem by Bullen, 1947; Jeffreys, 1951; Gutenberg, 1951, and Birch, 1952]. If true, then the extrapolation of the fusion curve to pressures of the order of 10^6 atm would help to fix a minimum temperature for the core boundary. This paper gives the experimental fusion curve of iron to 96,000 atm. An extrapolation of this curve to 10^6 atm was then made using Simon's [1929, 1937] semi-empirical fusion equation. The data for the three other Group VIII metals will be presented elsewhere [Strong and Bundy, to be published].

Simon's [1953] fusion equation has already received experimental and theoretical justification [Domb, 1951; DeBoer, 1952; Salter, 1954; Gilvarry, 1956a, 1957]. This encouraged both Simon [1953] and Gilvarry [1956b, 1957] to use the equation to extrapolate the melting point of iron to 10^6 atm using the one atmosphere melting point and initial slope of the curve as a base for the extrapolation. The core boundary temperatures obtained by them were about 3000 and 4000°C , respectively. Present experimental data indicate that the curve runs much lower in temperature than either of the two former curves.

In addition to the melting point data, the temperatures for the α - γ transition were obtained to 76,000 atm. The γ - δ transition could not be detected, so no data for its variation with pressure were obtained.

EXPERIMENTAL METHODS

At very high pressures the melting point of a metal can be detected by observing a sharp change in electrical resistance, an abrupt change in the thermal emf characteristics of a suitable pair of metals, or a step in a rising temperature-time curve caused by absorption of the latent heat of fusion. For determining the fusion curve of iron, all three of these methods were used. Incidental to the determination of the melting point, the α - γ transition temperature was also observed through resistance changes that accompany this transformation. The sample structures used in these measurements are illustrated in Figure 1.

In Figure 1a, the sample holder used for detection of melting by a step in the rising temperature-time curve is illustrated. The iron sample was surrounded by pure machinable alumina inside a graphite tube heater. A Pt-Pt 10 per cent Rh (P-PR) thermocouple was inclosed in a pure alumina tube which passed through the center of the iron slug. The slow and steady increase of temperature on the sample was interrupted by a small step at the melting point due to the latent heat of fusion. The cooling curve also exhibited a small step due to the release of latent heat upon refreezing. When the iron melted, some of the liquid metal inevi-

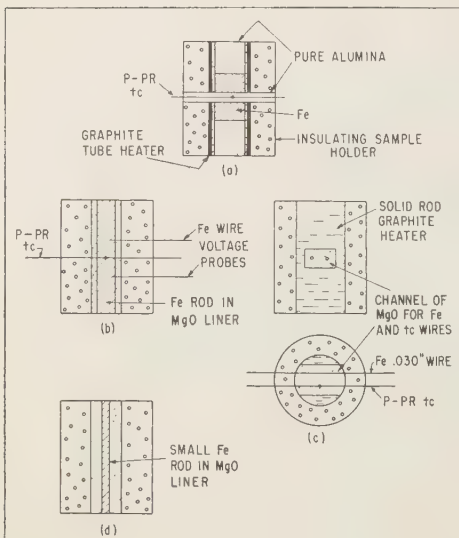


FIG. 1—Sample arrangements for the melting point of iron: (a) by step in temperature-time record due to latent heat absorption; (b) by resistance change and thermocouple maximum at melting point; (c) by resistance change; (d) by resistance change and heating power

tably found its way through the thin alumina wall into the graphite heater, and a sudden increase in current through the heater and a sharp rise in temperature resulted. The temperature, current, and voltage were automatically recorded so that the occurrence of melting was easily detected by the two phenomena described. An example of a thermocouple trace and associated current and voltage records are shown in Figure 2a as they appeared in the neighborhood of the melting point for an experiment at 48,500 atm.

Figure 1b illustrates the sample used for detection of the α - γ phase transformation and melting by resistance changes. An iron rod was heated directly by passage of a current. Because iron has a very small resistance change at the melting point [Powell, 1953, only 9 per cent] iron wire voltage probes were placed on either side of the melting zone so that the resistance change at melting could be observed to best advantage. The thermocouple itself served as a secondary detector of melting. Being in direct contact with the iron, it alloyed at the melting

point so as to give a millivolt reading which could not exceed the melting point. With a very fast rise in temperature, the thermocouple followed the temperature all the way to the melting point. This is illustrated in Figure 2b for an experiment at 76,000 atm. At slower rates of temperature rise, the thermocouple alloyed with the iron near the melting point in such a way as to cause a decrease in its thermal emf-temperature coefficient. In such cases, a plot of temperature versus heating power was used to obtain the final melting temperature by extrapolating the temperature from the power input

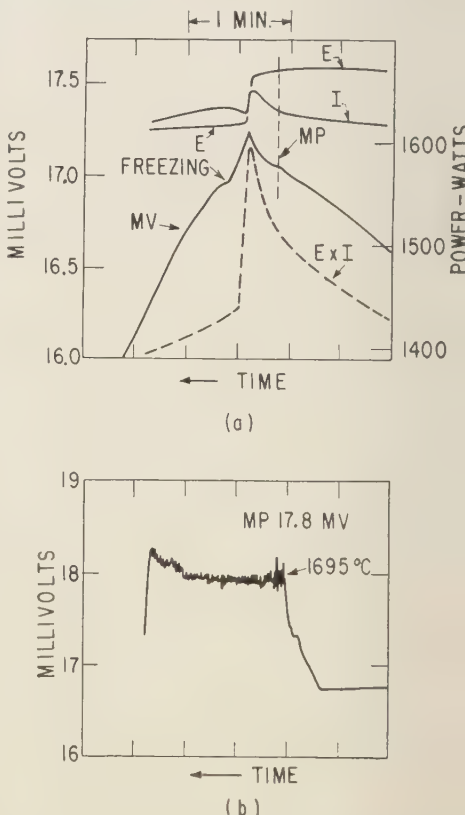


FIG. 2—Thermocouple output at the melting point: (a) temperature steps, current and voltage changes at the melting point by method of Figure 1a; (b) thermocouple peak output at the melting point and subsequent erratic behavior by method of Figure 1b. Pressure for experiments (a) 48,500 atm; (b) 76,000 atm; time marked in one-minute units

where the thermo-electric output showed signs of decreasing to the power input where melting occurred. This extrapolation was never more than 100° . The temperature was directly proportional to power input so that the extrapolation was linear. The amount of platinum available for alloying with the iron was less than 0.8 per cent and the effect of this much platinum on the melting point of iron is negligible, since metallurgical charts show that the melting points of Fe-Pt alloys are equal to or higher than the melting point of Fe. However, the thermocouple wires could alloy rapidly with iron near the melting point and cause a drift in its calibration. An example of the data obtained from this type of sample is illustrated in Figure 3.

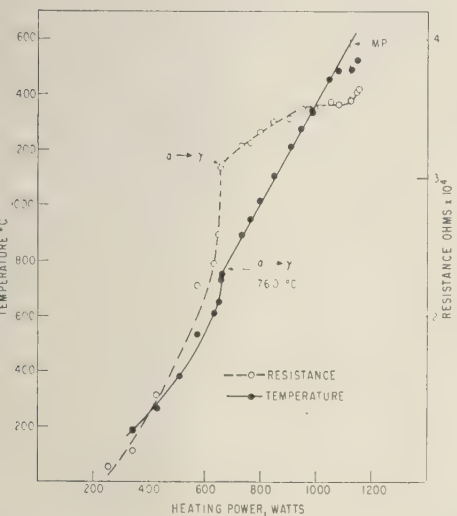


FIG. 3—Temperature and resistance versus heating power for sample of Figure 1b at 25,000 atm

In Figure 1c the iron specimen is in the form of a 0.020 inch wire which, with its thermocouple, was embedded in a trough of pure magnesium oxide powder. The trough of magnesia was centered in a graphite rod heating element. Short low-resistance leads were connected to opposite ends of the iron wire so that the specimen constituted most of the electrical resistance in the iron wire circuit. The temperature and resistance of the iron wire were recorded as the heating power was increased. The Fe resistance

was recorded as millivolts for a 10 milliampere dc current passing through it. The α - γ transformation and melting point could be observed in this manner. One observation was made with this type of sample.

Figure 1d shows a type of sample which depended on a resistance change to detect the melting point and the proportionality of temperature to power input to obtain an approximate value of the melting point. The location of the α - γ transition served as a check point.

All iron used in this work was 99.94 per cent iron by weight. It was vacuum melted and cast after being treated to reduce the oxygen content to 0.0023 per cent. The carbon content was 0.002 per cent. The largest single other impurity was 0.02 per cent Ni whose influence on the melting point was negligible.

The high pressure equipment of H. T. Hall's (to be published) general design was used for obtaining the required pressures.

PRESSURE AND TEMPERATURE MEASUREMENT

A calibration of pressure within the pressure chamber in terms of the applied load was obtained by substituting elements which undergo sharp resistance changes at certain pressures in place of the iron specimen. These elements are Bi(24,800 atm), Tl (43,400), Cs (53,500), and Ba (77,400). The transitions and the pressures at which they occur were discovered and measured by Bridgman [1952]. In the several years of experience with the apparatus of this work, it has been well established that its pressure calibration is linear with applied load and remains constant over very long periods of time.

Further details about pressure calibration and its probable errors are described elsewhere [Strong and Bundy, to be published]. For the present, it can be stated that the pressures quoted with the results are thought to be accurate to ± 10 per cent.

Temperature measurement depended upon the reliability of P-PR thermocouples over the full pressure range. By comparing different thermocouples over a wide pressure and temperature range, it was concluded that the handbook tables for P-PR probably agree with the true high pressure calibration to within $\pm 10^{\circ}$. Further details about these tests are given elsewhere [Strong and Bundy, to be published].

RESULTS

The α - γ transformation—This transformation was detected by an abrupt change in the slope of the electrical resistance-heating power (or temperature) curve. One such transition is illustrated in Figure 3. In any one sample, the temperature for the transformation was quite reproducible but the reverse transformation often occurred several degrees lower than the forward one. The α - γ transformation temperatures obtained are shown in Figure 4. The

0.06 per cent by weight of various foreign atoms which could reduce the transformation temperature to a certain extent. Also, different methods of observing the occurrence of the transformation do not generally give quite the same transformation temperature.

The heat of transformation computed from present data is in the range of 170 to 190 cal/gm atom. The generally accepted value is 215.

The γ - δ transformation—The γ - δ transformation was not detected. In the temperature regions where this transformation should have occurred, the electrical resistance of the sample fluctuated in such a way as to make detection of the transformation by a definite resistance change very doubtful. Data given by Ralston [1929], Tamman and Bandel [1934] and Birch [1940], show that the transformation temperature will increase with pressure. The initial slope of the transformation curve according to Tamman and Bandel is about 6.5° per 1000 atm, and according to Birch, about 17° per 1000 atm. If the former value is correct, the γ - δ transformation curve might not intersect the fusion curve, but with an initial slope of 17° per 1000 atm there should be a triple point between γ , δ and liquid in the neighborhood of 10,000 atm. No triple point was evident in the data obtained in this work, but the existence of one at pressures in the neighborhood of 10,000 atm is not excluded.

The fusion curve for iron—Figure 5 shows the fusion curve obtained for iron to 96,000 atm. The flags on the points indicate the estimated error of individual temperature readings exclusive of possible errors in P-PR calibration caused by pressure. A good fit to the experimental data was obtained with Simon's [1929, 1937] equation.

$$\frac{P}{a} = \left(\frac{T}{T_0} \right)^c - 1 \quad (1)$$

in which T is the absolute melting temperature at the applied pressure P (in atmospheres) T_0 is the melting temperature at the origin of the fusion curve, which in this case is one atmosphere, and a and c are constants to be determined from experimental data. Simon considered that a was essentially an "internal pressure." For iron, a and c were found to be 75,000 atm and 8 respectively. The error in c due to uncertainties in pressure and temperature calibration was estimated to be ± 1 . If 8 is assumed to be the

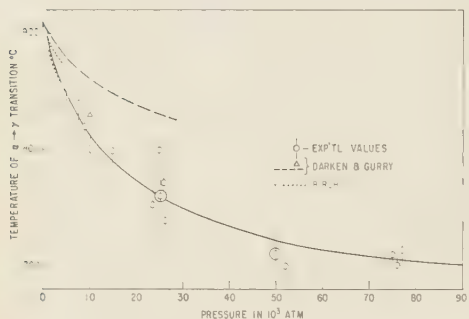


FIG. 4.—Temperature for α - γ transition at pressures to 76,000 atm

lowest pressure at which observations could be made was about 5000 atm. Included with the present experimental data are the data of Birch [1940] to 4000 kg/cm² and some calculated values of Darken and Gurry [1953]. The upper curve was calculated from the Clausius-Clapeyron equation after allowance had been made for the effect of pressure on the heat of transformation. The single point (triangle) was obtained by a simple Clausius-Clapeyron calculation. Recent theoretical calculations by Jamieson [1958] gave a pair of curves which straddled the experimental results up to about 40,000 atm.

A polymorphic transition was found in iron at 0.13 megabars by Bancroft and others [1956]. The transition was detected by shock-wave techniques as a discontinuity in the pressure-relative volume function. Their observations were made at near room temperature, hence the transition they observed is not consistent with the α - γ transition observed in this work.

In evaluating this experimental data, it should be remembered that the iron used contained

correct value of c the error in a due to pressure errors was estimated to be ± 5000 atm.

The dotted curve was drawn by use of equation (1) in which $T_0 = 1805^\circ\text{K}$, the melting point of the pure metal. The melting points actually obtained were a few degrees below that of the pure metal probably due to the presence of about 0.6 per cent by weight of foreign atoms in the iron.

It is interesting to compare the slope of the fusion curve at the origin obtained from the

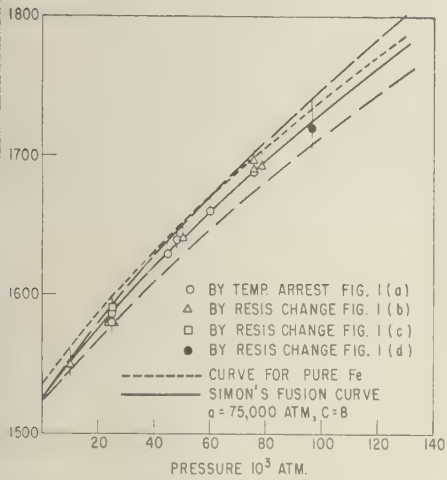


FIG. 5—Fusion curve for iron to 96,000 atm

experimental data in Simon's equation (1) with the slope obtained from the Clausius-Clapeyron equation. Differentiation of (1) gives

$$\frac{dP}{dT} = \frac{c \cdot a}{T_0} = \frac{8 \times 75,000}{1805} = 332 \frac{\text{atm}}{\text{deg}} \quad (2)$$

When allowance is made for the uncertainty in c , the error in dP/dT is about ± 40 atm/deg. The Clausius-Clapeyron equation gives

$$\frac{dP}{dT} = \frac{L}{T_0 \Delta V} = 330 \pm 30 \frac{\text{atm}}{\text{deg}} \quad (3)$$

When 3.63 kg cal/gm atom is used for the latent heat of fusion L [Awberry's unpublished work; see Simon, 1953] and 3 ± 0.5 per cent [Stott and

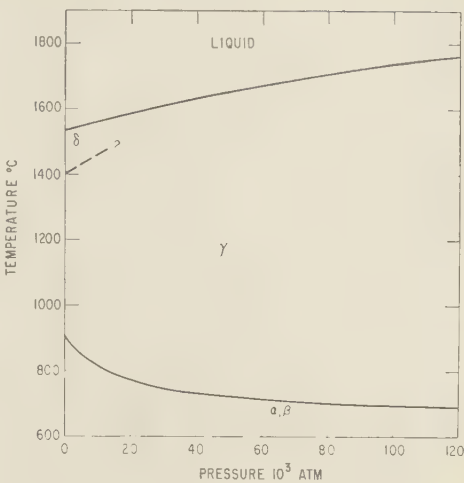


FIG. 6—Phase diagram for iron

Rendall, 1953; $\Delta V/V_i = 3 \pm 0.5\%$] is used for the relative volume change at the melting point.

A phase diagram for iron summarizing these results is shown in Figure 6.

DISCUSSION

Perhaps the point of greatest interest concerning the fusion curve for iron is its extrapolation to pressures equal to those in the core of the earth. Simon's equation for the fusion curve was used for this extrapolation and the resulting curve is shown in Figure 7 together with the curves proposed by Simon [1953] and Gilbarry [1956b, 1957]. The value of a used was 75,000 atm with curves also plotted for $a = 65,000$ and 79,000



FIG. 7—Extrapolated fusion curve for iron

to allow for possible errors in pressure calibration. The value of c used for the three curves was 8.

For a pressure of 1.4×10^6 atm corresponding to a depth of 2900 km [Bullen, 1947; Bullard, 1948, 1951] at the boundary between the core and the mantle, the extrapolated curve gives $2340 \pm 50^\circ\text{C}$ for the melting temperature of iron. However, if there are unsuspected phase changes in iron or if its electronic configuration is altered in such a manner that the iron in effect becomes a different element, the value of the melting point given would not necessarily be correct. Further, the iron may be alloyed so as to change its melting point somewhat. Alloying with nickel, however, would not likely produce a large change because the melting point of this metal to 100,000 atm has also been determined [Strong and Bundy, to be published] and its value extrapolated to 1.4×10^6 atm was 2200°C . Considering the great length of the extrapolation and the possible presence of impurities in the iron, perhaps an error of $\pm 200^\circ$ should be allowed in this determination.

Opinions about temperature for the base of the mantle cover the range from 2000 to $10,000^\circ\text{C}$. A good many of the arguments for various temperature choices are summarized by Gutenberg [1951], Bullen [1957], Gilvarry [1957], and others. The weight of opinion is for a temperature within the range of about 2000 to 4000°C . Recent work of Clark [1957a,b] on radiative transfer and of Lawson and Jamieson [1958] on radiative and exciton conduction indicated that heat transfer rates within the mantle may be substantially higher than was thought possible earlier. Thus, as expressed to the writer by G. C. Kennedy in a private communication, a temperature at the lower end of the range seems plausible. The melting point of iron found in this work, $2340 \pm 200^\circ\text{C}$, is consistent with the hypothesis of a liquid iron core and the concept of a lower temperature gradient within the mantle due to a rather high heat transfer rate through it. This melting point of iron represents the lower limit of temperature allowable for the core boundary.

A number of arguments have been advanced for the existence of an inner core of solid iron beginning at a depth of about 5000 km where the pressure is $\sim 3 \times 10^6$ atm. For these arguments the reader is referred to some of the original papers and review articles [Birch, 1940; Macel-

wane, 1951; Jacobs, 1953; Bullen, 1957]. Clearly the boundary between liquid and solid iron at the melting point of iron. A bold extrapolation of present data to 3×10^6 atm indicates a $2600 \pm 200^\circ\text{C}$ temperature at this point.

This $2600 \pm 200^\circ\text{C}$ temperature and the $2340 \pm 50^\circ\text{C}$ minimum at the core boundary imply a rather low temperature gradient through the core and mantle. Because no assurance can be given that the Simon extrapolation is valid at pressures much higher than 10^6 atm, these results require support from other evidence before they can be accepted.

The experimental fusion curve differs from the curves deduced by Simon and Gilvarry. Both their curves were drawn with the help of Simon's fusion equation, but their methods of selecting values for the constant c differed and neither was based on experimental fusion data for iron other than the value at zero pressure. To make a preliminary calculation of a Simon made use of the thermodynamic relation

$$a = \left(\frac{\partial u}{\partial V} \right)_T = \gamma \frac{C_V \cdot T}{V}$$

in which γ is the Grüneisen constant [1926] and T the melting point at zero pressure. He took a range of values for c from the fit of his equation to Bridgman's [1949] fusion curves to 12,000 atmospheres of Na, K, Rb, and Cs. The values of a and c so obtained were adjusted to a 150,000 atm and $c = 4$ so that the initial slope of the fusion curve calculated from equation (1) would agree with the Clausius-Clapeyron value of equation (3). Gilvarry [1956] derived the Simon fusion equation and an expression for c starting with a modified form of Lindeman's law for melting. He used a from equations (2) and (3) combined, after c was obtained from the expression

$$c = \frac{6\gamma + 1}{6\gamma - 2}$$

In (5), the Grüneisen constant γ , evaluated at the zero pressure melting point was used. Gilvarry gives as his choice of values for iron $a = 3.47 \times 10^6$ atm and $c = 1.9$.

Earlier, Salter [1954] had also derived Simon's equation from an equation of state for solid iron and Lindeman's law. His expression for c was exactly the same as Gilvarry's in equation (3).

evaluated a by equation (4). Salter did not apply his results to iron.

The experimental values of a and c differed widely from the calculated ones for iron as well as for three other Group VIII metals. Experimental c 's were much larger and the a 's smaller than their computed values from equations (4) and (5) in all cases. While it is evident that Simon's fusion equation and the Lindemann law both have a high content of physical truth, the evaluation of the Simon constants a and c still lack some essential features. This subject is discussed more fully elsewhere [Strong and Bundy, to be published].

Acknowledgments—The author is very grateful to Warren Moore and J. Schermerhorn for preparing the high purity iron in the various shapes used in his work, to Sherman Reed and Wilson Weir for their very careful work in constructing the samples, and to Roy E. Tuft for his valuable assistance in conducting the experiments.

REFERENCES

ANCROFT, D., E. L. PETERSON, AND S. MINSHALL, Polymorphism of iron at high pressure, *J. Appl. Phys.*, **27**, 291–298, 1956.

ARCH, F., α - γ transformation of iron at high pressures, and problem of earth's magnetism, *Am. J. Sci.*, **238**, 192–211, 1940.

ARTHUR, F., Elasticity and constitution of the earth's interior, *J. Geophys. Research*, **57**, 227–286, 1952.

RIDGMAN, P. W., *The physics of high pressure*, G. Bell and Sons, London, 445 pp., 1949.

RIDGMAN, P. W., The [electrical] resistance of 72 elements, alloys and compounds to 100,000 kg/cm², *Proc. Am. Acad. Arts Sci.*, **81**, 169–251, 1952.

ULLARD, E. C., The figure of the earth, *Monthly Notices Roy. Astron. Soc. Geophys. Suppl.*, **5**, 186–192, 1948; see also *Internal constitution of the earth*, chap. 13, B. Gutenberg, ed., 1951.

ULLEN, K. E., *An introduction to the theory of seismology*, Cambridge Univ. Press, 276 pp., 1947; see also *Internal constitution of the earth*, chap. 13, B. Gutenberg, ed., 1951.

ULLEN, K. E., *The planet earth*, Scientific American Book, Simon Schuster, New York, 167 pp., 1957.

LARK, S. P., Radiative transfer in the earth's mantle, *Trans. Am. Geophys. Union*, **38**, 931–938, 1957a.

LARK, S. P., Absorption spectra of some silicates in the visible and near infrared, *Am. Mineralogist*, **42**, 732–742, 1957b.

ARKEN, L. S., AND R. W. GURRY, *Physical chemistry* of metals, chap. 12, McGraw Hill, New York, 535 pp., 1953.

DEBOER, J., A discussion on theory of liquids: Theories of the liquid state, *Proc. Roy. Soc. London, A*, **215**, 4–28, 1952.

DOMB, C., The melting curve at high pressures, *Phil. Mag.*, **42**, 1316–1324, 1951.

GILVARRY, J., The Lindemann and Grüneisen laws, *Phys. Rev.*, **102**, 308–316; Grüneisen's law and the fusion curve at high pressure, 317–325; Equation of the fusion curve, 325–331, 1956a.

GILVARRY, J., Temperatures in the earth's interior, *Nature*, **178**, 1249–1250, 1956b.

GILVARRY, J., Temperatures in the earth's interior, *J. Atmospheric and Terrest. Phys.*, **10**, 84–95, 1957.

GRÜNEISEN, E., *Handbuch der Physik*, vol. 10, 1–59, Julius Springer, Berlin, 1926.

GUTENBERG, B., *Internal constitution of the earth*, chap. 7, Dover Publications, New York, 439 pp., 1951.

JACOBS, J. A., The earth's inner core, *Nature*, **172**, 297–298, 1953.

JAMIESON, J. C., Second annual report to ONR on high pressure research, Univ. of Chicago, Oct. 1958.

JEFFREYS, H., *Internal constitution of the earth*, chap. 2, B. Gutenberg, ed., Dover Publications, New York, 439 pp., 1951.

LAWSON, A. W., AND J. C. JAMIESON, Energy transfer in the earth's mantle, *J. Geol.*, **66**, 540–551, 1958.

MACEWANE, J. B., *Internal constitution of the earth*, chap. 10, B. Gutenberg, ed., Dover Publications, New York, 439 pp., 1951.

POWELL, R. W., The electrical resistivity of liquid iron, *Phil. Mag.*, **44**, 772–775, 1953.

RALSTON, O. C., Iron oxide reduction equilibria—a critic from the standpoint of the phase rule and thermodynamics, *Bull. U. S. Bur. Mines* **296**, 326 pp., 1929.

SALTER, L., The Simon melting equation, *Phil. Mag.*, **45**, 369–384, 1954.

SIMON, F. E., AND G. GLATZEL, Remarks on the fusion-pressure curve, *Z. anorg. u. allegem. Chem.*, **178**, 309–316, 1929.

SIMON, F. E., Range of stability of the fluid state, *Trans. Faraday Soc.*, **33**, 65–73, 1937.

SIMON, F. E., The melting of iron at high pressures, *Nature*, **172**, 746–747, 1953.

STOTT, V. H., AND J. H. RENDALL, The density of molten iron, *J. Iron Steel Inst. London*, **175**, 374–378, 1953.

STRONG, H. M., AND F. P. BUNDY, The melting points of four Group VIII metals to 100,000 atmospheres (to be published).

TAMMANN, G., AND G. BANDEL, Heat content and specific volume of iron-carbon alloys, *Arch. Eisenhüttenw.*, **7**, 571–578, 1934.

(Manuscript received February 19, 1959.)

On the Attenuation of Small-Amplitude Plane Stress Waves in a Thermoelastic Solid

SVEN TREITEL*

Department of Geology and Geophysics
Massachusetts Institute of Technology
Cambridge, Massachusetts

Abstract—All real materials have a finite thermal conductivity. This means that stress waves propagating through any physically real solid suffer energy losses due to heat conduction. The equations of motion and of temperature for an elastic solid with a finite thermal conductivity are derived with the aid of the irreversible form of the second law of thermodynamics. Their solution for frequencies of physical interest shows that the attenuation coefficient of a stress wave traveling in such a thermoelastic solid is proportional to the second power of the frequency.

Introduction—Although the literature dealing with the propagation of small-amplitude disturbances in perfectly elastic solids is quite extensive, few of the treatments published to date include the effect of a finite thermal conductivity upon the propagation mechanism. When a perfectly insulated solid element is compressed elastically by an applied stress $P(\epsilon)$, where $P(\epsilon)$ is a linear function of the elastic strain ϵ , it will return to its original state as soon as the stress has been removed. Since the element is insulated, there is no outward flux of heat, and the process is therefore adiabatic. Equivalently, one may say that the thermal conductivity of the medium, γ , is zero. No net entropy has been generated in this process, which is thus reversible. If $\gamma = \infty$, then any heat produced during compression will be conducted away instantaneously, so that there is no net rise of temperature in the element. This process is then isothermal, but it is no longer isentropic with respect to the element's environment. No physical medium has either a zero or an infinite thermal conductivity, and therefore any actual deformation of a solid must involve a net outward flux of heat and, consequently, the creation of irreversible entropy. In particular, the entropy which is thus generated will be in addition to that produced by any viscous or other dissipative mechanism. When speaking of an *elastic*

deformation, one should specify that the thermal conductivity of the medium is zero; otherwise the deformation process is not reversible, as is usually postulated. It is obvious, then, that any rigorous propagation theory must take thermal phenomena into account. Since the compression of a solid medium exhibiting a finite thermal conductivity involves the creation of irreversible entropy, a stress wave propagating through this medium will undergo progressive decay as it loses its energy in the form of heat. In accordance with prior treatments of this general subject [Synge, 1955; Biot, 1956; Hunt, 1957], a perfectly elastic medium of finite thermal conductivity will be termed a "thermoelastic solid."

Portions of the material contained in the following sections are not new; however, the writer feels that a thermodynamically more rigorous approach of the problem, such as is attempted here, will eliminate much of the confusion that currently exists in the pertinent literature.

Previous work—Markham and others [1951], Truesdell [1953], and Hunt [1957], have made exhaustive studies of sound absorption in fluids in the presence of viscosity and heat conduction. Synge [1955] has derived an equation of motion for a fluid exhibiting both viscosity and finite thermal conductivity. His work is based on that of Eckart [1940], and is thus thermodynamically rigorous, since it considers the production of irreversible entropy. Synge's equations of motion and of temperature (see below) contain non-

* Present affiliation: Cuba California Oil Company, Havana, Cuba.

linear terms, but these were dropped in his analysis. Solutions of the form

$$T = T_1 \exp j(\sigma x + \omega t) \quad (1a)$$

$$u = u_1 \exp j(\sigma x + \omega t) \quad (1b)$$

were assumed, and subsequent substitution of these relations into the equations of motion and temperature yielded a secular equation in the generally complex wave number σ . Here T is temperature, u is displacement, ω is circular frequency, and x and t are space and time variables, respectively. T_1 and u_1 are real constants which may be found explicitly by satisfaction of prescribed boundary conditions.

Synge did not solve his secular equation, which is biquadratic in σ . Lessen [1957] has solved this equation by approximation methods but has not investigated the frequency dependence of the attenuation coefficient α , where α is given by

$$\alpha = g m(\sigma) = g m(\nu + j\alpha) \quad (2)$$

and ν is the real part of the complex wave number σ .

Biot [1956] has developed a theory of thermoelasticity based on thermodynamical arguments. His approach is less general than that of Synge, since his actual equations are based on the reversible forms of the first and second laws of thermodynamics.

Deresiewicz [1957] has made use of Biot's equations in a study of plane wave attenuation in a thermoelastic solid. He found his secular equation to be algebraically intractable and proceeded to show that an assumed damping relation

$$\alpha = (\text{const}) \omega^2 \quad (3)$$

satisfies the secular equation for low frequencies.

The thermoelastic solid—The general form of the equation of state of a solid may be written in the form

$$dP = V \left(\frac{\partial P}{\partial V} \right)_T \frac{dV}{V} + \beta k_T dT \quad (4)$$

where P is pressure, V is specific volume, and β and k_T are the coefficients of thermal expansion and isothermal bulk modulus, respectively.

If one considers displacement in the x direction

only, the equation for conservation of momentum is

$$\rho \frac{\partial^2 u}{\partial t^2} = \frac{\partial P}{\partial x} \quad (5)$$

where $\rho = 1/V$ = density. In the one-dimensional case, (4) and (5) can be easily shown to yield the thermoelastic equation of motion

$$\rho \frac{\partial^2 u}{\partial t^2} = (\lambda + 2\mu)_T \frac{\partial^2 u}{\partial x^2} - \beta k_T \frac{\partial T}{\partial x} \quad (6)$$

where the infinitesimal strain $\epsilon = dV/V = \partial u/\partial x$ and λ, μ are the *isothermal Lamé* elastic parameters. Equation (6) contains two unknowns, the temperature T and the displacement u . Accordingly, we must seek a further relationship between these quantities.

The first and second laws of thermodynamics may be combined to yield [see, for example, Allis and Herlin, 1952, p. 105]

$$T_0 \frac{ds}{V} = c_e \frac{dT}{V} + T_0 k_T \beta \frac{dV}{V} \quad (7)$$

Here s is entropy per unit mass, c_e is specific heat at constant strain, and T_0 is equilibrium temperature. Differentiating with respect to time and again letting $1/V = \rho$ and $dV/V = \epsilon$, one has

$$\frac{\partial T}{\partial t} = \frac{T_0}{c_e} \frac{\partial s}{\partial t} - \frac{T_0 k_T \beta}{\rho c_e} \frac{\partial \epsilon}{\partial t} \quad (8)$$

The continuity relation for entropy [Denbigh, 1951] is

$$\rho \frac{\partial s}{\partial t} + \text{div } \mathbf{S} = \frac{\partial S_{irr}}{\partial t} \quad (9)$$

where \mathbf{S} is the entropy flux vector and S_{irr} the net entropy created in an *irreversible* process. The first term of (9) may be regarded as the total rate of increase of entropy in a given region, $\text{div } \mathbf{S}$ the rate of entropy outflow, and $\partial S_{irr}/\partial t$ the rate of creation of entropy per unit volume per unit time, which is always positive by the second law of thermodynamics. If heat is transferred by conduction alone, it has been shown [Bridgman, 1941; Denbigh, 1951] that

$$\frac{\partial S_{irr}}{\partial t} = \frac{\gamma}{T^2} (\nabla T)^2 \quad (10)$$

but

$$\mathbf{S} = \frac{\mathbf{Q}}{T} = -\frac{\gamma}{T} \nabla T \quad (11)$$

where \mathbf{Q} is the heat flux vector and $\mathbf{Q} = -\gamma \nabla T$ Fourier's heat conduction law. Substitution of (10) and (11) into (9) gives

$$\frac{\partial s}{\partial t} - \frac{\gamma}{T} \nabla^2 T + \frac{\gamma}{T^2} (\nabla T)^2 = \frac{\gamma}{T^2} (\nabla T)^2 \quad (12)$$

which, after some rearrangement, becomes

$$\frac{T_0}{c_e} \frac{\partial s}{\partial t} = \frac{\gamma}{c_e \rho} \nabla^2 T = \kappa \nabla^2 T \quad (13)$$

where κ is thermal diffusivity, and where we have replaced T by the equilibrium temperature $T_0(T = T_0 + \Delta T)$, a satisfactory approximation for small ΔT . Relation (13) may be substituted into (8) to yield the second desired equation in (T, u) , so that one has finally the system

$$\frac{\partial^2 u}{\partial t^2} = \frac{k_T + 4/3\mu}{\rho} \frac{\partial^2 u}{\partial x^2} - \frac{\beta k_T}{\rho} \frac{\partial T}{\partial x} \quad (14a)$$

$$\frac{\partial T}{\partial t} = \kappa \frac{\partial^2 T}{\partial x^2} - \frac{k_T \beta T_0}{\rho c_e} \frac{\partial^2 u}{\partial x \partial t} \quad (14b)$$

where we have replaced $(\lambda + 2\mu)_T$ by $(k_T + 4/3\mu)$ in (14a). Differentiating (7) with respect to the space variable x and rearranging terms, gives

$$\frac{\partial T}{\partial x} = \frac{T_0}{c_e} \frac{\partial s}{\partial x} - \frac{T_0 k_T \beta}{\rho c_e} \frac{\partial^2 u}{\partial x^2} \quad (15)$$

which, when combined with (14a) becomes

$$\begin{aligned} \frac{\partial^2 u}{\partial t^2} &= \left[\frac{k_T + 4/3\mu}{\rho} + T_0 \left(\frac{k_T \beta}{\rho} \right)^2 \right] \frac{\partial^2 u}{\partial x^2} \\ &\quad - \frac{\beta k_T T_0}{\rho} \frac{\partial s}{\partial x} \end{aligned} \quad (16)$$

The adiabatic bulk modulus k_s is related to the isothermal modulus by

$$k_s = k_i + \frac{T_0}{\rho c_e} (\beta k_T)^2 \quad (17)$$

see, for example, Mason, 1957], so that (16) may be written

$$\frac{\partial^2 u}{\partial t^2} = \frac{k_s + 4/3\mu}{\rho} \frac{\partial^2 u}{\partial x^2} - \frac{\beta k_T T_0}{\rho} \frac{\partial s}{\partial x} \quad (18)$$

The equations of motion (14a) and (18) thus express the same relationship, except that the former has temperature and the latter specific entropy as an independent variable. Now let us set $\partial T/\partial x = 0$ in (14a). In this case one has

$$\frac{\partial^2 u}{\partial t^2} = \frac{1}{V_{P,T}^2} \frac{\partial^2 u}{\partial x^2} \quad (19)$$

where

$$V_{P,T} = \sqrt{\frac{k_T + 4/3\mu}{\rho}} \quad (20)$$

defines the *isothermal* compressional, or P-wave velocity. If we set $\partial s/\partial x = 0$ in (18),

$$\frac{\partial^2 u}{\partial t^2} = \frac{1}{V_{P,S}^2} \frac{\partial^2 u}{\partial x^2} \quad (21)$$

where

$$V_{P,S} = \sqrt{\frac{k_s + 4/3\mu}{\rho}} \quad (22)$$

defines the *adiabatic* P-wave velocity. Since $k_s > k_T$ by (17), $V_{P,S}$ is always greater than $V_{P,T}$. The solutions of equations (19) and (22) are well known; in particular, neither model can give rise to attenuation, since neither contains dissipative terms. The isothermal and adiabatic cases correspond respectively to infinite and zero thermal conductivity of the medium.

It is evident from the foregoing that dissipation can only arise in a medium described by relations (14a, b). Accordingly, we next turn our attention to solutions of this system. Substitution of assumed solutions (1a, b) into (14a, b) yields

$$-\left(\frac{k_T \beta T_0}{\rho c_e} \sigma \omega \right) u + (\kappa \sigma^2 + j\omega) T = 0 \quad (23a)$$

$$(V_{P,T}^2 \sigma^2 - \omega^2) u + \left(j\sigma \frac{\beta k_T}{\rho} \right) T = 0 \quad (23b)$$

If non-trivial solutions of (23a,b) exist, the determinant of coefficients must vanish, and we thus derive the secular equation

$$(V_{P,T}^2 \kappa) \sigma^4 + (j\omega V_{P,S}^2 - \omega^2 \kappa) \sigma^2 - j\omega^3 = 0 \quad (24)$$

which is a bi-quadratic in the complex wave number σ , where $\sigma = \nu + j\alpha$, and in which $V_{P,S}$ has been inserted by virtue of (16). Its solution

is obtainable by standard, although quite laborious, algebra that is outlined in the Appendix of this paper. As is shown there, provided that

$$\omega \ll \frac{V_P^2}{\kappa} \quad (25)$$

where V_P is the compressional wave velocity, the attenuation coefficient α is given by

$$\alpha = \frac{1}{8} \frac{\kappa \omega^2}{V_P^3} \quad (26)$$

We have thus deduced the important result that the thermoelastic attenuation coefficient α is proportional to the square of the circular frequency ω for all ω satisfying (25).

In order to gain an idea of the order of magnitude of thermoelastic damping in actual solids, we consider two examples: first, copper, a medium of high thermal diffusivity κ ; and secondly, rock, which has a low value of κ .

For copper, $\kappa = 1.14 \text{ cm}^2/\text{sec}$ and $V_P = 4.6 \times 10^8 \text{ cm/sec}$. Thus equation (26) is applicable when

$$\omega \ll 1.8 \times 10^{11} \text{ rad/sec (copper)}$$

In the case of rock, $\kappa = 0.01 \text{ cm}^2/\text{sec}$, $V_P = 0(5 \times 10^8 \text{ cm/sec})$, and (26) holds, provided that

$$\omega \ll 2.5 \times 10^{13} \text{ rad/sec (rock)}$$

These values clearly show that the approximate formula (26) is applicable for all frequencies of physical interest. The attenuation coefficient α , plotted according to (26) as a function of ω for copper and rock, is shown in Figure 1.

Conclusions—Knopoff and MacDonald [1958] have made a thorough review of available experimental data on the frequency dependence of the attenuation coefficient α , and they were able to conclude that in most instances, with the notable exception of some metals and plastics, α was a linear function of ω . In these cases thermoelastic damping is either absent or too minute to permit detection. Nevertheless, a number of workers [see, for example, Zener, 1948; Kolsky, 1953] have reported measurements on metals that do reveal an ω^2 dependence of α . The latter results have been frequently explained in terms of the well-known theory of visco-elasticity, which also yields an ω^2 dependence of the attenuation coefficient [Kolsky, 1953]. However, the

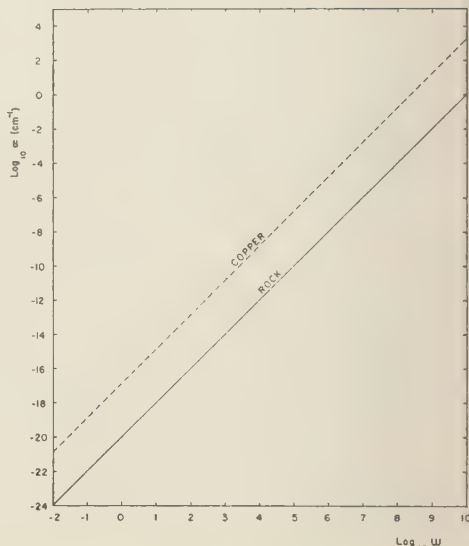


FIGURE 1

Fig. 1—The thermoelastic attenuation coefficient α as a function of circular frequency for copper and rock

question of solid viscosity is quite controversial and numerical values proposed for different materials by various workers differ by several orders of magnitude. The thermoelastic model examined in this paper, on the other hand, provides us with a plausible explanation for observed ω^2 damping in terms of the well-known quantities, κ (thermal diffusivity) and V_P (compressional wave velocity). Perhaps both mechanisms are actually operative; in any event, the question can only be settled by measurement of a much more refined character than have been carried out to date.

Acknowledgments—The writer wishes to thank Gordon J. F. MacDonald, now at the Institute of Geophysics, University of California, Los Angeles, for helpful comments made in connection with this work, which forms a part of the author's doctoral dissertation submitted to the Department of Geology and Geophysics at the Massachusetts Institute of Technology.

APPENDIX

In order to derive equation (26) in the text, we proceed as follows:

Solving (24) as an ordinary quadratic in σ^2 , we have

$$\sigma^2 = \frac{\omega}{2V_{P,T}\kappa} [(\omega\kappa + C_1) + j(D_1 - V_{P,S}^2)] \quad (\text{A1})$$

in which

$$C_1, D_1 = \left\{ \frac{V_{P,S}^4 - \omega^2\kappa^2}{2} \cdot \left[\sqrt{1 + \left(\frac{2\omega\kappa \Delta V_P}{V_{P,S}^4 - \omega^2\kappa^2} \right)} \pm 1 \right] \right\}^{1/2} \quad (\text{A2})$$

and

$$\Delta V_P = 2V_{P,T}^2 - V_{P,S}^2$$

Now,

$$\sigma^2 = \nu^2 - \alpha^2 + 2j\nu\alpha \quad (\text{A3})$$

If (A3) is substituted into (A1) and real and imaginary parts equated, one has the system

$$\begin{aligned} \nu^2 - \alpha^2 &= \frac{\omega(\omega\kappa + C_1)}{2V_{P,T}\kappa} \\ \nu\alpha &= \frac{\omega(D_1 - V_{P,S}^2)}{4V_{P,T}\kappa} \end{aligned} \quad (\text{A4})$$

If we solve this system for α , we obtain

$$\begin{aligned} \alpha &= \left\{ \frac{\omega(C_1 + \omega\kappa)}{4V_{P,T}\kappa} \cdot \left[\sqrt{1 + \left(\frac{D_1 - V_{P,S}^2}{C_1 + \omega\kappa} \right)^2} - 1 \right] \right\}^{1/2} \end{aligned} \quad (\text{A5})$$

Equation (A5), in conjunction with expressions (A2), constitutes the exact solution of damping in the thermoelastic solid.

However, we may write with slight error

$$V_{P,T} \approx V_{P,S} = V_P$$

and thus $\Delta V_P \approx V_P^2$. Furthermore, the second term underneath the radical in (A2) can then be written

$$\frac{2\omega\kappa \Delta V_P}{V_{P,S}^4 - \omega^2\kappa^2} = \frac{\frac{2\omega\kappa}{V_{P,S}^2}}{1 - \frac{\omega^2\kappa^2}{V_{P,S}^4}} \quad (\text{A6})$$

When $V_{P,S}^4 \gg \omega^2\kappa^2$ or, equivalently, when $\omega \ll V_{P,S}^2/\kappa$ (see Eq. 25), repeated application of the binomial expansion theorem to (A2) and (A5), retaining first order terms only, can be shown to lead to the approximate form (26). The algebra involved is laborious and will be omitted here for the sake of brevity.

REFERENCES

- ALLIS, W. P., AND M. A. HERLIN, *Thermodynamics and statistical mechanics*, McGraw-Hill Book Co., New York, 1952.
- BIOT, M. A., Thermoelasticity and irreversible thermodynamics, *J. Appl. Phys.*, **27**, 240-253, 1956.
- BRIDGMAN, P. W., *The nature of thermodynamics*, Harvard University Press, 1941.
- DENBIGH, K. G., *The thermodynamics of the steady state*, Methuen's Monographs on Chemical Subjects, London, 1951.
- DEREŚCIEWCZ, H., Plane waves in a thermoelastic solid, *J. Acoust. Soc. Am.*, **29**, 204-209, 1957.
- ECKART, CARL, The thermodynamics of irreversible processes, I—The simple fluid, *Phys. Rev.*, **58**, 267-269, 1940.
- HUNT, F. V., Propagation of sound in fluids, in *American Institute of Physics handbook*, pp. 3-25 to 3-56, 1957.
- KNOPOFF, L., and G. J. F. MACDONALD, The attenuation of small amplitude stress waves in solids, *Rev. Modern Phys.*, **30**, 1178-1192, 1958.
- KOLSKY, H., *Stress waves in solids*, Clarendon Press, Oxford, 1953.
- LESSEN, M., The motion of a thermoelastic solid, *Quart. Appl. Math.*, **15**, 105, 1957.
- MARKHAM, J. J., R. T. BEYER, AND R. B. LINDSAY, Absorption of sound in fluids, *Rev. Modern Phys.*, **23**, 353-408, 1951.
- MASON, W. P., Acoustic properties of solids, in *American Institute of Physics handbook*, pp. 3-74 to 3-88, 1957.
- SYNGE, J. L., The motion of a viscous fluid conducting heat, *Quart. Appl. Math.*, **13**, 271-278, 1955.
- TRUESELL, C. J., *J. Rational Mech. Anal.*, **2**, 643, 1953.
- ZENER, C., *Elasticity and anelasticity of metals*, Univ. of Chicago Press, 1948.

(Manuscript received February 27, 1959.)

Method for Obtaining the Optical Properties of Large Bodies of Water*

J. E. TYLER, W. H. RICHARDSON, AND R. W. HOLMES

*Scripps Institution of Oceanography, University of California
La Jolla, California*

Abstract—Radiative transfer within a hydrosol such as ocean or lake water can best be described by means of the inherent and apparent optical properties of the hydrosol. Equipment for obtaining the important optical properties of large bodies of water is described and a method for computing six optical properties from measurements of radiance distribution is given.

The optical properties of Lake Pend Oreille are computed for one condition of the lake and for one narrow region of the spectrum. The experimental values serve to substantiate certain theoretical relationships between the inherent and the apparent optical properties.

Introduction—In order to deal exactly with problems involving the penetration and transfer of light through water, it is necessary to specify not only the magnitudes of the optical properties but also the depth at which they are measured and whether they depend on the downwelling (−) or upwelling (+) stream of radiant flux. This is necessary because some of the optical properties of homogeneous water vary with depth, although the variation may be small. In order to be exact in meaning, the notation for the optical property or function is followed by the symbol (z) which means we are speaking of the property at a specific depth, z , and with the symbol (−) referring to properties associated with the downwelling stream of radiant flux or (+) referring to the upwelling stream of radiant flux.

In general the variation of the properties tends to diminish with increasing depth and with increasing cloud cover and overcast. When the water is nonhomogeneous the usual variation in depth of the optical properties may be obscured by the further variations caused by its nonhomogeneity.

List of symbols—The notation used in this paper is as follows:

$N(z, \theta, \phi)$ Field radiance at depth z in direction (θ, ϕ)

* This paper is based on research which has been supported by the Bureau of Aeronautics and the Bureau of Ships, U. S. Navy.

N_r/N_0	Ratio of the radiance of a beam after passage through a water path of length r to its initial radiance
$h(z, -)$	Downwelling scalar irradiance at depth z
$H(z, -)$	Downwelling irradiance at depth z
$h(z, +)$	Upwelling scalar irradiance at depth z
$H(z, +)$	Upwelling irradiance at depth z
T_r	Beam transmittance for path of length r
$s(z)$	Total scattering function* at depth z
$D(z, -)$	Downwelling distribution function
$D(z, +)$	Upwelling distribution function
$R(z, -)$	Reflectance of downwelling light by a hypothetical horizontal plane in the water at depth z
$K(z, -)$	Attenuation function for downwelling irradiance
$K(z, +)$	Attenuation function for upwelling irradiance
$a(z)$	Volume absorption function at depth z^*
$\alpha(z)$	Volume attenuation function at depth z^*

* In homogeneous media the term "function" as applied to these properties is replaced by the term "coefficient," since in homogeneous media these properties do not change with depth. The other functions generally vary with depth even in homogeneous media.

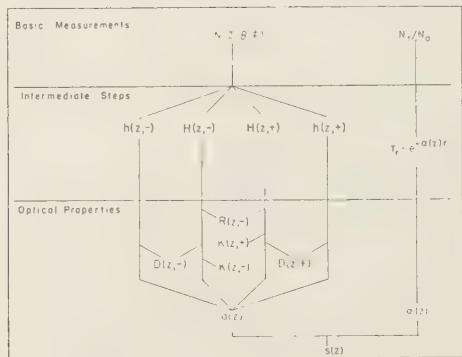


FIG. 1—Flow chart of optical constants and properties. The computational route is found by following the connecting lines in an upward direction from the desired optical constant or function

The important optical properties considered in this paper are shown in Figure 1 which also indicates in flow chart form one possible method of their determination from two basic physical measurements which were made at Lake Pend Oreille, Idaho [Tyler, 1958]. The two measurements were (a) radiance distribution as a function of depth, $N(z, \theta, \phi)$, and (b) beam transmittance, T_r .

Measurement of radiance distribution—The instrument used for the measurement of radiance distribution is shown in Figure 2 [Duniley and others, 1955]. When in use, this instrument is suspended on a single cable and powered by an electric cable looped into the underside at the vertical axis of rotation. Rotation about the vertical axis (azimuth position) is controlled by means of a servo system consisting of a gyrosyn compass assembly in the instrument with control transformer and indicator on the main control panel. The error signal resulting from an azimuth mismatch between the control transformer and the gyro heading is used to drive a propeller which rotates the instrument so as to minimize the error signal and thus keep the instrument oriented in azimuth. The optical system is designed to accept light through a cone of acceptance having apex angle of 6.6° , and the instrument thus measures relative values of the physical quantity radiance in the direction specified by θ (the angle from the zenith) and ϕ (the azimuth angle).

Data obtained with this instrument and the method of integration outlined in the next sections were used to compute the apparent optical properties $R(z, | -)$, $K(z, -)$, $K(z, +)$, $D(z, -)$, and $D(z, +)$ for Lake Pend Oreille and also the inherent optical property $a(z)$ (volume absorption function).

Computation of $H(z, -)$ and $H(z, +)$ from $N(z, \theta, \phi)$ —It is clear from Figure 1 that the functions $H(z, -)$, $H(z, +)$, $h(z, -)$, and $h(z, +)$ are essential to the determination of the functions $R(z, -)$, $K(z, -)$, $K(z, +)$, $a(z)$, $D(z, -)$, and $D(z, +)$. The basis for obtaining irradiance over a horizontal plane from radiance distribution data is expressed in equation (1)

$$H(z, \pm) = \int_{\pm} N(z, \theta, \phi) |\cos \theta| d\Omega \quad (1)$$

where \int_{\pm} signifies integration over the upper (-) or lower (+) hemisphere to obtain respectively $H(z, -)$ or $H(z, +)$. Stated precisely

$$\int_{-} = \int_{\theta=0}^{\pi/2} \int_{\phi=0}^{2\pi} \quad \int_{+} = \int_{\theta=\pi/2}^{\pi} \int_{\phi=0}^{2\pi}$$

$$d\Omega = \sin \theta d\theta d\phi$$

In order to perform the numerical integration expressed in (1) and thus obtain numerical values for $H(z, -)$ and $H(z, +)$, the radiance distribution solid was enclosed in a spherical grid divided by equal increments of θ and ϕ . The values of radiance at the centers of these increments were then weighted and summed in accordance with (2).

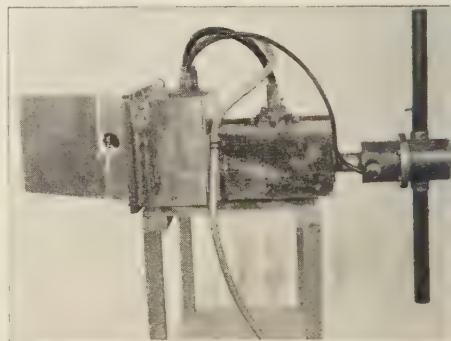


FIG. 2—Underwater photometer showing the radiance measuring head on the right and azimuth control propeller on the left

The mechanics of the integration process at given depth can be expressed in symbols as

$$H = \sum_{i=0}^m \sum_{j=0}^n N_{ij} \Delta\Omega_i' \quad (2)$$

here N_{ij} is the value of the radiance at the center of the increment specified by i in the θ direction and j in the azimuth direction. $N_{0j} = N_0$ for $j = 0, 1, \dots, n$; since the radiance in the zenith direction does not change with azimuth; and where the $\Delta\Omega_i'$ are weighted solid angles defined for the indicated zones ($i = 0, 1, \dots, m$) as follows

$$\Omega_i' = \sin \theta_i \cos \theta_i \Delta\theta \Delta\phi,$$

for $i = 2, 3, \dots, m - 2$

$$\Omega_0' = \Delta\Omega_m'$$

$$= \frac{3}{8} \sin \left(\frac{\Delta\phi}{4} \right) \cos \left(\frac{\Delta\phi}{4} \right) \Delta\theta \Delta\phi$$

$$\begin{aligned} \Omega_1' = \Delta\Omega_{m-1}' &= \left[\sin \Delta\theta \cos \Delta\theta \right. \\ &\quad \left. + \frac{\sin \left(\frac{\Delta\phi}{4} \right) \cos \left(\frac{\Delta\phi}{4} \right)}{8} \right] \Delta\theta \Delta\phi \end{aligned}$$

and

$$m = \frac{\pi}{2 \Delta\theta}, \quad n = \frac{2\pi}{\Delta\phi} - 1$$

$$i = 0, 1, \dots, m \quad j = 0, 1, \dots, n$$

$$\theta_i = i \Delta\theta \quad \phi_j = j \Delta\phi$$

The preceding equation (2) may be used for either $H(z, -)$ or $H(z, +)$. Figure 3 shows the geometrical arrangement and identifies centroid values of radiance for $H(z, -)$. To use (2) for the determination of $H(z, +)$, reflect the sphere in its equatorial plane.

Computation of $h(z, -)$ and $h(z, +)$ from $N(z, \theta, \phi)$ —The procedure for obtaining scalar radiance from radiance distribution data is expressed by

$$h(z, \pm) = \int_{\omega} N(z, \theta, \phi) d\Omega \quad (3)$$

The mechanics of numerical integration to obtain hemispherical scalar irradiance, $h(z, -)$,

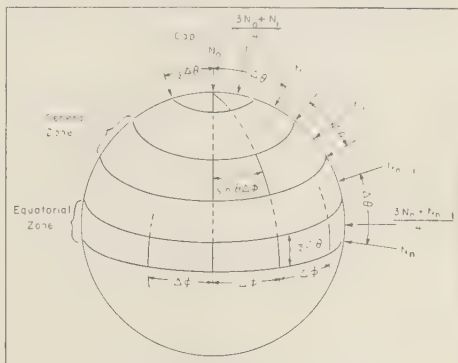


FIG. 3—Spherical grid used to perform the numerical integration to obtain irradiance and spherical irradiance. For simplicity, only three general zones are shown.

$h(z, \pm)$, are expressed in (4) in which the same general notation is employed as in (2) and Figure 3 and is used in the same general manner.

$$h_{(\text{hemispherical})} = \sum_{i=0}^m \sum_{j=0}^n N_{ij} \Delta\Omega_i \quad (4)$$

where

$$N_{0,i} = N_{0,0}$$

and where the $\Delta\Omega_i$ are weighted solid angles defined for the indicated zones ($i = 0, 1, \dots, m$) as follows

$$\Delta\Omega_i = \sin \theta_i \Delta\theta \Delta\phi,$$

for $i = 2, 3, \dots, m - 2$

$$\Delta\Omega_0 = \frac{3}{8} \sin \left(\frac{\Delta\theta}{4} \right) \Delta\theta \Delta\phi$$

$$\Delta\Omega_1 = \left[\sin \Delta\theta + \frac{\sin \left(\frac{\Delta\theta}{4} \right)}{8} \right] \Delta\theta \Delta\phi$$

$$\Delta\Omega_{m-1} = \left[\cos \Delta\theta + \frac{\cos \left(\frac{\Delta\theta}{4} \right)}{8} \right] \Delta\theta \Delta\phi$$

$$\Delta\Omega_m = \frac{3}{8} \cos \left(\frac{\Delta\theta}{4} \right) \Delta\theta \Delta\phi$$

In the numerical evaluation of (2) and (4) each hemisphere was divided into 8 increments

of $\Delta\theta$ and 2 increments of $\Delta\theta/2$ and into 18 increments of $\Delta\phi$. Substituting the values of

$$\Delta\theta = \pi/2m = 10^{\circ} = 0.1745 \text{ radians}$$

$$\Delta\phi = \pi/n = 20^{\circ} = 0.3491 \text{ radians}$$

into (2) and (4) a table of factors, $\Delta\Omega$ and $\Delta\Omega'$ was obtained (Table 1).

TABLE 1—Summation factors for computation of irradiance and scalar irradiance

θ_i (degrees)		$\Delta\Omega_i$	$\Delta\Omega_i'$
0 and 180		0.000 966	0.000 966
10	170	0.010 918	0.010 747
20	160	0.020 835	0.019 579
30	150	0.030 461	0.026 379
40	140	0.039 160	0.029 997
50	130	0.046 665	0.029 997
60	120	0.052 758	0.026 379
70	110	0.057 247	0.019 579
80	100	0.067 603	0.010 747
90	90	0.022 824	0.000 996

For each hemisphere the sum of the 18 values of N_{ij} for each i was multiplied by the corresponding $\Delta\Omega_i'$ or $\Delta\Omega_i$, and the sum of the results gave the irradiance or scalar irradiance, respectively, for the hemisphere.

Computation of optical properties—In modern two-flow theory the functions which describe the interaction of light with water must, in general, be associated with the specific stream to which they apply [Preisendorfer, 1958a]. For horizontally stratified scattering-absorbing media (for example, large bodies of water), there will be one set of functions for the downwelling stream (identified by the symbol $-$) and another set of functions for the upwelling stream (identified by the symbol $+$). The functions which have been computed in this experiment from the radiance distribution are shown in Table 2.

Computation of $K(z, -)$ and $K(z, +)$ —The attenuation functions, $K(z, -)$ and $K(z, +)$ for natural downwelling and upwelling light in the water are determined by the equation

$$K(z, \pm) = \frac{\ln \frac{H(z - \Delta z/2, \pm)}{H(z + \Delta z/2, \pm)}}{\Delta z} \quad (5)$$

TABLE 2—Optical properties associated with water

Item	Downwelling	Upwelling
Attenuation functions	$K(z, -)$	$K(z, +)$
Volume absorption functions	$a(z)$	$a(z)$
Reflectances of a hypothetical horizontal plane	$R(z, -)$	$\begin{cases} R(z, +) \\ 1/R(z, -) \end{cases}$
Distribution functions	$D(z, -)$	$D(z, +)$

This equation (5) is derived from the precise definition of $K(z, \pm)$,

$$H(z, \pm) = H(0, \pm)$$

$$\cdot \exp \left[- \int_0^z K(z', \pm) dz' \right]$$

where the primed symbols denote dummy variables of integration. Because the measurement of $H(0, \pm)$ is difficult, the definition of $K(z, \pm)$ can be restated for a depth difference Δz .

$$H\left(z + \frac{\Delta z}{2}, \pm\right) = H\left(z - \frac{\Delta z}{2}, \pm\right)$$

$$\cdot \exp \left[- \int_{z - \Delta z}^{z + \Delta z} K(z', \pm) dz' \right]$$

If Δz is sufficiently small, $K(z, \pm)$ may be treated as being constant over the interval $z - \Delta z/2, z + \Delta z/2$ and

$$\int_{z - \Delta z/2}^{z + \Delta z/2} K(z', \pm) dz' = K(z, \pm) \int_{z - \Delta z/2}^{z + \Delta z/2} dz'$$

$$= K(z, \pm) \Delta z = \ln \left[\frac{H\left(z - \frac{\Delta z}{2}, \pm\right)}{H\left(z + \frac{\Delta z}{2}, \pm\right)} \right]$$

The attenuation functions $K(z, \pm)$ generally vary with depth. Their values at any given depth z are determined by the operational procedure summarized in (5), which requires knowledge of the irradiances just above and just below z .

Computation of $R(z, -)$ —The reflectance $R(z, -)$ of a hypothetical horizontal plane i

ater with respect to the downwelling flux at a depth z below the surface was computed from the defining equation

$$R(z, -) = \frac{H(z, +)}{H(z, -)} \quad (6)$$

Note that

$$R(z, +) = \frac{H(z, -)}{H(z, +)}$$

Computation of distribution functions—Distribution functions $D(z, \pm)$ are measures of the directional distribution of the upwelling and downwelling radiance. They are defined [Preisendorfer, 1958a] by the equations

$$D(z, \pm) = \frac{h(z, \pm)}{H(z, \pm)} \quad (7)$$

Computation of the absorption function—The value of the absorption function $a(z)$ was determined from the equation

$$(z) = \frac{\ln \left[\frac{\bar{H}\left(z - \frac{\Delta z}{2}, +\right)}{\bar{H}\left(z + \frac{\Delta z}{2}, +\right)} \right] \bar{H}(z, +)}{\Delta z h(z)} \quad (8)$$

where $\bar{H}(z, +) = H(z, +) - H(z, -)$, net upwelling irradiance, and $h(z) = h(z, +) + h(z, -)$, the scalar irradiance. Equation (8) is developed as follows. The operational definition of the absorption function $a(z)$ is

$$a(z) = \frac{1}{h(z)} \times \frac{d\bar{H}(z, +)}{dz} \quad (9)$$

[Preisendorfer, 1957]

Now, by definition of $\bar{K}(z)$, we have

$$\frac{d\bar{H}(z, +)}{dz} = -\bar{H}(z, +)\bar{K}(z) \quad (10)$$

and

$$\bar{I}(z, +) = \bar{H}(0, +)$$

$$\cdot \exp \left[- \int_0^z \bar{K}(z') dz' \right]$$

Furthermore, between the two depths, $z - \Delta z/2$ and $z + \Delta z/2$, we have by definition of $\bar{K}(z)$

$$\begin{aligned} \bar{H}\left(z + \frac{\Delta z}{2}, +\right) &= \bar{H}\left(z - \frac{\Delta z}{2}, +\right) \\ &\cdot \exp \left[- \int_{z - \Delta z/2}^{z + \Delta z/2} \bar{K}(z') dz' \right] \end{aligned} \quad (11)$$

$\bar{K}(z)$ may be considered constant over the interval $z - \Delta z/2, z + \Delta z/2$ when Δz is sufficiently small. Therefore, from (11)

$$\begin{aligned} \int_{z - \Delta z/2}^{z + \Delta z/2} \bar{K}(z') dz' &= \bar{K}(z) \int_{z - \Delta z/2}^{z + \Delta z/2} dz' \\ &= \bar{K}(z) \Delta z = \ln \left[\frac{\bar{H}\left(z - \frac{\Delta z}{2}, +\right)}{\bar{H}\left(z + \frac{\Delta z}{2}, +\right)} \right] \end{aligned} \quad (12)$$

Substituting in (9) the values of $d\bar{H}/dz$ as given in (10) and $\bar{K}(z)$ as given in (12), we have the convenient operational equation (8) for $a(z)$.

Other physical measurements—In addition to the radiance distribution measurements described above, it was possible to measure some of the water properties by direct methods. The function $K(z, -)$ was obtained by direct measurement with a flat-plate collector used to obtain relative values of $H(z, -)$ at various depths. The collecting surface of this instrument (Figure 4) is carefully designed to collect radiant flux in accordance with the law

$$P(\theta) = P(0) \cos \theta \quad (13)$$

that is, the surface is a Lambert collector.



FIG. 4—Flat-plate Lambert collector for measuring relative values of irradiance

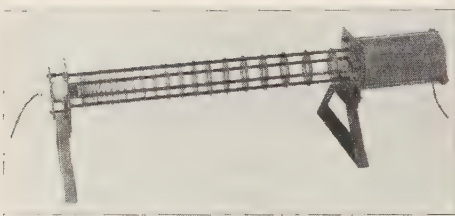


FIG. 5—Hydrophotometer for measuring the total attenuation coefficient

The volume attenuation function α was measured with a hydrophotometer (Fig. 5). The length of the path of the transmitted beam is $r = 1$ meter. This instrument is designed to be insensitive to changes in coupling (between the radiant flux and the detector) when the index of refraction of the medium changes over a wide range. It is also designed to minimize the effect of forward scattered light within the beam. Recent work by Preisendorfer [1958b] makes it possible to predict that the error created by forward scattered light within the beam of this instrument will be of the order of 0.3 per cent in the value of α .

Results—The experimental values obtained at a depth of 29 meters for eight optical properties of Lake Pend Oreille are given in Table 3. The total scattering coefficient for collimated light s can be found from a and α by

$$\alpha(z) = a(z) + s(z) \quad (14)$$

This table includes this calculated value of s

TABLE 3—The optical properties of Lake Pend Oreille at depth 29 meters and for a wavelength band 64 m μ wide (half-band width) peaking at 480 m μ

Property	April 28, 1957 Computed from $N(29, \theta, \phi)$	March 16, 1957 Measured directly	Calcu- lated indirectly
----------	--	--	-------------------------------

$K(29, -)$	0.169/m	0.184/m	
$K(29, +)$	0.164/m		
$R(29, -)$	0.0227		
$D(29, -)$	1.31		
$D(29, +)$	2.78		
$a(29)$	0.117/m		
$\alpha(29)$		0.442/m	
$s(29)$		0.325	

and also the directly measured value of $K(z, -)$ for $z = 29$ meters.

Discussion—These measurements were carried out in the spring of 1957 before the start of the spring plankton bloom and well before the development of any thermocline. The lake was tested extensively to determine its homogeneity and was found to be very nearly homogeneous by every test. Therefore the values of $\alpha(29)$ and $a(29)$ and $s(29)$ are representative values for all depths below 5 meters. The values of the properties given here should approach the minimum values for the year. The values $K(z, -)$, $K(z, +)$, $R(z, -)$, $a(z)$, $s(z)$ would be expected to rise in the upper layers of water during the plankton bloom and would probably be higher for all depths during the heavy spring run-off.

All of the constants reported here are associated with a half bandwidth of 64 m μ wide centered at 480 m μ .

In Table 3 the value of $K(29, -)$, measured directly, was obtained under overcast lighting conditions in March, whereas the value computed from $N(29, \theta, \phi)$ is for clear sunny conditions in April. These conditions may account for the difference in the two tabulated values of $K(29, -)$.

Table 4 gives relative values of irradiance and

TABLE 4—Integrated relative values of irradiance and scalar irradiance

z(meters)	$H(z, -)$	$H(z, +)$	$h(z, -)$	$h(z, +)$
4.24	721,000	15,500	899,000	41,900
10.42	329,000	6,040	413,000	16,500
16.58	109,000	2,230	141,000	6,190
28.96	13,100	298	17,200	830
41.30	1,660	39.0	2,190	108
53.71	221	5.19	289	14.33

scalar irradiance as obtained by the integration procedure. The array of properties for this range of depths may be readily computed from the tabular values.

One of the prime objectives of making these measurements was to provide numbers which could be used to confirm certain theoretical relationships which relate the various optical

properties. For example, it has been shown [Preisendorfer, 1958a] that in general

$$\begin{aligned} K(z, -) &= R(z, -)K(z, +) \\ &= a(z)[D(z, +)R(z, -) + D(z, -)] \end{aligned}$$

If the values for April 28 (column 2 of Table 3) are substituted in this expression the result is

$$.165 \sim .161.$$

REFERENCES

DUNTLEY, S. Q., R. J. UHL, R. W. AUSTIN, A. R. BOILEAU, AND J. E. TYLER, An underwater photometer, *J. Opt. Soc. Am.*, **45**, 904 (abstr.), 1955.

PREISENDORFER, R. W., Divergence of the light field in optical media, *Scripps Inst. Oceanog., Univ. Calif., Ref.* 58-41, 16 pp., 1957.

PREISENDORFER, R. W., Directly observable quantities for light fields in natural hydrosols, *Scripps Inst. Oceanog., Univ. Calif., Ref.* 58-46, 29 pp., 1958a.

PREISENDORFER, R. W., A General theory of perturbed light fields, with applications to forward scattering effects in beam transmittance measurements, *Scripps Inst. Oceanog., Univ. Calif., Ref.* 58-37, 22 pp., 1958b.

TYLER, J. E., Radiance distribution as a function of depth in the submarine environment, *Scripps Inst. Oceanog., Univ. Calif., Ref.* 58-25, 1958.

(Manuscript received February 19, 1959.)

Return Period Relationships

G. N. ALEXANDER

*State Rivers and Water Supply Commission
Melbourne, Victoria, Australia**

Abstract—The samples available in hydrology are often so small that it is desirable to take their size into account when estimating parameters. By using a simple classical model the relationship between various estimates of return periods derived from hydrologic time series has been obtained. Results for the 'annual' and 'base stage' series are compared with values given previously for a 'complete' series and also with empirical values used by the U. S. Weather Bureau. Effects of departures from the model assumed, caused by seasonal variation in probability of occurrence, or by correlation in magnitude, are reconciled with observed results.

Introduction—Although we regard 'time' and 'space' as being continuous, when we make quantitative measurements we express the result as a number of units which, provided the unit is small enough, can always be given as an integral number. However, the year, which is the time unit commonly used in hydrology in association with the 'return period' T cannot be considered 'small,' as the measurements used in time-series observations are made at much smaller time intervals. Hence we need the relationship between return periods based on finite samples using the year as the unit and those using other time units. In the limiting case the time unit approaches zero giving a 'continuous' variate. This continuity, which is mathematically desirable, raises problems of probability in a time continuum.

As the difference between estimated mean return periods of major hydrologic events, such as floods, using different methods of estimation, is small in comparison with their sampling error, the exact relationship between methods may appear academic. However, in statistical analysis in hydrology it is common practice to use a dimensionless number, formed by taking the ratio of the variate to an 'index' value whose mean return period is of the order of one to five years. It is particularly desirable, therefore, to know the relation between the

methods for such mean return periods and the effect of a given sample size N , so as to improve the estimates for this index value and hence the dimensionless ratio.

List of symbols

N	= number of years or cells
m	= rank of series $m = 1, 2, 3, \dots$
m_k	= expected number of events occupying k cells
k	= number of cells occupied, $k = 1, 2, 3, \dots, N$
p	= probability of an 'annual' event
T	= return period (generally)
T_a	= return period, annual series = N/k (N years)
T_b	= return period, base stage series = N/m
T_c	= return period, complete series
T_d	= return period, discrete series = N/k (N cells)
T_e	= return period, empirical series
T_f	= return period, finite N series = N/m_k
T_v	= return period, variable series

Probability models—The relationship between mean return periods for a finite N is one facet of 'distribution-free' methods in which order statistics play a fundamental role. Thus its determination is part of a reversion to a more fundamental approach and a healthy reaction against the hampering restrictions inherent in the use of a continuous distribution which is usually selected empirically. In hydrologic studies, the effective size of the sample is often equivalent to the number of years of observation. This number is usually small, so that if

* This paper was prepared while the author was at the U. S. Geological Survey, being on leave of absence from the State Rivers and Water Supply Commission, Victoria, Australia.

a continuous distribution is employed, some continuity is necessary.

In many cases before applying asymptotic results, that is, those which in theory assume an infinite sample size, we need to know the error caused by using a finite-sized sample. It is known, for instance, that although the 'extreme value' distribution [Fisher and Tippett, 1928] in its general form is 'distribution-free,' if it is regarded as being derived from a parent distribution, the rate of approach to the asymptotic form is greatly dependent on the parent form assumed. One objection to the use of the extreme value distribution is the excessively large sample required before the final asymptotic form can be obtained from a normal parent. This objection does not hold for certain other distributions of the parent form; for example, if the parent is the extreme value distribution (which, in hydrologic statistics it could be) there are no transitional forms, and a large sample is not required.

A better understanding of the role of basic probability theory, derived from rational models and freed as far as possible from the limitations of empirical distributions, is essential to the development of hydrologic statistics. The pioneer work of the Russian probabilists [Gnedenko and Kolmogorov, 1954], when translated into usable techniques in the manner so ably illustrated by Feller [1957], will speed this development.

The concept of hydrologic statistics examined in this paper by using a classical probability model, is that of the 'return period'. Although the term is commonly used by hydrologists, its characteristics are not well known to them; and as far as the author is aware, the effect of sample size on different measures of the mean return period has not previously been published.

Definitions—The theoretical model from which a series of floods or return periods is compiled consists of a continuous hydrograph with time as abscissa and rate of flow as ordinate. Each occurrence of a maxima can be regarded as a 'flood event' to which a magnitude X can be ascribed. From this model we can obtain the usual type of distribution with flood magnitude as the variate. Alternatively, by considering time as the variate, we can obtain distributions based on the observed inter-

vals or return periods between recurrence of specified flood events. This concept of the return period as a random variable is in accord with the definition given in Kendall and Buckland's "Dictionary of Statistical Terms" [1957]: "Return Period—In time series, the interval of time taken by the series to return to some assigned value, as for example 'the return period of flooding' in a river." Such a distribution, which is highly skewed [Alexander, 1957], may be specified by certain statistics, usually the mean and variance. It is to this mean value of return period that most hydrologic definitions refer, but the word 'mean' is often omitted. Linsley and Franzini [1955] define recurrence interval, which we regard as synonymous with return period, thus:

"Recurrence Interval—The recurrence interval is defined as the average interval in years between the occurrence of a flood of a specified magnitude and an equal or larger flood. The m th largest flood in a data series has been equalled or exceeded m times in the period of record, N years, and its recurrence interval is

$$T^* = \frac{N}{m}.$$

The estimate of the return period T of a given flood obtained by using this ratio of number of years N to number of events m will differ as m depends on the 'data series' used.

In this paper we are concerned primarily with the differences between the mean values which arise from the different methods of compiling the series of return periods, examining in particular the effect of the length of record N , or the finite sample size.

The two variates, flood magnitude and return period, are obviously related, but they should not be regarded as forming a bivariate distribution. In dealing with flood magnitude as the variate, time plays a secondary role, different series being obtained depending on

* The symbol t_* , in the original quotation has been changed to T as this symbol has been used throughout in this article. We are not concerned in this article with the distinction between sample and population values and will use T rather than the Greek τ , although it should be remembered that relationships as in Equation (3) are only correct for population values.

ow the time scale is divided in selecting flood vents. In the series using return period as the variate, the function of flood magnitude is merely to enable the flood events to be ranked in order so as to give the number of floods m , say, greater than X . In the distribution of the return period we ignore the different magnitudes of these m floods and use only the values n and X .

It might be noted that hydrologists usually refer to the return period of floods "equal to or greater than" (the m th flood). As flood magnitude may be regarded as a continuous variate, the probability of a flood being exactly equal to a given magnitude is negligible, and the words "equal to" appear redundant. We obtain the same value of the (mean) return period from a given sample if we omit "equal to" and write $m + 1$ instead of m , a form originally advocated by Kimball [1946] and employed by the U. S. Geological Survey and others. As we are not concerned here with the best estimate of the mean return period of floods, but only with the theoretical relation between mean return periods using different series, for simplicity we will use m and not $m + 1$ and also omit the words "equal to."

Selection of series—In the model given above, we define a series of either magnitudes or return periods which use all the maxima (flood-events) as comprising the 'complete' series. The mean return period estimator using all such observed values will be designated by T_c . (As we are concerned with seven different estimators, a mnemonic system is used for the subscripts; for example, $c = \text{complete}$).

This series of flood peaks has obvious drawbacks, the principal one arising from the inclusion of a number of correlated observations. Hence, in practice, a number of floods is eliminated from the complete series by considering (1) the flood magnitude and (2) the time scale.

Flood magnitude—The number in the complete series of flood magnitudes is truncated by excluding floods below a specified magnitude, usually termed the "base stage," giving the estimator T_b (base stage).

In the definition of the mean return period given, if the number of floods m exceeds the number of years of records N , then $T_b < 1$. We

cannot then invert this return period to obtain an estimate of probability P , as P will then exceed unity. Hence Linsley and Franzini's [1955] equations 5.2 and 5.3 must be restricted to the case where $T > 1$.

Time scale—To impose restrictions based on the time scale we may (a) select only the maximum flood within a prescribed unit duration, giving what we term the "discrete time series," or (b) prescribe a minimum time between successive flood peaks, giving a "truncated time series." These two methods will be considered in turn.

Discrete time series—The first procedure requires the division of the essentially continuous time scale into discrete time-units or durations. If no base stage is used and the duration selected is one year, we obtain from N years of record a series of N terms, giving the so-called annual flood series, with a mean return period designated herein by T_a (annual): for discrete durations other than the year, we may use the general symbol T_d (discrete). The general formula for mean return period is unchanged but the m th flood will in general have a different value from that in the complete series. The advantage of the year over other time units, such as the month, is that seasonal variation is eliminated and, provided there is no secular variation, the probability of occurrence is the same in each year. Fuller [1914] used the annual series, and so did Hazen [1930] who contended that the series based on magnitude only did not constitute a "proper" series.

Truncated time series—In the above method of subdividing the continuous time scale into equal units, it is theoretically possible for floods to be selected which have practically no time between them and hence to be correlated. This objection may be overcome by compiling a series which has a specified minimum time between peaks. The series so obtained is usually termed by hydrologists a "partial duration" series [*U. S. Geological Survey, Water Supply Paper 771, 1936*] to distinguish it from the full series based on all values in the daily flow duration curve. The number of floods in the partial duration series is also usually reduced by selecting a base stage, and to define such a series both restrictions should be specified.

The restrictions imposed by placing a lower limit on the time between peaks is equivalent to a truncation of the complete series based on the time scale. The minimum time interval used gives the point of truncation, and this interval should increase with stream size so as to minimize the correlation between adjacent peaks. In U. S. Geological Survey practice the usual interval is two days, but other limitations are imposed [U. S. Geological Survey Handbook for Hydrologists, chap. 1].

Relation between T_d and T_e .—There is loss of information in discarding all but the annual maxima; consequently hydrologists have endeavored to reconcile the mean return periods obtained from the different series.

In the draft report of the *Institution of Engineers, Australia, Stormwater Standards Committee* [1948] it was concluded from the agreement between the expected number of heavy storms, as given by the Poisson distribution, and the observed number, that storms could be regarded as occurring by chance. Hence for a mean return period of two years in the annual or primary series, the mean 1.45 years (incorrectly given as 1.48) was deduced for all storms (termed primary and secondary falls).

Langbein [1949] published the theoretical relation between the 'annual' and 'partial-duration' return periods, based on the concept that in the latter series the events (floods) occur 'at random' in time. This relationship, which may be expressed thus [*Alexander*, 1957],

$$1 - 1/T_d = \exp(-1/T_e) \quad (2)$$

is the basic relation of the Poisson process for

TABLE 1—Return periods

Continuous T_e	Discrete T_d
0.5	1.16
1	1.58
1.45	2.00
2	2.54
5	5.52
10	10.5
20	20.5
50	50.5
100	100.5

conversion of discrete probabilities to those assuming that the probability remains homogeneous in time [*Feller*, 1957, p. 399]. In Table 1 are the values of T_d and T_e , given by *Langbein*; these are linearly related if plotted with T_e on a logarithmic scale and T_d on an extreme value or log-log scale.

The value of $T_d - T_e$ may be expressed as $\frac{1}{2} + d$ where $0 < d < \frac{1}{2}$ with d increasing as T_e decreases. This asymptotic difference of $\frac{1}{2}$ for large T_e can be determined more accurately, if required, from the expansion of $\exp(-1/T_e)$, and is given by

$$T_d - T_e = \frac{1}{2} + \frac{1}{12T_e} - \frac{1}{720T_e^3} - \dots \quad (3)*$$

The persistent difference between T_d and T_e for large N arises thus. If we consider the first and last events to occur in a continuous time series of N complete years, the elapsed time between them will always be less than N , by approximately one half year. Hence in theory T_e is really based on a length of record about one half year less than T_d .

However we do not need to use this asymptotic relation requiring large N , and in the next section we derive values of the mean return period T_f , say, for a given finite N but with continuous or homogeneous probability. The method used also shows the connection between the basic probability assumptions and the 'law of logarithmic growth'. It is convenient to examine first the case where $T_d = 1$, its minimum value.

Relation between T_d and T_f for $T_d = 1$.—The author [1957] has previously used *Feller's* discussion of the classical occupancy problem to determine the effect of the 'base stage' on number of events in this series provided N is large. *Bizley* [1957] gives a lead to the same problem, but for finite N , which can be readily used to relate the return periods T_d and T_f in a discrete and finite series respectively.

Using the classical model of the distribution of 'balls' in 'cells,' we may regard the N years of record of some event as providing N cells which

* Equation 4.03 [*Alexander*, 1957] incorrectly gives the third term as $+1/144T_e^3$. Fortunately this error did not effect the conclusions drawn in the ensuing paragraph.

have to be occupied by balls or flood events. The phrase that the events occur 'at random' in time and are 'statistically independent' is equivalent to saying that the event is as likely to occur in any cell (or year) as in any other cell (or year). For the relation between T_d and T_f , we may regard all the floods as indistinguishable events; that is, their size is irrelevant. The model we use to relate the return periods is mathematically equivalent to placing, at random, flood events into the N cells until no cell remains unoccupied. We are interested in determining the number r of events that is required. This number r is a random variable, $\geq N$, whose mean m_N^* we seek. Since its distribution may be shown to be a negative exponential the mean is sufficient to define the distribution. It might be noted that even if N is as small as 7, the probability density that $r = N$ (that is, only 7 events are required to occupy 7 cells) is as small as 0.006, being given by $7!/7^7$ [Feller, 1957, p. 31].

When during the distribution process, i cells are occupied, leaving $N - i$ unoccupied, the probability of a random event occupying an empty cell is $(N - i)/N$; hence the expected number of events X_i required to reduce by one the number of unoccupied cells is the reciprocal of the probability, or $N/(N - i)$. The total expected number of events m_N required to occupy N cells will be found by summing X_i from $i = 0$ to $i = N - 1$.

Hence

$$\begin{aligned} m_N &= \sum_{i=0}^{i=N-1} X_i = \sum_{i=0}^{i=N-1} N/(N - i) \\ &= N[1 + 1/2 + 1/3 + \dots + 1/N] \quad (4) \end{aligned}$$

This is a harmonic series which is nonconverging. It is readily computed for small values of N , and an exceptionally good approximation is given by Buzley [1957, p. 122]; even for N as small as 5, the error is only 0.25 per cent.

$$m_N = N(\log_e N + \gamma + 1/2N). \quad (5)$$

For very large N we may drop the last two terms [Feller, 1957, p. 211] but this is inadvisable

in hydrologic statistics; for example, with $N = 65$, the error would be 14 per cent (For large N , (4) and (5) may be used to define Euler's constant $\gamma = 0.577$, which is the mean in the 'extreme value' distribution when the mode is zero). The value m_N is therefore the expected number of flood events required so that every cell or year is occupied, but there is at least one year when there is only one flood event. For example, if $N = 65$, $m_N = 309$. This value of m_N may be compared with the value of $n_b = 298$ for the median given previously [Alexander, 1957] but which assumed the mean given by the approximation $N \log_e N$. The number m_N of flood events is then the expected number in the base stage series with the base stage low enough to include the lowest annual flood. As T_f is defined as the number of years N divided by number of events m_N , we determine (for $T_d = 1$) values of T_f for selected values of N as given in Table 2. In this case the difference between T_d and T_f varies from zero to one depending on N .

TABLE 2—Values of T_f , for $T_d = 1$

N	T_f
1	1
5	0.44
10	0.34
20	0.28
50	0.22
100	0.19
∞	0

Relation between T_d and T_f for T_d greater than unity—In the model used in the previous section, flood events were allotted until all the N cells were occupied. For T_d greater than unity, we stop allotment when the k th cell is first occupied, the expected number of events being m_k . The m_k th event in the ordered series will then give the base stage. With N cells and m_k events occupying k of them, the mean return periods of the base stage flood T_d and T_f will be given by

$$T_d = N/k, \quad T_f = N/m_k \quad (6)$$

In the latter case the total expected number of events m_k will be given by summing the X_i

* We use m throughout rather than μ or $E(m)$ to denote population mean and to simplify nomenclature, but see footnote on p. 676.

from $i = 0$ to $i = k - 1$ instead of to $i = N - 1$. Hence

$$\begin{aligned} m_k &= \sum_{i=0}^{i=k-1} N/(N-i) \\ &= N/N + N/(N-1) \\ &\quad + \cdots N/\{N-(k-1)\} \end{aligned} \quad (7)$$

It should be noted that as $m_k = 1$ for $k = 1$ the expected return period for the rank 1 event is equal to N for both T_d and T_f . The difference between T_d and T_f again has a minimum of zero (when $k = 1$) and a maximum of unity (when $k = N \rightarrow \infty$).

For the values of N and k used in most hydrologic work, it is simplest to compute values for m_k for given N and k and hence T_d and T_f . As normally we will be estimating one or the other, Table 3 shows the difference $T_d - T_f$, enabling one to be computed from the other.

For the values of $T_d = 2, 5$, and 10 , we give in Table 4 the general relation for T_d/T_f , and the values for $N = 40$.

TABLE 4—Values of T_d/T_f

T_d	T_d/T_f	$T_d/T_f (N = 40)$
2	$1.386-1/N$	1.36
5	$1.115-1/1.6N$	1.10
10	$1.054-1/1.8N$	1.04

Empirical relation used by U. S. Weather Bureau—The theoretical relation given by Equation (2) and Table 1 is not used by the U. S. Weather Bureau, which employs an empirical factor for converting partial-duration to annual series [U. S. Weather Bureau, 1957]. For given T_d the corresponding values of T_f

Table 3—Values of $T_d - T_f$; $T_d = N/k$

N	k										
	1	2	3	4	5	10	15	20	30	40	50
5	0	0.28	0.39	0.47	0.56						
10	0	.26	.35	.41	.45	.66					
15	0	.25	.35	.39	.43	.53	.70				
20	0	.25	.34	.39	.42	.51	.57	.72			
30	0	.25	.34	.38	.41	.48	.52	.56	.75		
40	0	.25	.34	.38	.41	.47	.50	.53	.59	.77	
50	0	.25	.33	.38	.41	.47	.49	.51	.56	.61	.78

If we wish to estimate $T_d - T_f$ for other values of N or k we may obtain from (5), after a little algebra

$$\begin{aligned} m_k &= N \log_e N/(N-k) \\ &\quad - k/2(N-k) \dots \end{aligned} \quad (8)$$

This is accurate enough for all practical purposes; even for N as low as 10 and k as high as 5 (that is, $T_d = 2$), it is within $\frac{1}{2}$ per cent of the exact value.

For purposes of showing the effect of N on the ratio T_d/T_f we obtain from (6) and (8)

$$\begin{aligned} T_d/T_f &= T_d [\log_e \{T_d/(T_d-1)\} \\ &\quad - 1/2N(T_d-1)] \end{aligned} \quad (9)$$

(empirical) have been derived and are given in Table 5. It is understood that for $T > 20$, T_d and T_f are regarded as identical, and that the other values were derived from stations whose length of record is about 40 years. From Equation (9) or Table 4, we obtain values of T_f for $N = 40$ (Table 5). The difference between T_d and T_f is approximately constant, lying between 0.25 and 0.29 with T_f the smaller. For possible causes of this difference we re-examine the assumptions of the model used to derive T_f .

Variation in probability during the year—One basic assumption in the model used is that the probability remains the same for each cell. Thus if we regard the cell as covering a duration

TABLE 5— T_s and T_f for given T_a and N

T_a	T_s	T_f ($N = 40$)	$T_s - T_f$
2	1.76	1.47	0.29
5	4.80	4.55	0.25
10	9.90	9.62	0.28
20	20.0	19.72	0.28

such as a year it does not matter if the probability varies during the year so long as the mean probability for each year is constant.

Consider now the effect of what we may term seasonal variation in probability of an occurrence whose yearly probability is $p = 1/T_a$. If we have two seasons in the year with a probability of occurrence in one of $p_1 = 1/10$ and in the other of $4p_1$ or $p_2 = 2/5$, then the yearly probability $p = p_1 + p_2 = 1/10 + 2/5 = 1/2$; hence $T_a = 2$.

If $N = 40$, for example, from (8) the corresponding expected number of events m_k for $T_a = 2$ is $N \log_e 2 - 1/2 = 27.2$ and $T_f = 1.47$ as given in Table 4. If, however, the probability varies during the year it is easily shown that the total number of occurrences is always less than if it remains constant [Feller 1957, p. 216]. For example, with the above values of N and T_a , we obtain from (8) the total number m_s in the variable case

$$\begin{aligned} m_s &= m_1 + m_2 = N(2 \log_e 40 \\ &\quad - \log_e 36 - \log_e 24) - \frac{1}{2}(1/9 + 2/3) \\ &= 0.616N - 7/18 \\ &= 24.25 \text{ for } N = 40 \end{aligned}$$

As $T_s = N/m_s$, $T_s = 1.65$. Thus T_s is about 12 per cent greater than $T_f = 1.47$, but less than the Weather Bureau's value T_s of 1.76 for $T_a = 2$.

Thus 'seasonal' variation in probability of occurrence, which normally exists, will account for some of the difference between T_s and T_f . It would be possible to estimate T_s by using an empirical determination of the seasonal fluctuation in p .

Effect of correlation in magnitude—The other basic assumption in the original model is that

the events are independent of each other. We must again consider the two axes and distinguish between independence in (1) time of occurrence, and (2) magnitude of the event. Thus storms two days apart could be practically independent, but the magnitudes of the floods caused would be correlated because of persistence in base flows or runoff conditions. Hence, if the minimum time between flood peaks for the partial duration series is only two days, as in U. S. Geological Survey practice, we would expect to obtain a larger number of floods than in a purely random series, with a consequent reduction in the base-stage return period, T_b for a given T_a . Thus as indicated in Figure 1 of Langbein [1949], the difference between the observed values of T_b and T_a is of the order of one year, or higher than the maximum value for $N = 50$, say, of 0.78 as in Table 3.

Conclusion—Thus, these two natural departures from the model, (1) variation in probability throughout the year, and (2) a positive correlation between magnitudes, produce opposite effects in the theoretical differences ($T_s - T_f$) between the return periods; the former tends to reduce the difference and the latter to increase it. Hence, even if the theoretical relation between the return periods, T_s and T_f , as given in Table 3 were observed, this could be due to a nice balance between these two effects.

REFERENCES

- ALEXANDER, G. N., Flood flow estimation, probability and the return period, *J. Inst. Engrs. Australia*, 29, 263–278, 1957.
- BIZLEY, N. T. L., *Probability: an intermediate text book*, Cambridge Univ. Press, London, 224 pp., 1957.
- FELLER, W., *An introduction to probability theory and its application*, 2nd ed., John Wiley and Sons, New York, 461 pp., 1957.
- FISHER, R. A., AND L. H. C. TIPPETT, Limiting forms of the frequency distribution of the largest and smallest member of a sample, *Proc. Cambridge Phil. Soc.*, 24, 180–190, 1928.
- FULLER, W. E., Flood flows, *Trans. Am. Soc. Civ. Engrs*, 77, 564–676, 1914.
- GNEDENKO, B. V., AND A. N. KOLMOGOROV, *Limit distributions for sums of independent random variables*, Addison-Wesley Publication Co., 264 pp., 1954.
- HAZEN, A., *Flood flows: A study of frequencies and magnitudes*, John Wiley and Sons, New York, 199 pp., 1930.

INSTITUTION OF ENGINEERS, Australia, Stormwater Standards Committee, *Draft report on 1st term of reference*, 1948.

KENDALL, M. G., AND W. R. BUCKLAND, *A dictionary of statistical terms*, Oliver and Boyd, London, 493 pp., 1957.

KIMBALL, B. E., Assignment of frequencies to a completely ordered set of sample data, *Trans. Am. Geophys. Union*, 27, 843-846, 1946.

LANGBEIN, W. B., Annual floods and the partial-duration flood series, *Trans. Am. Geophys. Union*, 30, 879-881, 1949.

LINSLEY, R. K., AND J. B. FRANZINI, *Elements of hydraulic engineering*, McGraw-Hill, New York, 582 pp., 1955.

U. S. GEOLOGICAL SURVEY, *Water Supply Paper 771*, 1936.

U. S. WEATHER BUREAU, Rainfall intensity-frequency regime, Part I, *Tech. Pap. 29*, 44 pp., 1957.

(Manuscript received September 30, 1958; revised February 25, 1959; presented at the Thirty-Ninth Annual Meeting, Washington, D. C., May 1, 1958.)

Letters to the Editor

RADIO EMISSION FOLLOWING THE FLARE OF AUGUST 22, 1958

A. BOISCHOT AND J. W. WARWICK

*High Altitude Observatory
University of Colorado
Boulder, Colorado*

On August 22, 1958, a great flare, importance 3, was seen on the sun. The very active region in which the flare occurred gave, during its passage through the visible disk, 24 flares of importance 1, 4 flares of importance 2, and 3 flares of importance 3. On August 22, this center of activity was located at N20 W08. A small flare (importance 1+ by Naval Research Laboratory) was in progress when the great flare (importance 3 or 3+ as observed by Ottawa, McMath-Hulbert, and Ondrejov Observatories) appeared at 1417 UT. At 1700 UT this second flare was still continuing.

Coincident with the flare, the radio emission showed an intense outburst. Figure 1 gives the beginning of the bursts on different frequencies. It must be noted that for 18, 40, and 60 Mc/s the antennas were fixed, with maximum gain at 1900 UT, 1900 UT, and 1835 UT, respectively. We did not try in Figure 1 to make corrections for antenna gain because the burst began when the sun was very far from the maxima of the antenna pattern lobes; it was probably actually in its secondary lobes. The accuracy of such a correction would have been very poor. For 169, 470, and 2800 Mc/s, the antennas were tracking the sun, and the curves give the real evolution of the burst. The decrease of intensity which is seen at 18 Mc/s between 1430 and 1530 UT represents the ionospheric absorption of the cosmic noise background upon which the 18 Mc/s outburst occurred; this absorption reduces the apparent amplitude of the outburst itself.

Figure 2 gives, with a smaller time scale, the evolution of the emission on the same frequencies, now corrected (approximately) for the ef-

fect of lobe. The upper curve is the variation of cosmic rays (protons of about 170 Mev) as observed by Anderson [1958] in a balloon flight.

It seems that the spectrum of this event is somewhat different from that of typical outbursts and type IV bursts observed after great flares. Though the burst is quite normal in the microwave range, the great intensities reached on 40 and 18 Mc/s are very rarely observed. An

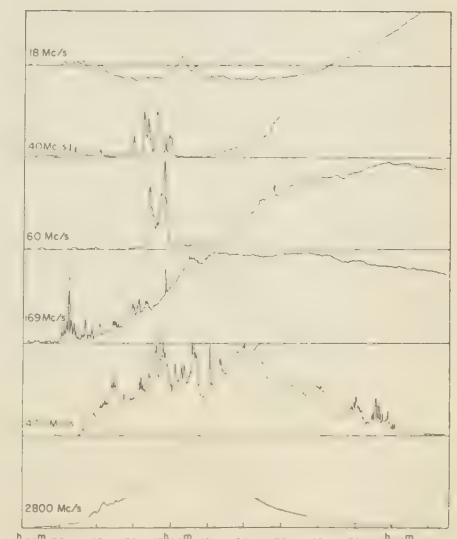


FIG. 1.—Beginning of the great radio outburst of August 22, 1958 on various frequencies. The authors are indebted to several other observatories for the records at 60, 169, 470 and 2800 Mc/s (see text). These records are uncorrected for antenna gain.

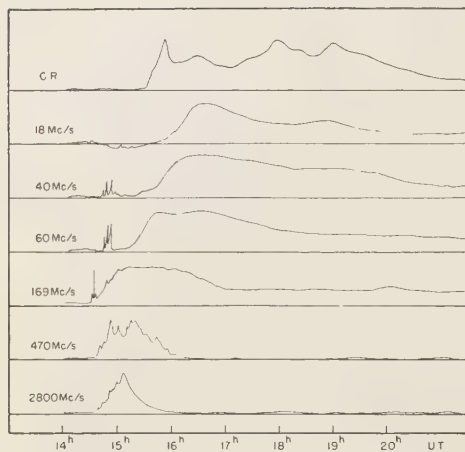


FIG. 2.—The complete records, on a smaller time base. Anderson's [1958] cosmic-ray data are plotted on the top graph. The intensity scales are different and arbitrary from graph to graph

estimate of the flux density at the peak of the 18 Mc/s burst is about $10^{-18} \text{ W} \cdot \text{m}^{-2} (\text{c/s})^{-1}$. In comparison with the flux densities reported by the other stations at higher frequencies, this value is equal or somewhat greater. The spectrum, therefore, was flat or it actually increased somewhat at the low-frequency end of our observed range. The low intensity on 470 Mc/s compared with both higher and lower frequencies is also infrequent.

It seems that we are dealing with two different types of emission: (1) the burst which appears on 2800 Mc/s and 470 Mc/s, the intensity of which decreases with decreasing frequency and disappears near 100 Mc/s; and (2) a long enduring continuum, which appears later than

the high frequency burst, and only on frequencies lower than 200 Mc/s. The lower the frequency, the later this emission seems to begin. It is important to note that the increase of cosmic rays corresponds better to this second part of the radio emission.

Another noteworthy point is that the type II emission on metric wavelengths, which generally immediately follows the beginning of the flare, is very weak or non-existent. It is not seen on 169 Mc/s records. Perhaps the increase at 1452 UT on lower frequencies may correspond to the type II burst, but it seems more probable that this is a group of type III bursts because of the delay between these bursts and the beginning of the flare and the observed shift in frequencies. It would be interesting, however, to look at the dynamic spectrum of the emission which has not been available to the authors.

The observations used in the present study on 18 and 40 Mc/s were from the High Altitude Observatory, Boulder, Colorado; on 60 Mc/s from Harvard College Observatory, Fort Davis, Texas; on 169 Mc/s from Nancy, France; on 470 Mc/s from the National Bureau of Standards, Boulder, Colorado; and on 2800 Mc/s from Ottawa, Canada. We wish to thank these observatories for the use of their records. This research was supported by the Electronics Research Directorate, Air Force Cambridge Research Center.

REFERENCE

K. A. ANDERSON, Ionizing radiation associated with solar radio noise storm, *Phys. Rev. Letters*, 1, 335-337, (1958)

(Received February 16, 1959.)

BALLOON OBSERVATION OF SOLAR COSMIC RAYS ON MARCH 26, 1958

P. S. FREIER, E. P. NEY, AND J. R. WINCKLER

*School of Physics
University of Minnesota*
Minneapolis, Minnesota*

A remarkable sequence of solar and terrestrial events occurred in late March 1958. The climax of these events was the observation of low-energy cosmic rays arriving at the earth. The phenomena which we will describe were probably initiated by a solar flare of importance three plus and of 248 minutes' duration which began at 0950 UT on March 23. This flare immediately produced a Type IV radio noise storm on the sun with radio emission at all frequencies observed from below 169 mc to 9400 mc. *J. F. Denisse* [Meudon Observatory, Paris; private communication] reports that on lower frequencies this flare produced one of the two or three largest and longest storms ever recorded. The flare produced on the earth a short-wave fade-out of importance three between 0953 and 1309 UT on March 23.

The solar cloud presumably ejected by the flare arrived at the earth on March 25 at 1540 UT as evidenced by the sudden commencement of a magnetic storm. This sudden commencement was shortly followed by a pronounced decrease in sea level cosmic rays. The decrease in sea level neutrons at Deep River, Canada, amounted to 9.8 per cent and this decrease occurred between March 25 and 26.

Figure 1 shows a plot of the neutron intensity at Deep River, Canada,** during the period March 20 to April 10, and it can be seen that the cosmic-ray counting rate recovered from the decrease by early April.

In addition, on Figure 1 are shown the data

of *Leinbach and Reid* [1959] on the absorption of cosmic noise at Ft. Yukon, Alaska. An extremely large and abrupt absorption of 10 Db began at the time of the sudden commencement on March 25. Leinbach and Reid's data show that even at night the absorption of cosmic noise was 3 Db on the nights preceding and following March 26. The detailed form of this absorption curve will be discussed by Leinbach and Reid in a subsequent publication, but it should be remarked that this type of polar cap cosmic noise absorption is presumed to be caused by the arrival of charged particles at the earth which increase the ionization of the D layer of the ionosphere. The March event represents probably the most intense event of this type so far observed, and it appears that at this time the particles were confined to the solar beam and were observed only when the earth entered this beam at 1540 UT March 25.

The data which we have obtained relate to the energy and composition of cosmic-ray particles at high altitude during this period near Minneapolis (geomagnetic latitude 55°). Balloon flights were carried out on March 21, March 26, and April 8. We refer to these flights as IGY 27, 28, and 29. The flights were instrumented with our standard geophysical year equipment which consists of a single counter, ion chamber, and photographic emulsions [Ney and Winckler, 1958; Peterson, Howard, and Winckler, 1958]. The ion chamber and single counter give a continuous record of the particle flux and ionization at high altitude, and the emulsions allow the determination of the precise nature of the particles involved.

In Figure 2 are shown the results of these high-altitude measurements at a pressure of 10

* This work supported by the USNC for the IGY through the NSF and by the ONR.

** These neutron data taken by H. Carmichael are available at World Data Center A for Cosmic Rays, University of Minnesota, Minneapolis.

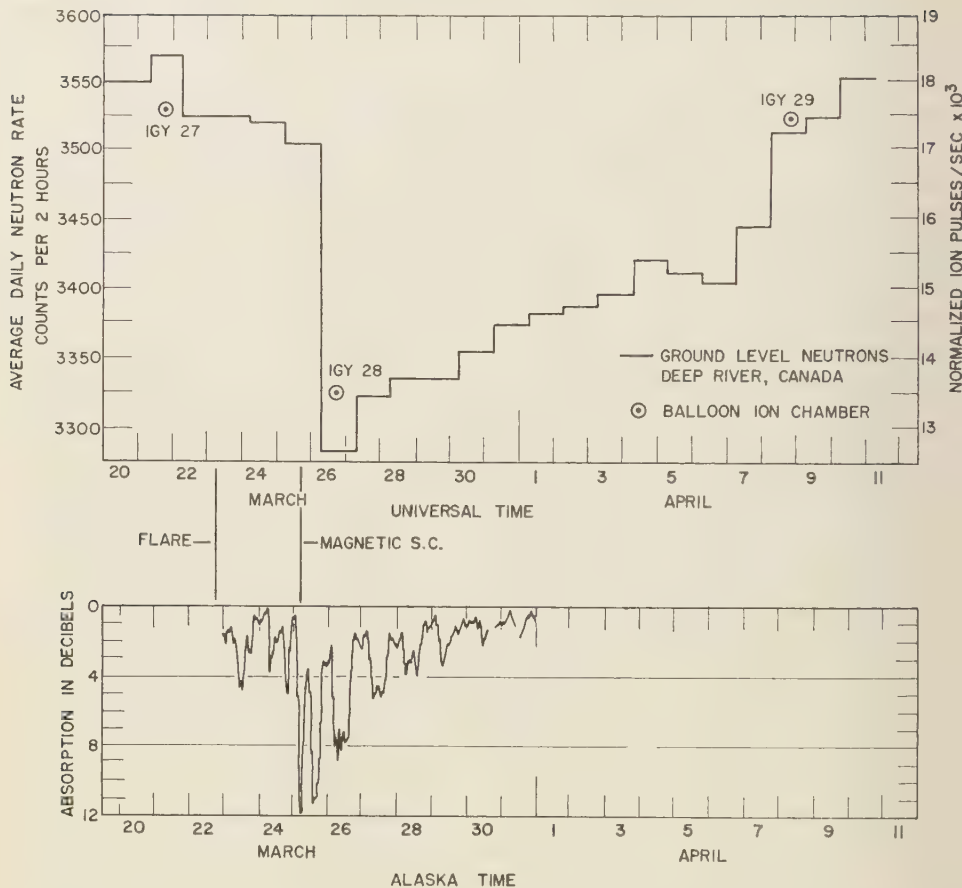


Fig. 1 *Upper:* Sea level neutron intensity at Deep River, Ont., Canada (courtesy of H. Carmichael), showing time of balloon flights and 10 g/cm^2 total ionization rate

Lower: 27.6 m.c. cosmic noise absorption at Ft. Yukon, Alaska. Widebeam vertical antenna. Courtesy of H. Leinbach and G. Reid

mb. We shall first discuss the counter and ion-chamber measurements. The ion-chamber curve of Figure 2 shows that the high-altitude ionization was constant and steady on March 21 and returned to this constant steady value by April 8. At the time of IGY 28 on March 26 the intensity as measured by the counter and ion chamber as the balloon reached ceiling at 1300 UT was less by 23.3 per cent than that measured on March 21. This is consistent with the behavior of cosmic rays during a Forbush decrease. The Forbush decrease is generally considered now to indicate the effect of the solar

beam in modulating pre-existing cosmic rays, and its effect at sea level and high altitude is to depress the cosmic-ray intensity. However, in this event, after the balloon reached ceiling and had been floating for about an hour, a slow increase in counting rate of the single counter and ionization in the ion chamber was observed, and this increase continued until the termination of the flight at 1900. No increase was observed in a simultaneous flight at Texas, geomagnetic latitude 41° . The ratio of the increase in the ion chamber reading to that of the single counter indicates particles ionizing approximately three

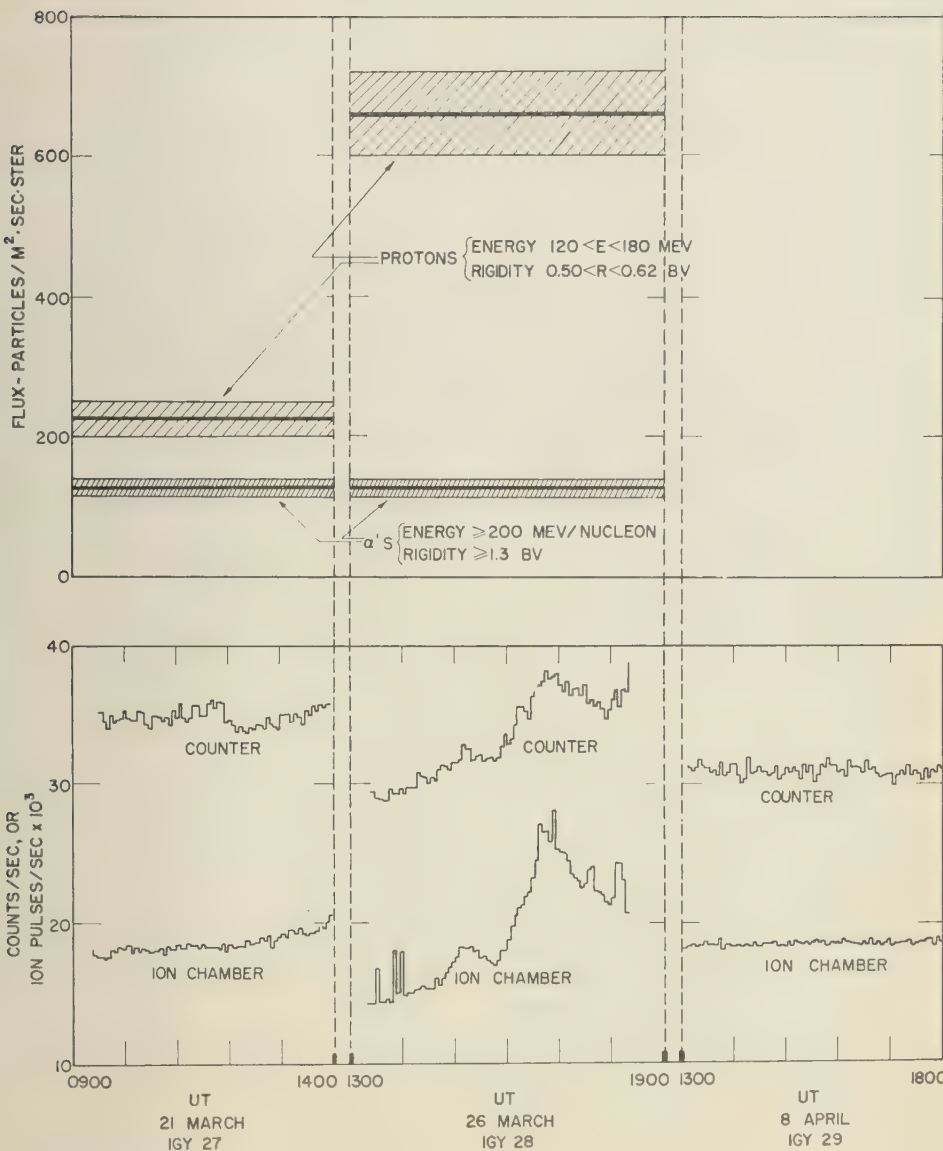


FIG. 2.—Upper: Nuclear emulsion flight average flux of protons and alpha particles

Lower: Total particle count rate and mean ionization. The increase in ionization rate observed on IGY 28 is in satisfactory agreement with the proton increase observed in the emulsions for the same flight

times minimum ionization. If these are protons their range is 33 g/cm² and their energy approximately 200 mev. The increase with time of IGY 28 may be in reality a latitude effect while the balloon drifted between Minneapolis and Sioux Ste. Marie, Michigan.

The emulsions were studied to determine in detail the nature of the particles associated with this cosmic-ray increase. In Figure 2 are shown the results of the measurements on alpha particles of energy greater than 200 mev/nucleon and protons of energy between 120 and 180 mev. It should be noted that the alphas measured consist of almost all the alpha particles in the primary beam but that the protons consist of a narrow rigidity interval between rigidities of 0.50 BV and 0.62 BV. The reason for the narrow proton slice is associated with the technique of carrying out the experiment and will be discussed in detail in a later publication.

The principal point to be made is that although alphas of rigidity greater than 1.3 BV did not change measurably in flux the protons in the narrow rigidity interval increased by a large amount. In fact, the increase in flux of protons between 120 and 180 mev consisted of 0.04 particles/cm²-sec-ster. The total flux of protons at solar maximum is about 0.1 particles/cm²-sec-ster. The increase in flux averaged over the flight of IGY 28 due to protons of 120 to 180 mev was therefore almost a half of the total primary proton flux. This figure can be checked from the ionization-chamber and single-counter readings, and the estimate on the basis of these detectors is that the average increase during the flight of protons of energy less than 200 mev was 0.06 particles/cm²-sec-ster. Since the emulsion measurement was made only to an energy of 180 mev the ion chamber to single-counter ratio is consistent with the measured increase in flux in the emulsions. The proton energies in this event are far below the geomagnetic cut-off. Protons arrived at rigidities as low as 0.5 BV whereas the cut-off inferred from previous direct energy measurements is 1.0 BV [Fowler, Freier, and Ney, 1958].

The significant features of this event are: (1) the presence of particles below the normal cut-off rigidities appropriate to the latitude of Minneapolis, and (2) the delayed arrival of cosmic rays relative to the flare of March 23.

We interpret the presence of low-rigidity particles to indicate the distortion of the Stoermer cut-offs by the solar beam.

The late arrival may be due to one of the following causes: (a) *Continuous acceleration and injection of cosmic rays at the sun*. The March 23 flare produced the magnetic channel, but subsequent solar activity accelerated and injected the cosmic rays. (b) *Storage of particles accelerated during the solar flare*. This storage could take place in the solar corona between March 23 and March 30, and the particles could arrive at the earth after diffusion into the magnetic channel. Alternatively the storage could take place in the solar gas cloud injected by the flare. (c) *Release of trapped particles in the Van Allen belt* (earth's corona) by the magnetic perturbation of the solar cloud.

We believe that (a) is ruled out by the lack of major flares during the period following the March 23 flare and that (c) is improbable because of the polar cap effects observed by Leinbach. It therefore seems likely that the particles observed on March 26 were accelerated in the flare of March 23, stored in the solar corona and propagated to the earth in the magnetic channel also arising from the March 23 flare.

Acknowledgments—The authors wish to acknowledge the major contribution to the balloon flight program reported here, made by L. Peterson, R. Hoffman, and R. Arnoldy; and the co-operation of H. Leinbach in making his experimental results available before publication.

REFERENCES

FOWLER, P., P. S. FREIER, AND E. P. NEY, *Il Nuovo Cimento*, 8 (Suppl.), 492, 1958.
LEINBACH, H., AND G. C. REID, *Phys. Rev. Letters*, 2, 61, 1959.
NEY, E. P., AND J. R. WINCKLER, *Geophysical Monograph* 2, Am. Geophys. Union, 1958.
PETERSON, L. E., R. L. HOWARD, AND J. R. WINCKLER, *Electronics*, 31, 76, 1958.

(Received May 22, 1959.)

Abstracts of papers presented at the
Pacific Southwest Regional Meeting
Stanford, California, February 5-6, 1959
listed in the order of the last name of the first author

G. ABRAHAM (Department of Civil Engineering, University of California, Berkeley, Calif.) *Water gravity waves generated by a moving circular low pressure area*—In a towing tank the disturbance of the water level due to the movement of a low pressure area over the water surface has been studied. Results of two-dimensional experiments (line pressure disturbance) have been described earlier by Wiegel, Snyder, and Williams. This paper will describe three-dimensional experiments (circular pressure disturbance).

The extent of the pressure disturbance, its advancing velocity, and the water depth were varied. The model data were compared with the theories of Havelock (1908) and Inui (1936). It was found that the main features of the generated waves, such as wave pattern and the magnitude of wave heights, followed the trends given by the theories. The disturbance of the ocean surface due to a hurricane and the generation of 'wind waves' by a gust may be considered as prototype applications for this model study.

J. AMOROCHO (Woodward, Clyde, Sherrard and Associates, Oakland, Calif.) *Seasonal rainfall-runoff relationships in tropical and subtropical areas*—A method of correlation between precipitation and runoff is presented for those areas where snowfall is nonexistent or negligible. This method permits the computation of seasonal runoff values on the basis of rainfall data alone. The procedure is based on the analysis of concurrent mass diagrams of rainfall and runoff and has been applied successfully for the extension of the flow history of a number of tropical streams, as well as for streams located in California. A discussion of the theoretical basis of the method is presented, together with an analysis of the degree of accuracy that can be obtained, as shown by comparisons between computed and measured runoff values.

E. P. ANDERSON (San Jose State College, San Jose, Calif.) AND R. A. HELLIWELL (Stanford University, Stanford, Calif.) *Reflected radio signals from the sea surface at 1.85 megacycles*—Short range echoes associated with Loran pulse transmissions at 1.85 Mc/s exhibit three particularly interesting characteristics: (1) a systematic amplitude fading at a frequency of 0.139 cps, (2) discrete but time-varying ranges up to 250 km, and (3) irregular fading of much lower frequency. An investigation showed that these echoes were returned from the sea. They were doppler shifted by 0.139 cps, correlating with the velocity of approaching water-waves of half-radio-wavelength crest-to-crest spacing. The mechanism of the systematic amplitude-fading appears to require a reference signal component closely associated with

the reflecting area; however, no such component was identified. The possibilities for using the phenomenon as a tool in the study of sea wave spectra are discussed.

J. A. B. BJERKNE (Department of Meteorology, University of California, Los Angeles, Calif.) *North Atlantic sea surface temperatures and atmospheric circulation*—Trends in ocean surface temperature of more than one year's duration seem to arise from three main meteorological influences: (1) change in ocean current heat advection, dictated by corresponding changes of average winds, (2) change in heat supply to the atmosphere as determined by sea-air temperature difference and strength of average wind, and (3) dynamic upwelling or downwelling produced by variations in the vorticity of wind drag. Empirical illustrations of the three types of meteorological influence are shown.

NORMAN H. BROOKS (Department of Civil Engineering, California Institute of Technology, Pasadena, Calif.) *Lateral diffusion of mass in a steady current in the ocean or atmosphere*—The solutions of problems of sewage disposal in the ocean, or gaseous waste discharge to the atmosphere, involve analyses of turbulent diffusion. If the polluting substance is introduced at a steady rate into a uniform current in the ocean or atmosphere, the material will diffuse laterally as it moves down-current. The width of the pollution band increases as the maximum concentrations at the center of the band decrease, because of the turbulent mixing with adjacent unpolluted fluid.

A Fickian-type diffusion equation is applicable, provided the diffusion coefficient is considered to increase with scale. Assuming that the diffusion coefficient (or eddy diffusivity) is proportional to the 4/3-power of the scale, and that the scale is proportional to the standard deviation of the distribution of concentration across the stream, it is possible to derive an exact mathematical solution of the diffusion equation. Results are expressed in a form usable for engineering problems; an example is presented which applies the equation to dispersal of sewage effluent in the ocean.

FRED A. CAMP (Los Angeles Department of Water and Power, Los Angeles, Calif.) *Hydrologic processes of snow and ice at high altitude*—This paper covers two subjects: (1) *An aspect of deglaciation and increased aridity in the high mountain regions in the Lahontan area, central Sierra Nevada range, California, and in the Alps of Central Europe*. The slight increase in average temperature coupled with a weather pattern change in 1919-1920 has produced radically differ-

ent hydrologic conditions in the temperate latitudes of the areas studied. This is illustrated by the 30-year recession of the Palisade Glacier in the central Sierra Nevada range and the Pasterze Glacier in Hohe Tauern, Province of Carinthia, Austria. (2) *An analysis of desiccated snow.* A wind-slab, a summer remnant of seasonal snow, was found on Mt. Whitney, elevation 4340 meters (14,200 feet), on July 22, 1958. At high altitudes (up to 4360 meters) in the temperate latitudes the hydrologic processes are considerably altered. The apparent changes are affected by motive power of heat in the following order of effectiveness: intense radiation of sun and sky, conduction from the earth, and atmospheric convection. It was found that on the crest and high transverse passes of the Sierra range, all three modes of heat transference are simultaneously operative in a greater or lesser degree.

Included are several meteorologic patterns of the distinct Sierra wave showing variants of precipitation and atmospheric temperature.

S. W. GRINNELL (Stanford Aerosol Laboratory, Stanford, Calif.) *The simplification of meteorological data recording systems by use of an electronic integrator.*—The outputs from various types of meteorological sensing elements are converted into series of square wave pulses, the heights of which represent the analogs of the true arithmetic means of the quantities being measured, averaged over a continuous series of fixed time intervals. For a group of instruments these averaging periods are simultaneous, but the height of square wave pulses can be sampled successively, thus permitting a multiple record of all data to be taken on a single instrument or to be telemetered over a single channel. Because of the inherent variability of the usual meteorological quantities, recording the successive mean values of these quantities accumulates significant data more rapidly than would be the case if spot samples of the meteorological quantities were to be multiply recorded by the same equipment. Equipment now in use can provide averaging periods varying from one second to about five minutes. It has been applied to producing continuous station records of wind speed, wind direction, vector wind travel, and air temperature at several levels, as well as to obtaining short-period records for turbulence studies and to making convenient intercomparisons of various types of temperature sensing elements.

MAHDI S. HANTUSH (New Mexico Institute of Mining and Technology, Socorro, N. Mex.) *Non-steady flow to flowing wells in leaky aquifers.*—Potential distribution is found for a flowing well discharging by natural flow from a uniform confined aquifer into which there is leakage in proportion to the drawdown. The leaky aquifer is of uniform compressibility and uniform transmissibility. Three cases are considered: (1) a well draining an infinite leaky aquifer; (2) a well at the center of a circular aquifer with zero drawdown on its outer boundary; and (3) a well situated at the center of a closed circular aquifer, that is, the flow across the outer boundary is zero. The variation of the discharge with time in the

three cases considered is formulated. The drawdown distribution and the discharge variation for the corresponding systems of non-leaky aquifers are obtained. It is shown how the formation constants, namely, the coefficient of transmissibility, the coefficient of storage, and the coefficient of leakage, will be obtained from variations in the rate of discharge of wells flowing at constant drawdown.

RAYMOND A. HILL (Leeds, Hill, and Jewett, Los Angeles, Calif.) *Inflow to Lake Titicaca.*—Lake Titicaca forms part of the great system of internal drainage of the Altiplano of Peru and Bolivia between the Cordillera Oriental and the Cordillera Occidental. The lake has an area of about 8300 square kilometers (3300 sq mi) and it is about 3800 meters (12,500 ft) above sea level. The adjacent ranges are about 2000 meters (6500 ft) higher. Lake Titicaca normally fluctuates about 60 centimeters (2 ft) each year and there have been cyclic fluctuations aggregating 4.6 meters (15 ft). Such fluctuations, of which there is a record since 1914, are indicative of variations in inflow but do not reflect the true magnitude of such variations because the rate of outflow is a function of the lake level. There are no records of inflow to Lake Titicaca and few of the outflow from it. Hence, estimates of inflow and outflow must be based on solutions of the equation of hydrologic balance with due allowance for precipitation on and evaporation from the lake surface. Trial solutions of these equations were made by months until a reasonably consistent set of values was determined. The results are set forth in tabulations of the probable inflow to Lake Titicaca and the outflow from it for each month of the 40-year period from 1915 to 1954, inclusive.

C. E. JACOB (Northridge, Calif.) *Salt-water encroachment in unconfined island aquifers.*—This is a theoretical study of the encroachment of sea water into unconfined aquifers under nearly circular islands and under islands approximating infinite strips. Simultaneous partial differential equations are obtained by the method of Dupuit for the salt-water flow and the fresh-water flow. Non-steady states are readily approximated by graphical integration between successive steady states or uniformly varying states. Influences of inhomogeneity and anisotropy are considered, also effects of partial confinement near the coast and adjustments of the Dupuit profiles to allow for them. The hodograph transformations are discussed. Simultaneous finite-difference equations are set up for numerical integration by digital computer. The long-term characteristics of the systems are studied, also the lagging of the encroachment behind any natural or artificial lowering of the water table. Tidal phenomena, diffusion, and dispersions are also discussed.

JOHN F. KENNEDY (California Institute of Technology, Pasadena, Calif.) *Anti-dunes and standing waves in alluvial channels.*—At near-critical or supercritical velocities, alluvial streams exhibit standing surface waves. These waves, once initiated, increase in amplitude until they reach a certain height and then break upstream. This be-

havior of the surface is intimately related to the accompanying behavior of the bed. The breaking of the waves dissipates energy in addition to that which would be dissipated by the same discharge flowing at an equivalent uniform depth. The friction factor for the anti-dune regime may be smaller or larger than that of the lower velocity regimes depending on the character of the bed material and the accompanying bed configuration. The agitation of the bed accompanying the wave-breaking entrains bed material, radically increasing the sediment discharge of the stream.

Laboratory flume experiments were made to study the behavior of the free surface and the bed and the relation between them, as well as their effects on the gross parameters of the flow. The behavior of the flow can be best explained in terms of the Froude number, size of the bed material, and depth of flow. It is consistent with that predicted by the solution of the problem of potential flow over a bed of sinusoidal form. No simple relation was found which would predict the behavior of a stream with any combination of governing parameters. The actual mechanism of wave growth and breaking and accompanying behavior of the bed was studied by means of still and motion pictures.

KENNETH R. KNOERR (California Forest and Range Experiment Station, USDA, Forest Service, Berkeley, Calif.) *Summer evapotranspiration measurements using a radioactive soil moisture probe*

—Changes in soil moisture storage were used to estimate summer evapotranspiration from some Sierra Nevada forest sites. These sites varied widely in cover type, cover density, and slope exposure. Soil moisture was measured periodically throughout the summer and fall. Normal gravimetric methods of soil-moisture measurements were used in 1957, but progress was slow because of the stony, glaciated soils of the region. In 1958, however, a commercially available, radioactive probe was used to obtain the soil-moisture measurements. This probe allowed repeated measurements at exactly the same point and depth. During the first year of the probe's use, measurements were made for only part of the summer evapotranspiration season, the 75-day period from July 31 to October 15. Average losses from the top 4 feet of soil for this period were: old red fir—5.1 inches; young red fir—4.8 inches, *wyethia* (a wild sunflower)—3.5 inches; and bare ground—1.3 inches. In addition, the 2.0 inches of precipitation received during the summer was lost by interception or by direct evaporation from the soil surface.

E. C. LAFOND (U. S. Navy Electronics Laboratory, San Diego, Calif.) *Sea-surface slicks off Mission Beach*—Slicks are streaks or patches of relatively calm surface water surrounded by rippled water. Off Southern California, slick films are prevalent on the sea surface in summer when the organic production is greatest and the thermocline is near the surface. At this time slicks in 50-foot shelf waters average 13 yards across and are spaced 130 yards apart. The oceanic environment associated with sea-surface slicks has been investigated by means of continuous-recording temperature, transparency and chemical equipment.

It was found that the water in or near the slick zone has a different transparency, oxygen content, bubble content, and surface tension than has adjacent water.

Slicks are associated with the motions created by internal waves. The vertical motion of near-surface water in such waves is upward on the face of the advancing wave and downward on the after face of the wave. The latter motion creates a convergence at the surface which concentrates the lighter film in the form of slicks at a location just behind the crest. As the subsurface progressive wave moves shoreward, the convergence zone and consequently the surface film with associated debris moves with it. Dye-marker studies show that a lateral motion occurs at the surface in the slick. This motion is believed to be due to geostrophic flow. The dye marker also reveals that currents move in different directions above and below the density boundary. These motions have been measured and treated theoretically. The speed and direction of band-type slicks was established by means of time-lapse motion pictures. These slicks move shoreward with decreasing speeds. Their speed depends on the nature of the associated internal wave and the characteristics of the vertical water strata. In summer at a depth of 50 feet they travel at an average rate of 10 yards per minute. From these studies, it appears that sea-surface slicks provide valuable information on the near-surface water structure and water motion.

JAN LAW (P. O. Box G, Seal Beach, Calif.) *In-place measurement of deep seated compaction*—The Long Beach, California, subsidence involves an area of 6 by 3 miles which includes 32 miles of water front. Subsidence initiated in 1938 has, as of 1958, created an elliptical bowl of subsidence of approximately 160,000,000 cubic yards. The profile of the bowl may be generalized by giving the radius of the major axis of the elliptical isobase lines. The 24, 12, 6, and 3 foot isobases are located respectively 1,000, 5,800, 9,000 and 13,500 feet from the center. The bowl is underlain by 2000 feet of fresh water sediments, 1500 feet of loosely consolidated oil sand and shale, 2500 feet of indurated oil sand and shale and the basement is the schist prevalent west of the Inglewood-Newport line. This basement schist is presumed to be stable.

The in-place measurement of compaction is based upon the following line of reasoning. Provided 6000 feet of casing is placed in a 6000 foot hole (which penetrates into basement), and provided the casing does not protrude when surface subsidence occurs, then it follows that the casing has been shortened. The earth forces of adherence or skin-friction in association with the weight of material in motion are such that the casing is shortened at depth locations which coincide with the depth location of compacting strata. Instruments lowered into the cased hole and raised with care are able to measure the in-place lengths of each joint of casing. The comparison of joint lengths obtained by surveys made at intervals during subsidence demonstrates the location and magnitude of deep seated compaction such that increment 'compaction-shortening' approaches increment subsidence.

RAY K. LINSLEY (Department of Civil Engineering, Stanford University, Stanford, Calif.) *Hydrology in Europe*—This paper reports some impressions gained during a sabbatical year spent as visiting Fulbright Professor at Imperial College, London. In general, there seems to be far more concern with precision of measurement of basic data than in the United States. Less effort has been devoted to statistical correlations such as rainfall-runoff relations and to unit hydrograph techniques. Emphasis is given to what may be called hydroclimatology—determination of normals and extremes, and to problems amenable to theoretical solutions. Some excellent experimental and analytical work is in progress. The differences in approach and viewpoint between hydrologists in Europe and in the United States can be explained by differences in the type of problems encountered, the data available, and fundamental philosophy.

The World Meteorological Organization may shortly take over responsibility for hydrology within the framework of the United Nations. This will not materially affect the United States, but may considerably accelerate world progress in hydrology.

EDWARD M. LITTLE (U. S. Navy Electronics Laboratory, San Diego, Calif.) *Fluid permeability profile of sea ice as a good index of its condition*—Vertical holes were drilled quickly in the sea ice with an ice auger about 10 cm in diameter to depths of 10 cm, 20 cm, 30 cm, etc. The rate of collection of brine in each hole was measured. This permitted calculation of the fluid permeability profile. Usually in midwinter the fluid permeability of new sea ice increases toward the bottom of the ice sheet because of the unfrozen brine occupying a larger fractional space due to the higher temperatures there. Rates of collection and brine temperatures were measured to give approximate temperature profiles. Salinity of the unfrozen brine, often as much as 120‰, is greater near the top in new sea ice. Permeability for brine in cm/sec for a pressure gradient of 1 atmosphere per cm was calculated. This was multiplied by the viscosity of salt water, salinity 70‰ and a temperature of -3.5°C. This gave intrinsic permeability independent of the fluid used. The intrinsic permeability range was from about 0.2 darcy near the top of the ice, at -7°C, to 2.5 darcys near the bottom of the 2-ft-thick ice. Sandstone has about the same order of permeability, a range of about 0.01 to 1 darcy.

A. R. McBIRNEY (1036 Haight Street, San Francisco, Calif.) *Theoretical aspects of hydrothermal power resources*—The first important utilization of long-neglected, hydrothermal power resources in the United States is now being undertaken at "The Geysers" in California. Successful exploitation of natural steam in New Zealand, Iceland, and Italy has demonstrated the importance of several factors governing potentialities of thermal areas. Of primary importance in predicting temperatures, pressures, and quality of steam that wells will produce is determination of the origin of the steam. Production from wells in areas of heat-saturated ground water is likely to be limited by depth-pressure relationships to mix-

tures of steam and water, and possible rates of heat withdrawal over extended periods are only slightly greater than initial surface heat losses. If heat is of primary, magmatic origin, however, dry or superheated steam can be expected, and total possible heat withdrawal is unrelated to surface heat losses. Physical, chemical and geological criteria for evaluating surface manifestations and exploratory borings can facilitate appraisal of a thermal area's economic potential.

DON J. MILLER (U. S. Geological Survey, Menlo Park, Calif.) *Giant waves in Lituya Bay, Alaska*—At least four times in little more than a century, giant waves have rushed out from the head of Lituya Bay, Alaska, leaving trimlines in the forest much like those formed by glaciers. The earliest known wave, dated by tree ring studies as occurring in 1853 or 1854, destroyed trees to a height of 395 feet two miles from the head of the bay. Old photographs indicate another wave about 1900; its trimline was obliterated by waves on October 27, 1936. The latest and largest wave closely followed the major earthquake of July 9, 1958, and in about four minutes killed two persons, wrecked two fishing boats, and destroyed the forest over about four square miles. Trees were washed out to altitudes higher than 1700 feet. The 1958 wave probably was generated by a large rockslide that was triggered by the earthquake and plunged into deep water at the head of the bay, but displacement along the Fairweather fault, under water in this area, may also have contributed. Evidence is lacking for either an earthquake or a rockslide at the time of the 1936 waves.

C. E. PALMER (Department of Geophysics, University of California, Berkeley, Calif.) *The stratospheric polar vortex*—Recent high-level balloon observations at polar stations, during the Arctic and Antarctic nights, have increased in number and range, especially during IGY. The new data indicate that above 15 km horizontal temperature gradients in the neighborhood of the edge of the earth's shadow become very large as the winter progresses. Thermal-wind arguments show that the shadow should be surrounded by a strong cyclonic vortex, increasing with height; and the wind observations confirm this expectation. At the limit of observation (about 30 km) the cyclone is very intense; wind velocities at this level in excess of 50 m/s are not uncommon; the increase in intensity could, plausibly, be expected to continue at least to 50 km and possibly beyond. The vortex appears to be unstable in the north polar regions, breaking down into cells at intervals of approximately three weeks. The cells appear on horizontal stratospheric maps as discrete high and low pressure regions which travel from west to east. Evidence will be presented, however, to show that the breakdown of the vortex is initially due to strong meridional motions, producing large temperature changes (30°C in four days, for example) within the earth's shadow. Application of theoretical criteria of stability (especially that due to Kuo) indicates that the vortex is indeed unstable with respect to toroidal perturbations. The breakdown of the polar vortex appears to be followed by readjustments in the tropospheric circulation

in high latitudes to the very great pressure and temperature changes in the lower stratosphere. So far, no breakdown in the south polar stratospheric vortex has been observed.

D. A. PHOENIX AND D. W. PETERSON (U. S. Geological Survey, Salt Lake City, Utah, and Denver, Colo.) *General geology of the Lees Ferry—Glen Canyon dam area*—Three groups of sedimentary formations crop out in the canyons of this deeply dissected plateau area; they are well exposed near Lees Ferry about 9 miles downstream from the dam site. The oldest, of Permian age, comprises about 800 feet of limestone, quartzite, and shale; it forms cliffs and steep slopes along Marble Canyon southwest of Lees Ferry. The middle group, of Triassic age, is about 1600 feet of chiefly claystone and mudstone; it underlies extensive landslides at the base of the cliffs near Lees Ferry. The youngest group, of Triassic(?) and Jurassic age, comprises about 2000 feet of fine-to medium-grained sandstone; it forms vertical cliffs above the middle group and in Glen Canyon. Regionally the strata dip gently northward, but west of the dam they are arched upward along a northward-trending monocline. Displacement along this monocline is sufficient to raise the impermeable rocks of the middle group above the proposed lake level downstream from the dam site.

The region has been prospected for uranium, gold, and mercury; the chief value, however, seems to be recreational, and to it the lake will add greatly. Economical development of tourist facilities will require intensive local studies of the availability of ground water. The migration of water away from the reservoir will probably take place along westerly trending joints but these losses should not be large and will be intercepted by the stream gaging station at Lees Ferry. It is expected however that additions to ground-water storage from the reservoir will be appreciable and this water may be useful in periods of prolonged drought.

ARTHUR M. PIPER (U. S. Geological Survey, Menlo Park, Calif.) *Derivation of a master record of rainfall*—A procedure is presented for deriving a master long-term record of rainfall to which records of shorter term may be fitted. The example is for the region of San Francisco Bay. Records for San Francisco (108 years, 1850–1957), Oakland (83 years, 1875–1957), and San Jose (83 years, 1875–1957) are used. 'Double-mass' plots of yearly rainfall at San Francisco against that at Oakland and San Jose approximate straight lines. However, each plot comprises several straight-line segments of somewhat different slopes, and the points of inflection correspond to years in which the location of one or two of the three stations was changed.

By the method of least squares, mean double-mass lines are computed from the present (1957) back to the latest significant change in station location (1940). For years prior to 1940, measured rainfall is adjusted so that the double-mass plot falls on the projected mean line of 1957–1940 in each year of significant station change. Adjustments are minimized by certain standardized procedures. For each of the three stations, adjusted yearly rainfall is reduced to accumulated devia-

tion from the average, expressed as a percentage of that average. From the three, mean values of accumulated deviation then are derived. Through these mean values, the straight line of closest fit is computed, and the array of values is 'sheared' so that the line of closest fit becomes the axis of reference. This step yields the master regional record from which probable long-term values of average rainfall can be derived for individual stations regardless of their terms of record.

JOSEPH L. REID, JR. (640 Loring Street, San Diego, Calif.) *Evidence of the existence of a South Equatorial Countercurrent in the Pacific*—The distribution of properties along a surface of equal potential density ($\sigma_t = 26.81$) suggests that at the depth of this surface near the equator there is in addition to the North Equatorial Current, Equatorial Countercurrent, and South Equatorial Current, a flow from west to east between 3°S and 7°S from 150°E to 100°W. The acceleration potential (or Montgomery function) of this surface with respect to 1000 decibars, from whose gradient the geostrophic flow is computed, decreases to the south in this region. The decrease is documented by eleven cross sections, including those of the Carnegie and Equapac expeditions. If it is geostrophically balanced, there must be flow to the east at the depth of this surface, which is between 300 and 350 meters in this region, at speeds between 10 and 24 cm/sec. The path of the eastward flow is also a tongue of high salinity extending eastward from the Coral Sea between the lower salinities of the westward-flowing Equatorial Current and the westward-flowing waters to the south.

ELMER ROBINSON (Bay Area Air Pollution Control District, San Francisco, Calif.) *Meteorological factors of air pollution in the San Francisco Bay Area and along the California Coast*—The coastal region of California is an area with many common factors of weather which indicate that air pollution should be an important consideration of California coastal communities. In the San Francisco Bay Area there is a wide range of climatic conditions which in turn contribute to a variety of air pollution situations. A description of both local and area-wide pollutants in the Bay Area shows how local weather conditions contribute to the evaluation of regional air pollution situations.

HALBERT E. Root (U. S. Weather Bureau, San Francisco, Calif.) *Rain probability forecasting on the West Coast*—Operational rain probability forecasts made for the San Francisco Bay Area during the 1956–1957 rainy season and for both the San Francisco and Los Angeles areas during the 1957–1958 season are evaluated by comparing the observed occurrence with the forecast probability and by 'P' score. When considered in 20 per cent groups, the weighted mean of the difference between the forecast probabilities and the observed relative frequency of occurrence ranges from 4 to 7 per cent for these two seasons and areas. In addition, 70 per cent of all forecast probabilities are concentrated in the upper and lower fifths of the probability range. 'P' score comparisons show that the scores made are superior to scores based on either climatological frequency or climatological persistence.

ABSTRACTS

J. F. T. SAU AND L. E. EBER (U. S. Fish and Wildlife Service, Stanford, Calif.) *On the preparation and significance of monthly mean sea-surface temperature charts of the North Pacific Ocean*—Sea-surface temperature observations from ships are probably the only historical data available from which to infer long-term changes of circulation in the open ocean. Bureau of Commercial Fisheries, Biological Laboratory, Stanford, California, has obtained from the U. S. Navy Hydrographic Office and the U. S. Weather Bureau over two million observations of sea surface temperature in the Pacific for the period from 1935 through June 1957 and the area north of 20°S latitude. The listings are organized and summarized by month and by 2-degree squares for the purpose of studying certain areas and preparing selected monthly charts of mean sea-surface temperature. Qualitative examination indicates that the data contain errors arising from (a) incorrect ship position, (b) use of different thermometric scale, (c) instrumental error, (d) observational error, and (e) personal and machine processing error. However, test charts constructed for June 1956 and June 1957 after gross errors have been eliminated by preliminary editing, indicate that internally consistent isotherm patterns can be drawn from the summarized data with relatively little smoothing.

The temperature change between the two months shows the warm water of 1957 off the west coast of North America and in the Gulf of Alaska, and colder conditions along the Japanese coast and extending eastward as a tongue between 33° and 39°N latitude to about 155°W. These changes in sea temperatures may have resulted from a decrease in circulation in the current gyre comprised of the Kuroshio, North Pacific Drift, California, and North Equatorial Currents and an increase in the Oyashio and Alaskan Currents. Indices of the mean monthly geostrophic wind for each of these current regions have been computed from the mean monthly sea-level pressure charts for the spring months of these years. The indices indicate changes in wind stress which agree well with the inferred current changes.

WARREN C. THOMPSON (Department of Oceanography and Meteorology, U. S. Naval Post-graduate School, Monterey, Calif.) *Modifications to the application of the Pierson-Neumann theory in the forecasting of ocean swell*—Estimation of the dimensions of ocean swell by use of the New York University (Pierson-Neumann-James) wave forecasting technique, described in H.O. 603, involves computation of the range of spectral components (wave trains of given period or frequency) that can be present at a given location at any given time. The range of spectral components, which determines the energy in the swell, and hence the swell height, is computed by the use of energy-dispersion equations. These equations can be rearranged so that the spectral properties of the swell can be more readily visualized, and so that the forecaster can keep better track of the energy. The rearranged equations yield the times of arrival and departure of those wave trains having the various periods produced in the sea. Further, for some synoptic situations (for example, the stationary fetch) the N.Y.U.

dispersion equations assume that all spectral components that ultimately occur in the sea extend to the windward edge of the fetch; also, they make no allowance for the wave energy present in the sea before the sea is fully developed. The rearranged equations can be modified in order to eliminate these difficulties.

JOHN E. TYLER (Visibility Laboratory, Scripps Institution of Oceanography, University of California, San Diego, Calif.) *The directional distribution of natural light at various depths under water*—The directional distribution of radiance for natural light in homogeneous water has been measured in detail for clear sunny sky conditions at seven depth stations between 4 and 66 meters and for overcast sky conditions at five depth stations between 12 and 49 meters. These data clearly illustrate the phenomena of flux transfer within the hydrosol, the dependence of the value of the attenuation coefficient for natural light on the lighting conditions, and the approach to asymptotic radiance distribution as depth increases. From these data one can compute the attenuation coefficient for natural light, the reflection factor at any depth, the up-and-down-welling distribution functions, and the absorption coefficient.

JOHN E. TYLER (Visibility Laboratory, Scripps Institution of Oceanography, University of California, San Diego, Calif.) *Some current hydro-optical research in the USSR*—The program of research undertaken by scientists on board the Russian Oceanographic Vessel *Vityaz* includes extensive hydro-optical measurements. Total transmittance of ocean water is being measured with a modulated-lamp hydrometer employing vacuum photo tubes. The instrument is depth limited to 200 meters, but it can be used to measure captive samples obtained from greater depths. Directional scattering measurements are being made on water samples placed in a visually balanced nephelometer of unusual design. The attenuation coefficient for natural light is being determined by means of a photoelectric underwater photometer employing five selenium photocells mounted behind convex Lambert collector plates. The measurements are all being made in selected regions of the spectrum and the data are being correlated with the location of ocean currents, with temperature, nitrate concentration, and the concentrations of phyto-plankton.

ARVI O. WAANANEN (U. S. Geological Survey, Menlo Park, Calif.) *Studies in land-water relations: hydrological effects of urbanization*—The hydrologic effects of changes in land use through development of suburban, industrial, and urban communities include, among others, modification of the natural surface drainage patterns, volume and intensity of runoff, channel hydraulics, infiltration and ground-water recharge, and sediment yield. Urbanization also is accompanied by sharp changes in the demands for water and the need for measures for disposal of surplus waters and municipal and industrial wastes. The social, economic, and political problems associated with urban development are receiving increasingly

greater attention. Frequent press items about flood, drainage, and other water problems indicate that the hydrologic effects are well recognized. However, only a few researchers are studying these problems; and there is a paucity of quantitative data and documentary material useful for defining or forecasting the magnitude, nature, and extent of the changes.

The Geological Survey has begun studies of the hydrologic changes resulting from urbanization of lands. Three small areas in the San Francisquito Creek basin near Menlo Park, California, are being studied to observe the changes that occur during the transition from rural to residential use. Other investigations include study of runoff characteristics of natural and seweried areas, effects of changes in vegetative cover, and review of hydrologic design criteria available.

F. X. WEBSTER AND F. S. DUCKWORTH (Stanford Aerosol Laboratory, Stanford, Calif.) *Comparative atmospheric travel of a gas and an aerosol*—A series of 24 field trials was conducted to compare the atmospheric travel and diffusion behavior of FP aerosol (a finely powdered solid material of density 4 with particles 1 to 5 microns in diameter) with the behavior of SO₂ gas. The comparisons are made on the basis of coincidentally measured FP-SO₂ dosages obtained along sampling arcs at 48, 100, and 200 yds downwind, and in a few trials up to 400 yds, from a common source point. The FP-SO₂ cloud was generated at a constant particle-to-gas ratio for a period of five minutes. Conditions affecting the FP-SO₂ cloud behavior included winds ranging from 2.6 to 16.4 mph, and temperature gradients (1/2 to 4 meters) ranging from 2.6°F lapse to 2.6°F inversion. The diffusion behavior of the gas and aerosol was studied from the standpoint of the comparative dosage-area patterns, the cross-wind integrated dosages, and the ratio of the dosages measured at all individual sampling stations. Average dosage-area coverage for the FP aerosol showed no statistically significant differences from those for

SO₂. For any two trials conducted under closely similar conditions, coincidently-obtained FP-SO₂ dosage areas were predominantly more nearly equivalent in area-coverage and configuration than other combinations of non-coincidently obtained dosage areas. Configurations of corresponding FP and SO₂ crosswind dosage profiles were very similar. There was no statistically significant tendency for individual station FP/SO₂ dosage ratios to change progressively with downwind distance.

J. B. WICKHAM, J. BLONDIN, AND J. NEGELE (U. S. Naval Postgraduate School, Monterey, Calif.) *Some ocean wave spectra at Davenport, California*—Spectra of ocean swell and local wind waves in shallow water off Davenport, California, are obtained by application of Tukey's method of analysis to wave records given by pressure-sensors mounted near the ocean bottom. The analyzed records cover 12-hour intervals over a five-day period during winter of 1954. For the same five-day period, wave spectra at Davenport are inferred from the wind areas on analyzed weather charts. Spectra in the generating areas, according to Neumann, simple forms of dispersion and angular spreading, and shoaling and refraction effects as described in Pierson, Neumann, and James in H.O. 603, were assumed in the analysis. Within the limits of the accuracy of the technique used in analyzing the wave records it is clear that long swells persist throughout the period, that local wind waves are occasionally present, and that in the middle frequencies spectral 'holes' are often observed. These holes are not explainable in terms of the meteorological conditions in the generating areas and the processes assumed to operate during propagation of the wave energy to Davenport. Some form of attenuation en route is therefore postulated. The meteorological data suggest that cross-sea interference, discussed briefly in H.O. 603, is the mechanism by which attenuation occurs. Its effects may frequently be non-negligible and must be accounted for in a complete wave theory.

AMERICAN
GEOGRAPHICAL
UNION

UNSELFISH
COOPERATION
IN RESEARCH

AMERICAN GEOPHYSICAL UNION

1515 Massachusetts Avenue, N.W., Washington 5, D.C.

Established by the National Research Council in 1919 for the development of the science of geophysics through scientific publication and the advancement of professional ideals.

APPLICATION FOR MEMBERSHIP

Please refer to qualifications on reverse side and designate below type of membership desired:

Member (\$10)

Associate (\$10)

Student (\$3)

Application forms for Corporation Membership are available upon request.

1. Surname First Name Middle Name

2. Preferred mailing address for publications

Permanent address

3. Place Month Day Year of Birth 4. Country of citizenship/naturalization

5. Nature of work and title and/or military rank; name and address of organization with which you are associated.

6. Check section or sections with which affiliation is desired.

<input type="checkbox"/> Geodesy	<input type="checkbox"/> Oceanography
<input type="checkbox"/> Seismology	<input type="checkbox"/> Volcanology, Geochemistry, and Petrology
<input type="checkbox"/> Meteorology	<input type="checkbox"/> Hydrology
<input type="checkbox"/> Geomagnetism and Aeronomy	<input type="checkbox"/> Tectonophysics

EXPERIENCE (List below)

Dates: From To Name and address of organization Title, duties, nature of work

EDUCATION (List below)

Dates: From To School Address Major Subject Degree, if any

*9. References: Please list below names and addresses of two or three references; include members of the AGU or others who know you well.

*10. Titles of technical contributions or publications, particularly those in the geophysical sciences, and where published.

*11. Brief statement of any special interests or qualifications in the geophysical sciences.

Date _____ Written Signature

* Applicants for student membership may omit Questions 9, 10, and 11, but must fill in Question 12. Please return form with check or money order payable to American Geophysical Union, 1515 Massachusetts Ave., N.W., Washington 5, D.C.

(over)

12. (STUDENT MEMBERS ONLY) The person whose signature appears on the reverse side is known to me and is a student majoring in _____ (subject) at _____
(Name of college or university) expected to graduate in _____ (year) with the degree of _____
 He is a full-time student, or a teaching or research assistant enrolled in more than half of a full-time academic program.

(Signature of faculty sponsor)

Check here if faculty sponsor is a member of AGU and willing to act as a regular sponsor for associate membership as well.

(Typed or printed name of sponsor)

(Title)

QUALIFICATIONS FOR MEMBERSHIP IN THE AMERICAN GEOPHYSICAL UNION

The membership of the AGU shall consist of Members, Associate Members, Student Members, and Corporation Members.

Those eligible as candidates for election to the grade of MEMBER shall be:

MEMBER (a) Persons who have made an active contribution to geophysical research through observation, publication, teaching, or administration. Definite evidence should be presented to the Membership Committee. "Publication" may include books, articles, unpublished manuscripts, inventions, or development of geophysical instruments.

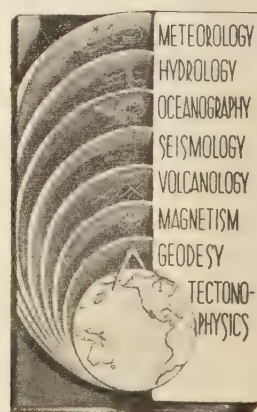
(b) Persons who have made active practical application of geophysical research. It should be shown that the nominee's work has not been purely routine, but that it has tended to create new knowledge of, or to broaden or strengthen the application of, geophysical research. In general, the minimum qualifications for membership will be not less than three years of professional experience in some phase of geophysics.

Those eligible as candidates for election to the grade of ASSOCIATE MEMBER shall be:

ASSOCIATE MEMBER Persons who have an active interest in physical processes of the Earth or technical assistance in the application of geophysics. In general, the minimum qualification for associate membership will be acceptable training or experience in some field of geophysics or allied science.

CORPORATION MEMBER Corporations and other interested organizations shall be eligible as candidates for election to CORPORATION MEMBERSHIP. They shall have the privilege of designating a representative who has the rights and privileges of Members (use special form).

STUDENT MEMBER Those eligible as candidates for election to the grade of STUDENT MEMBER shall be persons who are graduate or undergraduate students in residence at least half-time and who are specializing in the geophysical sciences. Teaching or research assistants enrolled in more than half of a full-time academic program may also be eligible for Student Membership. Student Members shall have all the privileges of Members except that they shall not vote or hold office.



Information for Contributors to the *Journal of Geophysical Research*

Manuscripts—Send manuscripts to J. A. Peoples, Jr., Department of Geology, University of Kansas, Lawrence, Kansas. Manuscripts, including proof copies of figures, should be submitted in triplicate to expedite review and publication. Manuscripts should be in English, typewritten on heavy paper on one side of page only, double spaced (including abstracts and references), with generous margins.

Ample space should be allowed for mathematical expressions, which should be typed or very plainly written by hand. Particular attention should be given to legibility of subscripts and superscripts and to differentiation between capital and lower case letters. Unusual symbols and cumbersome notations should be avoided. Fractional exponents should be used in preference to root signs, and the solidus (/) should be used for fractions wherever its use will save vertical space.

Authors are urged to have their papers critically reviewed by their associates for scientific validity, manner of presentation, and use of English before submitting them for publication.

Abstracts—An abstract must accompany each manuscript. It should be a concise but comprehensive condensation of the essential parts of the paper, suitable for separate publication, and adequate for the preparation of general indexes to geophysical literature.

References and footnotes—References should be indicated in the text by the insertion in brackets of the author's name and the year of publication, thus: [Trelease, 1951]. If the author's name is part of the text, only the year is bracketed. If there are two or more references citing different papers published in the same year by the same author, distinguish them by the letters a, b, c after the year. At the end of the paper, list all references alphabetically by the authors' names. Include in each entry the following: name of senior author, followed by his initials; names of junior authors, each preceded by his initials; title of paper (or book); title of publication or journal; volume number; inclusive page numbers; year of publication. Abbreviations of journals follow the style used in *Chemical Abstracts*. If in doubt, give the full title of the publication or journal. When a book is cited, add the publisher's name, the city of publication, and the total number of pages. Reference to specific pages may be made in the text if appropriate. Acknowledge unpublished reports and private communications in the text, not as references. Avoid footnotes to the text; use parenthetical sentences instead of footnotes if possible.

Tables and figures—Material suitable to tabular form should be arranged as a table and may be type-written on a separate page. Tables must be numbered according to their sequence in the text, and each table should have a title. Column headings should be short and self-explanatory; more complete explanation may be given in footnotes to the table. Authors should avoid repeating in the text material which is given in tables or figures.

Figures should be prepared with the column width of this Journal in mind (a scale of two to four times that of the published figure is usually adequate). Lettering and symbols should be large enough to stand reduction and remain legible. Captions should be typed on a separate page, not lettered in the figures. Necessary legends or lettering in the figures should be executed to meet competent drafting standards, not typewritten. If the author cannot arrange for suitable lettering, he may send the drawings with the lettering lightly penciled in or shown on a proof copy, and the lettering will be done at the editorial office.

Line drawings should be in India ink on white paper or tracing cloth. Coordinate paper should be avoided, but, if used, it must be blue-lined and the coordinate lines which are to show must be inked.

Photographs are acceptable only if they have good intensity and contrast. They should be unmounted, glossy prints.

Figures should be identified by numbering lightly in pencil, and 'top' of each figure should be indicated.

Acknowledgments—Acknowledgments should be made only for significant contributions by the author's professional associates. A brief closing statement will usually suffice.

REFERENCES

AMERICAN CHEMICAL SOCIETY, *List of periodicals abstracted by Chemical Abstracts*, Chemical Abstracts Service, Ohio State Univ., Columbus, 314 pp., 1956.

AMERICAN INSTITUTE OF PHYSICS, *Style Manual*, American Institute of Physics, New York, 28 pp., 1951.

AMERICAN MATHEMATICAL SOCIETY, A manual for authors of mathematical papers, *Bull. Am. Math. Soc.*, 49, no. 3, pt. 2, 1-16, 1943.

EMBERGER, M. R., AND M. R. HALL, *Scientific writing*, Harcourt, Brace and Co., New York, 468 pp., 1955.

TAFT, K. B., J. F. McDERMOTT, AND D. O. JENSEN, *The technique of composition*, 3rd ed., Farrar and Rinehart, New York, 628 pp., 1941.

TRELEASE, S. F., *The Scientific paper—how to prepare it, how to write it*, Williams and Wilkins Co., Baltimore, 175 pp., 1951.

U. S. GEOLOGICAL SURVEY, *Suggestions to authors of the reports of the United States Geological Survey*, 5th ed., U. S. Govt. Printing Office, Washington, 255 pp., 1958.

WILLIAM BYRD PRESS, *Mathematics in type*, Richmond, 58 pp., 1954.

Contents

	PAGE
Some Wind Determinations in the Upper Atmosphere Using Artificially Generated Sodium Clouds. <i>Edward Manring, J. F. Bedinger, H. B. Pettit, and C. B. Moore</i>	587
The Propagation of World-Wide Sudden Commencements of Magnetic Storms	V. B. Gerard
	593
Auroral X-rays, Cosmic Rays, and Related Phenomena during the Storm of February 10–11, 1958 <i>J. R. Winckler, L. Peterson, R. Hoffman, and R. Arnoldy</i>	597
On the Excitation Rates and Intensities of OH in the Airglow	Joseph W. Chamberlain and Clayton A. Smith
	611
A Preliminary Model Atmosphere Based on Rocket and Satellite Data	H. Korf Kallmann
	615
Cosmic-Ray Intensities and Liquid-Water Content in the Atmosphere <i>H. Arakawa</i>	625
Recent Seasonal Interactions between North Pacific Waters and the Overlying Atmospheric Circulation <i>Jerome Namias</i>	631
A Practical Equal-Area Grid <i>Emanuel M. Ballenzweig</i>	647
The Experimental Fusion Curve of Iron to 96,000 Atmospheres <i>H. M. Strong</i>	653
On the Attenuation of Small-Amplitude Plane Stress Waves in a Thermoelastic Solid <i>Sven Treitel</i>	661
Method for Obtaining the Optical Properties of Large Bodies of Water	J. E. Tyler, W. H. Richardson, and R. W. Holmes
	667
Return Period Relationships <i>G. N. Alexander</i>	675
Letters to the Editor:	
Radio Emission Following the Flare of August 22, 1958	A. Boischot and J. W. Warwick
	683
Balloon Observation of Solar Cosmic Rays on March 26, 1958	P. S. Freier, E. P. Ney, and J. R. Winckler
	685
Abstracts of papers presented at the Pacific Southwest Regional Meeting, Stanford, California, February 5–6, 1959	689

